JOURNAL OF APPLIED PHYSICS

Acc 1124 48

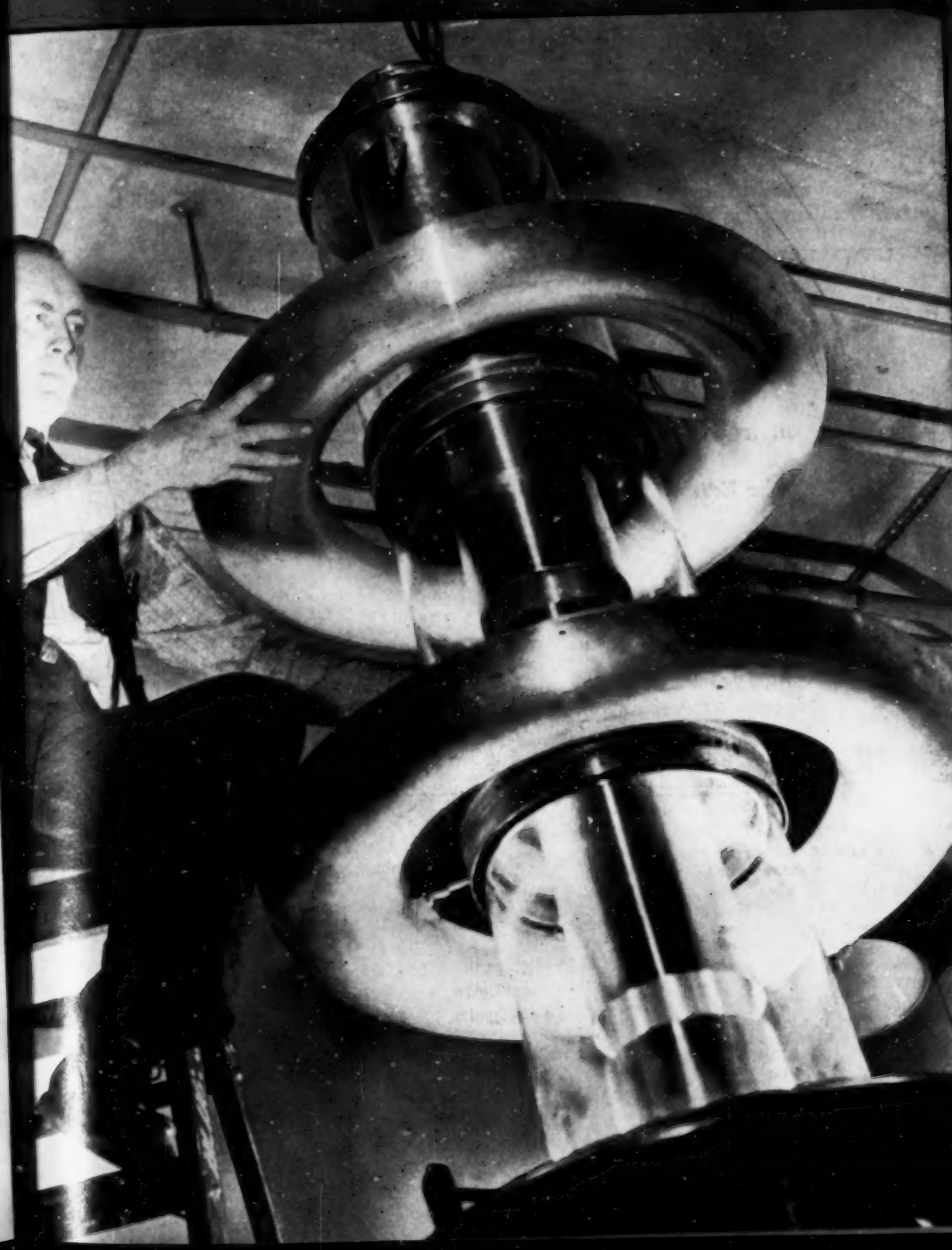

MARCH
1940
Vol. 11 No. 3

Giant X-Ray Tube

JOURNAL OF APPLIED
PHYSICS

MARCH, 1940 Vol. 11, No. 3

In This Issue

Page

Atom Smashing *Versus* Humanity Smashing 159

Ferromagnetic Domains and the Magnetization Curve
WILLIAM FULLER BROWN, JR. 160

Glass as an Electrical Insulator C. J. PHILLIPS 173

Resumés of Recent Research 182

Contributed Original Research

Remarks on the Study of Structural Viscosity in Liquids, and the Derivation of Equations for the Flux of Such Liquids Through Tubes FRANCIS BREAZEALE 187

Relation of Fluidity to Volume in Organic Liquids
EUGENE C. BINGHAM AND PAUL W. KINNEY 192

Conductivity Measurements on Potassium Halides
CORNELIUS G. BRENNECKE 202

Studies in Lubrication. VII. The Lubrication of Plane Sliders of Finite Width
M. MUSKAT, F. MORGAN AND M. W. MERES 208

Formation and Maintenance of Electron and Ion Beams
LLOYD P. SMITH AND PAUL L. HARTMAN 220

Letter to the Editor

Mechanism of Static Friction M. E. MERCHANT 230

In Every Issue

Here and There 183

Contributors to This Issue 185

Innovations in Instruments 186

Index to Advertisers viii

BOARD OF EDITORS

ELMER HUTCHISSON, *Editor*

Associate Editors

F. BITTER
W. E. FORSYTHE
L. A. JONES
B. E. WARREN
J. B. WHITEHEAD

Publication of the American Institute of Physics

ADMINISTRATIVE STAFF

HENRY A. BARTON, *Director*

MADELINE M. MITCHELL, *Publications Manager*

GOVERNING BOARD

JOHN T. TATE, *Chairman*
KARL T. COMPTON
WHEELER P. DAVEY
FLOYD A. FIRESTONE
HARVEY FLETCHER
R. C. GIBBS
ARTHUR C. HARDY
GEORGE R. HARRISON
A. STUART HUNTER
PAUL E. KLOPSTEG
H. R. LILLIE
FREDERIC PALMER, JR.
GEORGE B. PEGRAM
W. B. RAYTON
WALLACE WATERFALL

THE JOURNAL OF APPLIED PHYSICS, published monthly at Prince and Lemon Sts., Lancaster, Pa., is devoted to physics in its role as the science basic to other natural sciences and to the arts and industries. Previous to 1937 this publication was known as PHYSICS. It aims to be of service not only in physical laboratories, but also in the laboratories of industrial, chemical, geological, geophysical, meteorological, radio, and similar concerns. THE JOURNAL OF APPLIED PHYSICS publishes editorials, news of physicists and reviews, as well as technical papers of applied physics.

SUBSCRIPTION PRICE

	U. S., POSS. AND CANADA	FOREIGN
To members of scientific societies	$5.00	$5.70
To all others	7.00	7.70

Manuscripts should be submitted to Elmer Hutchisson, Editor, University of Pittsburgh, Pittsburgh, Pennsylvania.

Changes of address and proofs should be addressed to the Publications Manager.

Subscriptions and orders for back numbers should be addressed to Prince and Lemon Streets, Lancaster, Pa. or to the American Institute of Physics, 175 Fifth Avenue, New York, N. Y.

Advertising rates supplied on request. Orders, advertising copy and cuts should be sent to the American Institute of Physics.

Entered as second class matter at the Post Office at Lancaster, Pennsylvania, under the Act of March 3, 1897. Accepted for mailing at the special rate of postage provided for in the Act of February 28, 1925, authorized May 2, 1932.

Copyright 1940, by the American Institute of Physics.

4 QUICK STEPS TO STANDARDIZE

1 Hold switches at "1". Balance galvanometer by turning knob "1".

2 Hold switches at "2". Balance galvanometer by turning knob "2".

3 Set switch at "3". Balance galvanometer by turning knobs "3" and "3'".

4 With a standard 4 pH solution in place, set scale to 4 pH and balance galvanometer by turning upper knob.

ONE TO MEASURE

With unknown solution in place, balance galvanometer by turning lower knob and read results.

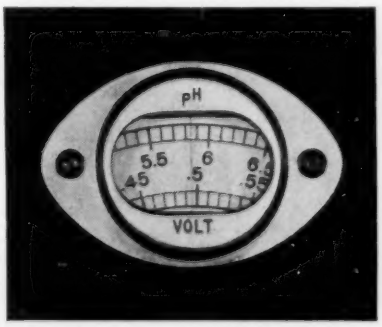

The hand-drawn scale is easily read.

pH is Easily Measured With a UNIVERSAL pH INDICATOR

Once it's standardized, measurements are made with a single adjustment. An occasional run through steps 1 to 4 gives a quick check on the accuracy of results. One reason for the Universal's consistent accuracy is the separate standardization of each variable. By making these four adjustments individually, errors arising from their interrelated effects are avoided.

Write for Catalog E-96 (1)

LEEDS & NORTHRUP COMPANY, 4978 STENTON AVE., PHILA., PA.

LEEDS & NORTHRUP

Measuring Instruments : Telemeters : Automatic Controls : Heat-Treating Furnaces

Jrl Ad E–96(15)

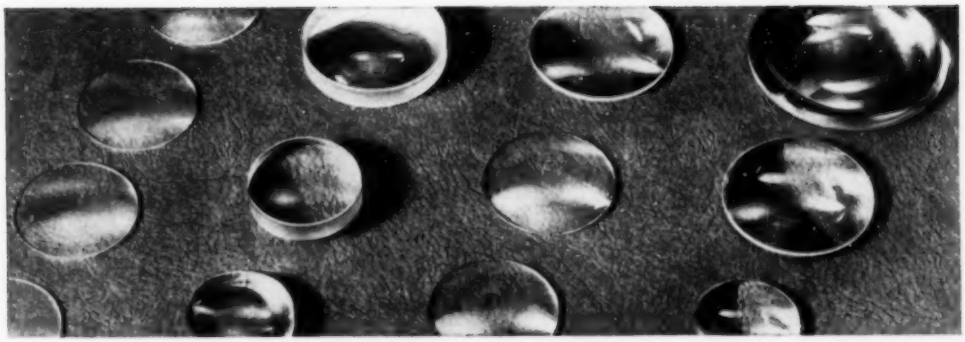

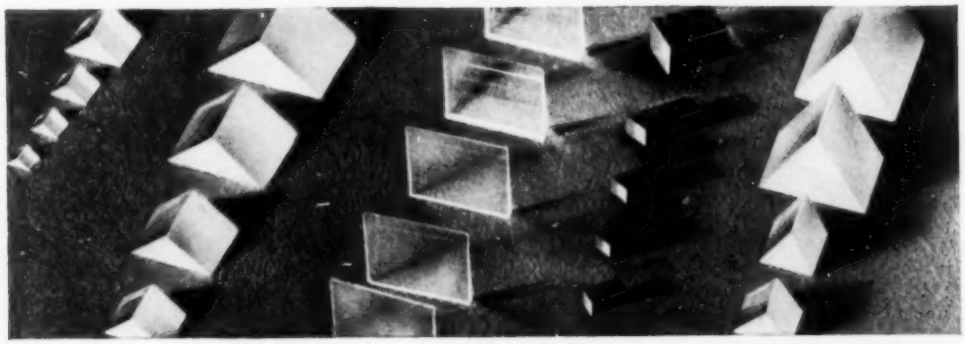

B&L OPTICAL PARTS

A Single Lens or a Complete Optical Unit

B&L Optical Parts—lenses, prisms and mirrors—are made to the same high standards as those used in B&L Instruments. That is why so many research workers and teachers of optics make their selections from the complete line of B&L Optical Parts. . B&L Catalog D-10 lists the widest variety of lenses, prisms, mirrors and complete optical sets for every requirement in teaching or research work. Glass, calcite and quartz parts are included. Write for the complete catalog to Bausch & Lomb Optical Co., 670 St. Paul St., Rochester, N. Y.

BAUSCH & LOMB

FOR YOUR EYES, INSIST ON BAUSCH & LOMB EYEWEAR, MADE FROM BAUSCH & LOMB GLASS TO BAUSCH & LOMB HIGH STANDARDS OF PRECISION . . . . . .

HARVARD COLLEGE
MAR 8 1940
LIBRARY

Journal of Applied

Physics

Volume 11 March, 1940 Number 3

Atom Smashing *Versus* Humanity Smashing

DR. Arthur H. Compton was reported recently as declaring that the progress made in breaking up atoms and putting a portion of their energy to other uses is of far more importance to the world today than the war in Europe. To those who are familiar with the rich and continuing rewards of research in all fields of science such a reminder is scarcely needed. Yet it must be repeated again and again in the daily press if the population as a whole is ever to recognize that promoting research is just as much a part of its responsibility as promoting big armies and big navies for defense purposes.

The need for emphasizing the importance of research was never greater than at the present time. We have before us the strange spectacle of nations which have themselves reaped countless benefits from science forsaking the methods of research for those of bloodshed and destruction. Their purpose is said to be to uphold national honor and to give their people a better living. Yet with the very finite area of this world on which we live it is perfectly obvious that, if a nation expands its geographical frontiers, it can do so only at the expense of other people. How different the situation is if its intellectual frontiers are expanded. There is no conceivable limit to the expansion which is possible. No one will lose anything and all will gain.

In his book, *Atoms in Action*, Dr. G. R. Harrison estimates that, if we could discover a way to use the energy of the sun in an efficient manner, we could increase the wealth (in terms of available energy which is the only sensible unit) of every person on earth by a factor of 200,000 times. Some way must be used to bring to the attention of the so-called "man in the street" such examples of the potentialities of research. Strong statements coming from leading scientists like Dr. Compton will undoubtedly do a great deal of good. If the benefits which can accrue from scientific research become generally known, there will be no chance for the rise of dictatorial governments bent upon the destruction of humanity for the sake of a small geographical expansion.

For April

Magnetic Cooling: the Production and Measurement of Temperature Below 1°K, *by* CHARLES F. SQUIRE

Stellar Temperatures, *by* GERARD P. KUIPER

Also contributed research papers on:

Tension and Birefringence in a Vinylite Plastic,

The Use of Radioactive Phosphorus in Soil Studies,

The Solution of Torsion Problems by Numerical Integration of Poisson's Equation,

A Note on Heaviside's Expansion Theorem.

Ferromagnetic Domains and the Magnetization Curve

BY WILLIAM FULLER BROWN, JR.

Palmer Physical Laboratory, Princeton University, Princeton, New Jersey

The magnetization curve and hysteresis loop of a ferromagnetic material used to be explained qualitatively through the interaction of "molecular magnets." It is now known that interaction of the atoms produces, directly, only magnetic saturation, and that the "magnets" whose interaction is responsible for the details of the hysteresis curve are much larger things—magnetically saturated regions big enough to be seen under a microscope. These "spontaneously" magnetized regions are known as "domains," and with them progress is being made toward a quantitative theory of the magnetization process. The basic ideas of the domain theory are described in this article.

Introduction

THE magnetization curve of a typical ferromagnetic specimen, Fig. 1, may for theoretical purposes be divided into three parts: saturation (III), reversible magnetization at high fields (II), and the low field range (I) in which hysteresis occurs. It is with Part I that we shall be particularly concerned in this article, but in order to arrive at an understanding of it something must first be said about Parts II and III.

Saturation (III)

The large magnetic moments observed in ferromagnetic materials at saturation are attributed, in modern theory, to the "spins" of atomic electrons. The forces alining these spins are ones whose *origin* can be explained only by quantum mechanics, but whose *effect* can be taken into account, for our purposes, by attributing to every pair of neighboring atoms a classical potential energy

$$u = -\tfrac{1}{2} I \cos \phi, \tag{1}$$

where I is a positive constant, and ϕ is the angle between the directions of the two magnetic moments: see Fig. 2. Since u is a minimum when $\phi = 0$, the tendency of these forces is to produce perfect alinement of all the atomic moments. At the absolute zero of temperature there is nothing to oppose this tendency, and there results a magnetic moment per unit volume

$$J_0 = n\mu_0, \tag{2}$$

where n is the number of atoms per cubic centimeter and μ_0 is the magnetic moment per atom.

Temperature agitation tends to break up this perfect alinement of atomic moments; the "spontaneous" magnetization J_s therefore decreases as the temperature rises, and finally vanishes at a critical temperature θ, the Curie point. This occurs when the thermal agitation energy kT becomes of the same order of magnitude as the energy per atom associated with the alinement forces; or

$$k\theta \cong I. \tag{3}$$

From the value of θ ($=631°$K for nickel) and of Boltzmann's constant k ($=1.37\times10^{-16}$ erg per degree) it follows that I for nickel is of order of magnitude 10^{-13} erg, and the corresponding energy per unit volume is of order of magnitude $In \cong 10^{-13}\times10^{23} = 10^{10}$ ergs per cm^3. This is much greater than the energy density associated with interatomic magnetic forces, which is given in order of magnitude by $\frac{2}{3}\pi J_s^2 \cong 2\times(500)^2 = 5\times10^5$ ergs/cm^3. Magnetic forces, as is well known, are much too weak to account for ferromagnetism.

At room temperature J_s is only slightly smaller than the value J_0 at absolute zero, and the problem may be simplified by supposing that the atomic moments are perfectly alined but have a slightly decreased value μ, such that

$$J_s = n\mu. \tag{4}$$

The alinement of spins is accompanied by a distortion of the lattice (saturation magnetostriction). The magnetic forces exerted by the atoms on each other are capable of producing such a distortion. A calculation by classical theory, however, leads to a result that is correct only in its order of magnitude. No calculation by quantum mechanics has been carried out. The saturation magnetostriction must at present be evaluated from experimental data.

Reversible Magnetization at High Fields (II)

The atomic theory of spontaneous magnetization predicts that the magnetization should have the saturation value J_s even in zero applied field. The theory of Parts I and II of the magnetization curve must therefore take account of factors that were neglected in the simple atomic theory.

The most obvious of these is the crystalline nature of the material. Ordinary polycrystalline material is made up of crystal grains with their crystal axes oriented in different directions. Within such a crystal, we may expect the spontaneous magnetization to orient itself along certain axes of symmetry, unless a sufficiently

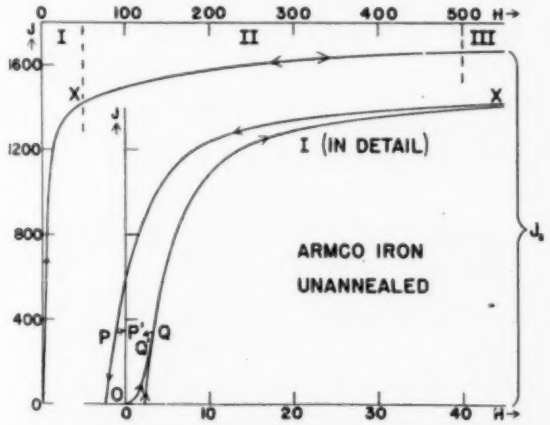

FIG. 1. Typical magnetization curve. H = magnetic field; J = magnetic moment per unit volume, or magnetization. *III*, saturation; *II*, slow and reversible magnetization; *I*, rapid and largely irreversible magnetization; *O*, demagnetization. Arrows indicate the directions in which the curves are traversed. At points *P* and *Q* the magnetization is the same, but the field is different. The "reversible susceptibility" is the slope of PP' or QQ'.

strong field is present to pull the magnetic moments into the field direction. In Part II of the magnetization curve of a polycrystalline specimen, the magnetic moments of the individual crystals are gradually turned out of directions determined by the crystalline forces, and into the direction of the field. The components of magnetization normal to the field direction cancel each other for the specimen as a whole, so that only the component in the field direction contributes to the observed magnetization.

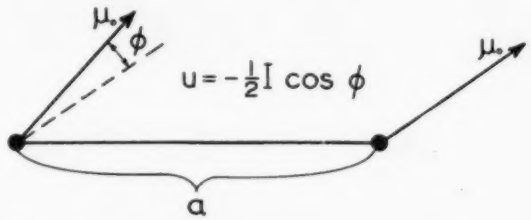

FIG. 2. Energy u of the alining forces between the magnetic moments μ_0 of atoms that are nearest neighbors.

In single crystal specimens, the normal component should be observable; moreover, if the field is along a direction in which the magnetization tends to point because of crystalline forces, Part II of the magnetization curve should be absent, and saturation should be attained in much smaller fields. Both of these conclusions are verified experimentally: the normal component of magnetization is observed, and certain directions in the crystal are found to be "directions of easy magnetization."

The theory that has been successful here is a formal one that says nothing about the nature of these atomic forces, but deduces formulas for their macroscopic effects from the requirements of thermodynamics and of crystalline symmetry. Such a theory involves a number of constants which cannot be determined from the theory but which can be evaluated from the experimental data. It is then the problem of atomic theory to explain the values of these constants. This portion of the atomic theory is still incomplete, although the general nature of the atomic forces involved is understood. The formal theory is sufficient for our purposes, and we need consider only two very simple cases.

The first is crystalline cobalt. At room temperature the direction of easy magnetization is the hexagonal axis, and the crystal is magnetically isotropic about this axis. The magnetization vector therefore lies in the plane determined

by the direction of easy magnetization and the field direction, as is shown in Fig. 3(a). It may be regarded as subject to a torque L_K, due to "anisotropy" forces, tending to pull it into the direction of easy magnetization, and to a torque $L_H = HJ_s \sin(\phi - \theta)$, due to the field, tending to pull it into the field direction. It is simpler, however, to consider not torques, but an energy function $W(\theta)$, the thermodynamic "free energy" per unit volume, from which the torque L acting

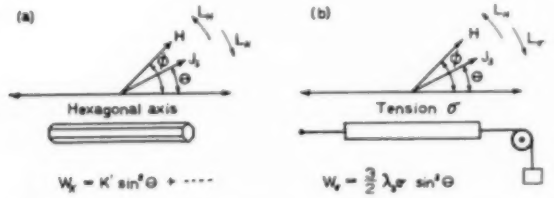

FIG. 3. Two simple cases of magnetic anisotropy: (a) cobalt crystal; (b) isotropic material under tension (magnetostriction positive). The spontaneous magnetization (J_s) is pulled toward the direction of the field (H) by a torque L_H, and toward the direction of easy magnetization by a torque L_K or L_σ. The torque L_K or L_σ may be derived from an energy function W_K or W_σ.

on the magnetic moment of unit volume can be derived by means of the relation $L = -\partial W/\partial\theta$. The condition for stable equilibrium at a given H is that θ shall have such a value as to make W a minimum. The part of W due to the external field is the potential energy of a magnet of moment J_s oriented at an angle $(\phi - \theta)$ to the field H, namely $W_H = -HJ_s \cos(\phi - \theta)$. The part of W due to the crystalline forces must by symmetry be of the form

$$W_K = K' \sin^2\theta + K'' \sin^4\theta + \cdots. \qquad (5)$$

Good agreement with experimental magnetization curves is obtained by setting $K' = 5.1 \times 10^6$, $K'' = 2.2 \times 10^6$ (both ergs/cm³), and neglecting higher powers of $\sin\theta$.

The second case, illustrated in Fig. 3(b), is that of an isotropic material subjected to uniform and constant tension σ dynes/cm² by the action of forces of external origin. In this case W_K is replaced by W_σ, the potential energy of the weight producing the tension. The saturation magnetostriction λ_s (fractional elongation in the direction of the spontaneous magnetization) will be assumed to be positive; in this case the length of the specimen in the direction of the tension is greatest when $\theta = 0$ or π. Thus the weight is lowest, and in the absence of a field the minimum of W is attained, for $\theta = 0$ or π—that is, the direction of the tension is a direction of easy magnetization. It can be shown that for any θ, the potential energy per unit volume due to the tension is

$$W_\sigma = \tfrac{3}{2}\lambda_s\sigma \sin^2\theta. \qquad (6)$$

Thus W_σ is of the same form as the first term in W_K.

The Demagnetized State (O)

Since the atomic theory requires the existence of spontaneous magnetization even in zero applied field, it might be supposed that in the demagnetized state the microcrystals are magnetized to saturation, and that the zero large-scale magnetization observed in ordinary measurements results from the random orientation of the different crystals in the polycrystalline specimen. But the experiments on single crystals show that they, too, can be demagnetized, and in fact Part I of the magnetization curve is about the same for them as for ordinary specimens. The conclusion is that even within a crystal, the uniform magnetization required by the atomic theory extends only over limited regions or "domains," and changes its direction from one direction of easy magnetization to another at boundaries between such domains. This involves less offense to the quantum and anisotropy forces than would a complete lack of alinement of the atomic magnets; for only the comparatively few atoms at the boundaries between domains will feel the difference between this and a completely uniform magnetization.

According to this picture, Part I of the magnetization curve begins (O, Fig. 1) with equal volumes magnetized along each of the directions of easy magnetization, and ends (X) with the entire crystal or microcrystal magnetized along the one of these directions that is nearest to the field direction. A further increase of field rotates the magnetization vector closer to the field direction, giving Part II of the curve, unless the angle between the field and the nearest direction of easy magnetization happens to be zero, in which case the crystal is already saturated at the end of Part I.

We shall consider later the process by which the crystal passes from an initial state of demagnetization to a final state in which only favored directions of easy magnetization are occupied. First, we shall consider the following questions: (1) What direct experimental evidence is there that such domains exist, and what information do the experiments give us about their nature? (2) What theoretical reason is there why the spontaneous magnetization should extend only over such limited regions, rather than over the entire specimen? (3) Can theory explain the observed size and shape of the domains?

(1) Experimental Evidence for Domains

The domains are not merely abstractions required by theory: they can be both heard and seen.

They can be heard by surrounding the specimen with a test coil connected to an amplifier and phones, and gradually applying a magnetic field. Loud cracks are heard, indicating sudden, discontinuous changes of the magnetic flux through the test coil—as might be expected if small chunks of the specimen change their directions of magnetization one by one as the field is increased. This is the well-known Barkhausen effect.

They can be seen by a refinement of the familiar "iron filings" experiment. A properly prepared magnetic powder or colloid, placed on a polished surface of a ferromagnetic specimen, forms patterns (visible in a microscope) that not only reveal the presence of magnetized domains in the macroscopically demagnetized material, but give considerable information about their size, shape, and arrangement.

The original crude method of observing the Barkhausen effect, by listening to noises made by the domains, can be replaced by a more sophisticated procedure in which the phones are replaced by a photographic record and quantitative information is obtained. The information relates to the regions that change their directions of magnetization discontinuously; these are not necessarily identical with the spontaneously magnetized domains, since it may occur that only part of a domain is involved in such a discontinuous change. The conclusions reached by Bozorth and Dillinger from experiments of this sort are: (1) The effect occurs in single crystals as well as in polycrystalline material. (2) The size of the Barkhausen regions does not vary much with the material or with its mechanical or thermal history; they may be larger or smaller than the crystal grains. (3) In wires 60 cm long and 1 mm in diameter, the average volume of a Barkhausen region varies from 1.2×10^{-9} cm^3 for iron to 45×10^{-9} cm^3 for a 50 percent iron-nickel alloy. These experiments leave open the question, which had not been raised at the time they were performed, of a possible dependence of the domain size on the dimensions of the specimen.

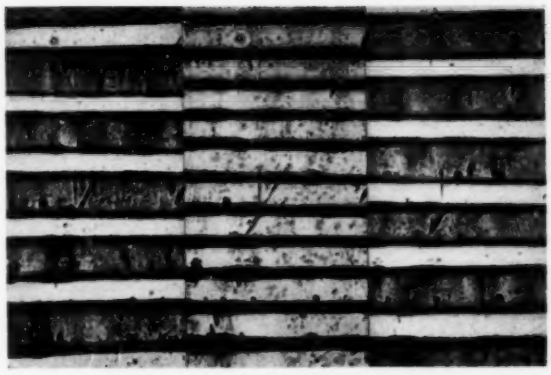

(a) (b) (c)

Fig. 4. Magnetic colloid patterns obtained by Elmore on a cobalt surface approximately perpendicular to the basal plane with applied normal field (a) outward; (b) zero; (c) inward. The lines run parallel to the hexagonal axis. Magnification approximately 65×.

The surface patterns, discovered by Bitter, have been studied in great detail by Elmore. One of his photographs is shown in Fig. 4. This is a photograph of patterns obtained on a cobalt surface; the direction of easy magnetization is approximately in the plane of the figure, and the lines of the pattern run parallel to that direction. In the middle pattern, the average spacing of the lines is about 6×10^{-3} cm. The spacing varies somewhat from one crystal grain to another; the lines are closer together in the smaller grains.

(2) Origin of the Domain Structure

The quantum forces described by Eq. (1) tend to produce a spontaneous magnetization extending throughout the whole specimen. The anisotropy forces of Eq. (5) or (6) can orient this

magnetization in certain preferred directions, but have no tendency to orient different regions in different ones of these directions.

With magnetic forces the situation is different. Magnetic atoms, regarded as small current circuits, tend to line up so as to link as much magnetic flux as possible. Fig. 5(a) shows the effect of this tendency in the case of two atoms.

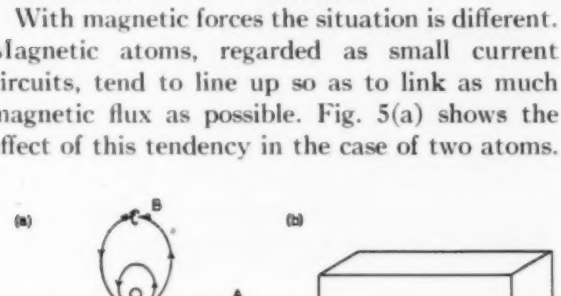

FIG. 5. Influence of magnetic forces. (a) Field lines of an atomic magnet of moment μ located at O. The arrow with head and tail points in the direction of the magnetic moment; the circular arrow shows the direction of the atomic currents producing it. A second atomic magnet at A or at B tends to set itself as shown. (b) Arrangement favored by quantum forces: a uniform magnetization of the specimen. (c) Arrangement favored by magnetic forces: long, narrow domains. (d) Arrangement opposed by magnetic forces: short, wide domains.

One is located at O; its field lines are shown. The second atom, if placed at A, alines itself in the same direction; but if placed at B, it alines itself in the opposite direction. In the case of a specimen containing many atoms, the uniform magnetization shown in (b) is less acceptable magnetically than the arrangement shown in (c), in which the flux is kept in closed paths inside the material rather than being allowed to escape to the outside.

This rough argument may be made more rigorous by considering the field $\mathbf{h}$, at a lattice point, produced by all the atoms at other lattice points. Stability requires that this be in the direction of the magnetic moment $\boldsymbol{\mu}$ of the atom at the lattice point in question, and as large as possible, in order that the mutual magnetic energy of all the pairs of atoms, $-\frac{1}{2}\Sigma\mathbf{h}\cdot\boldsymbol{\mu}$, may be a minimum. The overwhelming majority of the atoms are far enough from any surface of discontinuity so that this field is given by the Lorentz formula

$$\mathbf{h}=\mathbf{H}+\tfrac{4}{3}\pi\mathbf{J}, \qquad (7)$$

where $\mathbf{H}$ is the macroscopic field and $\mathbf{J}$ is the vector magnetization in that vicinity. $\mathbf{J}$ has the same direction as $\boldsymbol{\mu}$ and a fixed magnitude J_s, in (c) as well as in (b); the energy per unit volume contributed by this part of $\mathbf{h}$ is $-\frac{2}{3}\pi J_s^2$, a quantity already mentioned in the discussion of saturation. But $\mathbf{H}$ is oppositely directed in (b), being the demagnetizing field due to the poles at the ends of the specimen; while in (c), $\mathbf{H}$ is zero, since there are no poles. Thus (c), though not necessarily the best arrangement, is at least better than (b) as far as magnetic forces are concerned. On the other hand (d) would be worse than (b).

The requirements of the quantum forces are not satisfied by arrangement (c) at the boundaries between domains. Consider for simplicity a simple cubic lattice with lattice constant a, and suppose first that the boundary between oppositely magnetized domains is sharp, as indicated in Fig. 6(a), where each arrow represents an atomic magnet. The mutual energy of neighboring atoms on opposite sides of the boundary is increased, according to Eq. (1), from $-I/2$ to $+I/2$ by having the magnetic moments antiparallel instead of parallel; there are $1/a^2$ such pairs of atoms per unit area of the boundary, and therefore a sharp boundary involves additional energy of amount I/a^2 per unit area. A gradual transition (Fig. 6(b) and (c)) requires less energy. Here the angle θ between the magnetic moments of the atoms and the direction of easy magnetization is a slowly varying function of x, and the angle ϕ between the magnetic moments of successive atoms is the small quantity $ad\theta/dx$. Thus their energy exceeds the value for parallel alinement by $\frac{1}{2}I(1-\cos\phi)$ $=\frac{1}{4}I\phi^2=\frac{1}{4}Ia^2(d\theta/dx)^2$. If we now imagine the transition made more gradual by stretching out the curve in (c) over a greater thickness d, the number of pairs of atoms affected increases as d, but the excess energy of each pair decreases as $1/d^2$, so that the net effect is a decrease as $1/d$. Thus the quantum forces tend to make the transition as gradual as possible. In order of magnitude $d\theta/dx=\pi/d$, the number of pairs of

atoms per cm² of boundary $=\frac{1}{2}(1/a^3)d$, and hence the energy per unit area $=\frac{1}{4}Ia^2 \times(\pi^2/d^2)\cdot\frac{1}{2}(d/a^3)\leqq I/ad$, a decrease by a factor of about a/d as compared with the value for an abrupt transition.

But now the anisotropy forces come into play. We suppose that the anisotropy energy per atom is of the form $A\sin^2\theta$; this corresponds to the first term in Eq. (5) or to Eq. (6), with A equal to $K'a^3$ in the one case and to $\frac{3}{2}\lambda_s\sigma a^3$ in the other. Then the atoms in the transition layer have excess energy because their moments are turned out of the direction of easy magnetization. If the transition is made more gradual, the number of atoms affected increases as d, and since in this case there is no compensating decrease in the energy per atom, the total anisotropy energy per cm² of boundary increases as the boundary thickness d. In order of magnitude this energy is $A(\sin^2\theta)_{\text{Av}}\cdot(1/a^3)d\leqq A(d/a^3)$.

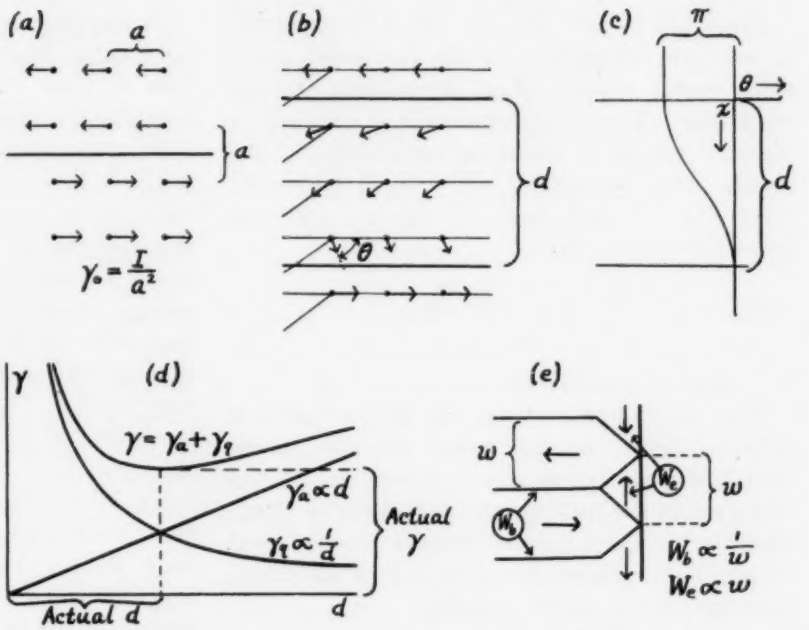

FIG. 6. Factors determining thickness of interdomain boundaries (a–d) and of domains (e). (a) A sharp boundary: too large quantum energy. (b) A gradual transition. (c) Graphical representation of (b). (d) Dependence of boundary energy per unit area, γ, on thickness of the boundary, d. γ_q, quantum energy; γ_a, anisotropy energy; γ, total energy, a minimum when $\gamma_a=\gamma_q$. (e) Dependence of total boundary energy, W_b, and end energy, W_e, on thickness of the domains, w.

Thus the total energy associated with unit area of the interdomain boundary consists of a term γ_q proportional to $1/d$, due to the quantum forces, and a term γ_a proportional to d, due to the anisotropy forces. The former tend to thicken the boundary layer and the latter to thin it. The actual thickness d will be that for which the sum of these terms is a minimum (see Fig. 6(d)).

It is easily shown that the function

$$\gamma(d)=\alpha d+\beta/d$$

is a minimum when the two terms are equal; then $d=(\beta/\alpha)^{\frac{1}{2}}$ and $\gamma=2(\alpha\beta)^{\frac{1}{2}}$. Here $\alpha\leqq A/a^3$ and $\beta\leqq I/a$. Thus, except for numerical factors of order of magnitude unity, we have

$$d=a(I/A)^{\frac{1}{2}},\quad \gamma=2(IA)^{\frac{1}{2}}/a^2=\frac{I}{a^2}\cdot\frac{2a}{d}. \qquad (8)$$

If $I\leqq10^{-13}$ and $A=K'a^3\leqq10^{-17}$, we get $d\leqq100a$, that is, a transition layer about 100 atoms thick between domains. The total energy per cm² of boundary is less than the value for a sharp boundary in the ratio $2a/d$, or $1/50$.

A more rigorous analysis verifies the results just obtained, and gives also the form of the function $\theta(x)$.

(3) Size and Shape of the Domains

Returning to Fig. 5(c), we may now endeavor to determine the thickness w of the domains themselves. In the expectation that this is much greater than the thickness d of the boundaries between them, we may take the boundaries into account sufficiently well by treating them as surfaces of discontinuity with a surface energy density γ given by (8). This energy by itself would tend to make the boundary area as small as possible, and thus to decrease the number of domains and increase their thickness. In fact there are c/w boundaries each of area bl, and the total boundary energy of the specimen is $\gamma bcl/w$, decreasing as w increases.

Thick domains, however, involve large regions at the ends (see Fig. 6(e)), in which the mag-

netization is turned squarely out of the direction of easy magnetization and the maximum anisotropy energy density, A/a^3, is realized. The two triangular prisms at opposite ends of a boundary together form a rectangular prism of length b and square cross section $(w/\sqrt{2})^2=w^2/2$; and since there are c/w such pairs of prisms, the total anisotropy energy is

$$\frac{A}{a^3}\cdot\frac{bw^2}{2}\cdot\frac{c}{w}=\frac{1}{2}\frac{A}{a^3}bcw,$$

increasing as w increases.

Thus the boundary energy tends to make the domains thick, the end energy to make them thin. The actual thickness is determined by the minimum of the total energy, $bc(\frac{1}{2}Aw/a^3+\gamma l/w)$, which is the same type of function encountered before. The equilibrium value of w is found by equating the two terms, whence

$$w=\left(\frac{2a^3\gamma l}{A}\right)^{\frac{1}{2}}=\left[\frac{2a^3l}{A}\cdot\frac{2(IA)^{\frac{1}{2}}}{a^2}\right]^{\frac{1}{2}}=2(ld)^{\frac{1}{2}}. \quad (9)$$

According to this the size of the domains depends on the size of the specimen, a result that is to be expected if surface as well as volume energies are present. For specimens of linear dimensions $\geqq 1$ cm, with $d\geqq 100a\geqq 10^{-6}$ cm, we get $w\leqq 10^{-3}$ cm, the order of magnitude observed in surface patterns. The volumes observed in the Barkhausen effect, 10^{-9} cm^3, are consistent with this, if they are interpreted as chunks of domains whose linear dimensions are of the same order of magnitude as the thickness of the domains.

We began by objecting to the large magnetic energy accompanying a uniform magnetization; have we ended up with an energy enough smaller to justify our more complicated arrangement? Insertion of (9) in the formula for the total energy, and division by the volume bcl, gives for the mean energy per unit volume

$$W=\frac{2A}{a^3}\left(\frac{d}{l}\right)^{\frac{1}{2}}\leqq\frac{10^4}{\sqrt{l}}\ \text{ergs/cm}^3. \quad (10)$$

The magnetic energy of a uniformly magnetized specimen is given approximately in terms of a demagnetization factor D by the formula

$$W_{\text{mag}}=\tfrac{1}{2}DJ_s^2\leqq 10^6D\ \text{ergs/cm}^3. \quad (11)$$

For $l=100$ cm, $W<W_{\text{mag}}$ provided $D>0.001$. This requires that the diameter of the specimen be greater than 0.4 cm. The theory therefore fails to give a satisfactory description of the domain structure of long thin specimens.

In other respects, too, the analysis is incomplete. It has been shown that a certain arrangement of the magnetic moments in domains leads to a lower energy than some other arrangements; but it has not been shown that this is the lowest energy attainable. A complete analysis would determine the magnetization direction as a function of position in such a way as to minimize the total energy. The problem can be stated mathematically in this form, but the differential equations that result are too complicated to give much information. Moreover the details of the domain arrangement are probably determined very largely by accidental factors, such as irregular strains and impurities, which have not been included in the simplified theory.

Low Fields (I)

We now understand how a specimen can be demagnetized and yet possess spontaneous magnetization throughout domains. By what process does the specimen pass from this state to one of uniform magnetization throughout each of its constituent crystals? And how does the magnetization become reversed when the field is decreased from a high value to zero and then to a high negative value? A detailed theory has been worked out only for specimens in which the conditions are particularly simple. We shall consider these cases first, and then discuss their bearing on the properties of ordinary materials.

(1) Materials With Positive Magnetostriction Under High Tension

Iron-nickel alloys of a certain range of composition have positive magnetostriction. If a specimen of such a material is subjected to a high longitudinal tension, its hysteresis curve assumes the rectangular shape shown in Fig. 7(a). There is 100 percent remanence, which persists until an opposing field H_s is reached; then the magnetization reverses in a single Barkhausen jump, AB or $A'B'$. If, on the other hand, the specimen is demagnetized by heating and a field is then applied, the magnetization increases or decreases reversibly with the field along the curve OP, as

long as the field remains less than a critical value H_c which is considerably smaller than H_s. As soon as H becomes equal to H_c, the irreversible jump PQ occurs.

The discontinuous processes AB, $A'B'$ have been investigated in great detail, especially by Sixtus and Tonks. In order to produce the jump $A'B'$ it is not necessary to apply a field H_s throughout the whole specimen: it is sufficient to have a field this great in a small part of the specimen, provided the field in the remainder of the specimen exceeds the critical value H_c. With this arrangement, shown in Fig. 7(b), a nucleus of reversed magnetization first forms at a point where the field is H_s, and then grows until it swallows up the whole specimen. The boundary of the nucleus of reversed magnetization moves forward with a finite speed v of order of magnitude 10^4 cm/sec.

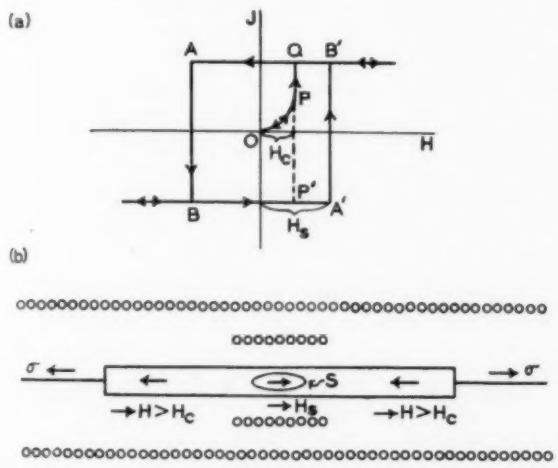

FIG. 7. Magnetic behavior of alloys with positiye magnetostriction under strong longitudinal tension σ. (a) Hysteresis loop ($B'ABA'B'$) and virgin curve ($OPQB'$). H_s="starting field," H_c="critical field." (b) Formation and propagation of a nucleus of reversed magnetization. The main field H exceeds H_c but is less than H_s; an auxiliary coil increases the field to H_s over a short part of the specimen.

We may therefore interpret the "starting field" H_s as the field necessary to produce a nucleus of reversed magnetization, and the "critical field" H_c as the field at which the reversal, once started, will be propagated through the remainder of the specimen. When the specimen has been demagnetized by heating, it contains many domains magnetized in each direction, instead of a single one magnetized in the wrong direction as is the case on BA'. The nuclei are therefore already present, and the field need only reach the value H_c in order that the rightly magnetized domains may swallow up the wrong ones (PQ).

The speed of propagation v is found, in the experiment of Fig. 7(b), to be a linear function of the excess of H over the critical value H_c:

$$v = B(H - H_c). \tag{12}$$

This is easily explained, if we assume merely the possibility of a displacement of the boundary S (Fig. 7(b)) and the presence of internal forces that interfere with this displacement when the field is less than H_c. If the boundary moves forward, the magnetic induction changes, e.m.f.'s are induced, and eddy currents flow. The magnetic field of these eddy currents is in such a direction as to oppose the motion that produced it, and its magnitude is proportional to the speed v with which the boundary moves. The effective field acting at the boundary is the resultant of the applied field H and this eddy-current field, and may thus be written $H - Cv$, where C is a constant. If the eddy currents were not present the boundary would move forward almost instantly, but because of them it cannot exceed the speed at which the effective field is reduced to H_c; thus the actual speed is determined by

$$H - Cv = H_c, \tag{13}$$

which is (12) in another form.

The constant B or C can be computed theoretically, in approximate agreement with experiment. It does not depend on the tension σ, but the critical field H_c does. The significance of this critical field may be understood better by considering the nature of the *reversible* change OP.

At O the specimen consists of domains, presumably of the approximate size and shape described before; but the exact position and shape of any boundary will be determined by the irregular internal stresses that were neglected before. Following Kersten, let us idealize this internal stress system to a succession of alternate regions of longitudinal tension and pressure, the variation being along a direction x perpendicular to the axis of the specimen and to

the domain boundaries. When this is superposed on a large externally applied tension σ_0, the result is a tension σ fluctuating with x as shown in the σ *vs.* x graph in Fig. 8(a). The energy γ per cm^2 of an interdomain boundary is given by Eq. (8) with $A=\frac{3}{2}\lambda_s\sigma a^3$. γ therefore varies with position of the boundary because of the variation of σ with x. γ is a minimum when the boundary is located at a minimum ($x=0$) of σ, as shown in (b), and increases if the boundary is displaced from this position a distance x as shown in (c). The forces acting in the boundary layer are equivalent in their effect to a hydrostatic pressure p_γ tending to push the boundary toward the position of minimum energy, $x=0$. In fact, if $\gamma(x)$ represents the potential energy per cm^2 of boundary expressed as a function of boundary displacement x, then $p_\gamma=d\gamma(x)/dx$; p_γ is zero at the minimum point $x=0$, and reaches its maximum value at the point x_c where the slope of the σ *vs.* x curve is greatest.

In zero field, the boundary will be at $x=0$. If a small field H is applied in the direction indicated in (c), the favorably oriented domain A tends to grow at the expense of its neighbor B. The potential energy in a given field H is decreased by $2J_sHdx$ per cm^2 of the boundary if the boundary is displaced dx; the field is therefore equivalent to a hydrostatic pressure $p_H=2J_sH$ pushing the boundary downward in the diagram. The equilibrium position of the boundary under a given field is that at which the two pressures p_γ and p_H just balance each other, as shown in (c); this requires

$$d\gamma(x)/dx=2J_sH. \qquad (14)$$

If the field is slowly increased, the boundary is gradually displaced, adjusting itself to the equilibrium position at each value of H, and returning through its previous positions if H is again decreased, as long as it does not reach the position x_c. This gives us the reversible magnetization curve OP of Fig. 7. But when H reaches a field H_c corresponding to displacement x_c, the equilibrium becomes unstable: for a very slight further displacement *decreases* instead of increasing the opposing pressure p_γ, and the boundary moves on without opposition, at a speed limited only by the eddy currents, until B is completely absorbed. This gives us the irreversible jump PQ.

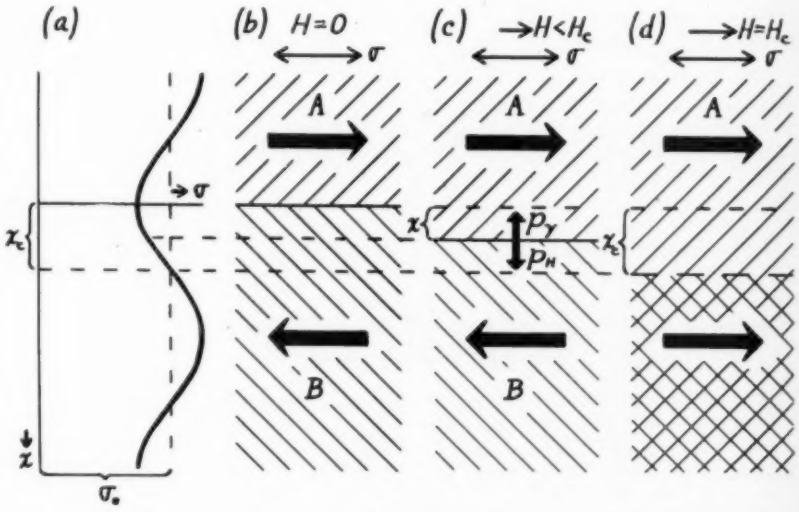

FIG. 8. Reversible and irreversible boundary displacement. (a) Stress distribution resulting from superposition of constant applied stress σ_0 on irregular internal stresses. (b) Position of the boundary with no field. (c) Reversible displacement of the boundary for $H<H_c$. (d) Barkhausen jump for $H=H_c$: the boundary, upon reaching x_c, is propagated irreversibly through the remainder of region B.

(2) Materials With Negative Magnetostriction, Under High Tension

An entirely different magnetization process occurs if longitudinal tension is applied to a wire whose saturation magnetostriction λ_s is negative, for instance nickel. In this case the tension causes all the domains to be magnetized in a plane *perpendicular* to the axis of the specimen, though at random orientations in this plane. With relation to a longitudinal field the domains are all equivalent, and there is therefore no tendency for one to absorb another; the only effect of the field in this case is to rotate the magnetic moments of all the domains simultaneously so that they are at an angle $\theta<\pi/2$ to the field direction; the resulting magnetization, $J=J_s\cos\theta$, can be found as for crystals by

minimizing the total energy. The conclusions of the theory have been verified experimentally by Becker and Kersten, who also extended the rotation theory to the case of domains in which the stresses are of internal origin and vary from one domain to another. Although this rotation theory leads to correct orders of magnitude for many quantities, it now seems unlikely that the rotation process plays more than a minor role in ordinary ferromagnetic materials.

(3) Ordinary Materials

There seems little doubt that the two processes described in (1)—reversible and irreversible displacements of the boundaries between domains—are the ones by which magnetization proceeds in the steep part (I) of the magnetization curve of ordinary ferromagnetic materials. Boundaries are displaced reversibly in regions where a stable equilibrium is possible under the joint action of external and internal forces. They move irreversibly, with a speed limited by the eddy currents, when a point of instability is reached. Both these processes may be observed in the surface patterns of Fig. 4 when a field is applied with a component in the direction of the strips. As the field is increased, alternate strips widen and the ones between them narrow. The process consists partly of a slow displacement that can be made to run backward by decreasing the field again, and partly of sudden jumps after which the boundary does not return to its previous position if the field is decreased.

Remanence and coercive force depend on the irreversible jumps. The problem is much more complicated than the simple case considered in (1), and the quantitative theory is still in its infancy.

Reversible processes are easier to handle theoretically, and here more quantitative results have been obtained. There are some properties of ferromagnetic materials that are, to a first approximation, dependent only on the magnetization J and not on the procedure by which this value of J was reached, so that they are the same for instance at points P and Q, Fig. 1. This is true of the "reversible susceptibility," which is the ratio $\Delta J/\Delta H$ measured in a small change ΔH carried out in the opposite direction to that by which the original state was approached—as indicated by the small arrows PP' and QQ', Fig. 1. This susceptibility is called "reversible" because such a change is comparatively free from discontinuous Barkhausen jumps. In dealing with properties of this sort, one can obtain fairly satisfactory theoretical results by ignoring the irreversible properties and considering a hypothetical reversible specimen to which the actual specimen is, as far as these properties are concerned, equivalent.

In the idealized specimen of Fig. 8 we may expand the function $\gamma(x)$ in a Taylor's series,

$$\gamma(x)=\gamma_0+\tfrac{1}{2}\gamma_2 x^2+\cdots, \tag{15}$$

with the first-order term absent and with the coefficient of x^2 positive because γ is a minimum at $x=0$. Then (14) gives

$$\gamma_2 x+\cdots=2J_s H, \tag{16}$$

and in a small reversible displacement δx produced by a change of field δH,

$$(\gamma_2+\cdots)\delta x=2J_s\delta H, \tag{17}$$

where the omitted terms are small if x is small. Hence for x not too large,

$$\delta x=k\cdot 2J_s\delta H, \tag{18}$$

where k is approximately constant. If the total boundary area in unit volume is S, the change in magnetization is

$$\delta J=2J_s\cdot S\delta x=4kSJ_s^2\delta H. \tag{19}$$

We shall now follow Kondorsky in assuming that, because of the irregularity of the internal stresses, the shapes of the domains are irregular, and Eq. (19) holds with a constant average value of k throughout the whole magnetization process.

The area S will now depend on the relative volumes v_A and v_B occupied by domains of the two types A and B, Fig. 8(c). It vanishes when either of these vanishes (saturation in either direction), and may be expected to be a maximum when they are equal (demagnetization). Kondorsky assumes the relation

$$S=sv_Av_B, \quad s=\text{constant}, \tag{20}$$

which, though impossible to justify rigorously, is simple and satisfies the conditions just stated.

Since the magnetization is given by $J=J_s(v_A-v_B)$, and since $v_A+v_B=1$, we have $v_A=(1+J/J_s)/2$, $v_B=(1-J/J_s)/2$, and Eqs. (19) and (20) lead to the following relation between the reversible susceptibility $\delta J/\delta H$ and the magnetization J:

$$\delta J/\delta H = ksJ_s^2(1-J^2/J_s^2). \qquad (21)$$

By a similar procedure in the more general case, Kondorsky is able to obtain formulas for the reversible susceptibility of various types of crystal. No experimental data are available with which to test the legitimacy of Kondorsky's assumptions. It is possible, however, to extend the analysis to polycrystalline material by making use of the concept of the "equivalent reversible specimen."

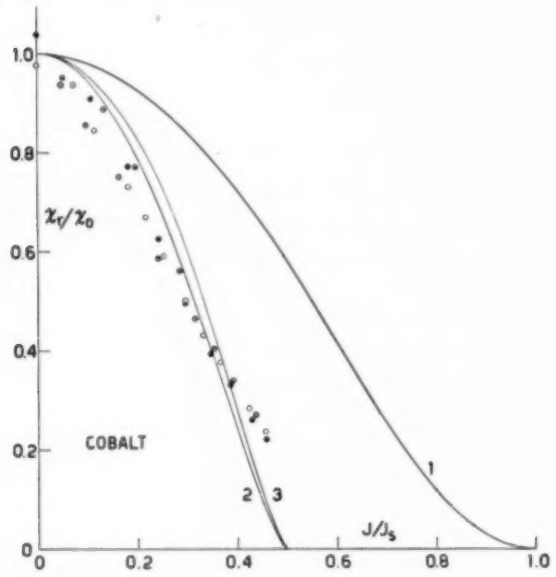

FIG. 9. Reversible susceptibility χ_r of polycrystalline cobalt. Experimental points (M. Samuel): open circles, virgin curve; solid circles, "ideal" or "anhysteretic" curve; circles black at bottom, descending branch of hysteresis curve; black at top, ascending branch. Theoretical curves: 1, boundary displacement, directions of easy magnetization isotropically distributed; 2, boundary displacement, correct crystalline symmetry; 3, artificial model with permanent internal fields, but with correct crystalline symmetry. χ_0 is the initial susceptibility.

For a reversible specimen, J is a single-valued function of H which can be found by integrating (21); this gives for the specimen of Fig. 8 or for a cobalt crystal

$$J=J_s \tanh ksJ_sH. \qquad (22)$$

If H is inclined at an angle θ to the direction of easy magnetization, H must be replaced by its component $H\cos\theta$ along this direction, and the whole expression must be multiplied by $\cos\theta$ to get the component of magnetization in the field direction; then for a polycrystalline specimen, the result must be averaged over all orientations of the crystals. This leads to an expression $J=f(H)$ for the magnetization curve of a fictitious reversible polycrystalline specimen of cobalt. Its derivative $\chi=f'(H)$ is the susceptibility. These may be regarded as parametric equations determining χ as a function of J. According to the hypothesis of the equivalent reversible specimen, the reversible susceptibility χ_r of an actual specimen is this same function of J, although the parameter H no longer has any simple physical meaning.

In Fig. 9 the predictions of this theory (curve 2) are compared with experimental data for polycrystalline cobalt. Although the agreement is far from perfect, the curve fits the data distinctly better than does curve 1, which is calculated from a formula proposed long ago by Gans. Gans' formula represents a limiting case, a crystal with many directions of easy magnetization distributed uniformly over the unit sphere; it holds fairly well for polycrystalline iron and nickel.

Curve 3 is calculated by a different theory, in which the symmetry of the crystals is taken into account but a different mechanism of magnetization is assumed. The close agreement between curves 2 and 3 and the wide deviation between them and curve 1 show that the crystalline nature of the material has a more decisive influence on the magnetic properties than does the specific mechanism of magnetization. Two conclusions follow from this. The first is the rather discouraging one that an agreement between theory and experiment does not necessarily prove the correctness of the mechanism assumed in the theory. The second is the more cheering one that a knowledge of the exact mechanism of magnetization is not necessary in order to carry out an approximate calculation of magnetic properties.

A number of properties have been calculated fairly successfully by a theory in which no mechanism is assumed, but the domain structure is taken into account in a very general way. Let

us suppose that we observe a ferromagnetic specimen through a large number of peep-holes, each small compared with the domains, and far enough apart so that what we see through one does not help us much in guessing what we shall see through another. By averaging over the peep-holes we shall get a good representation of the average magnetization, magnetostriction, and so on of the specimen as a whole. If the domain arrangement is governed largely by irregular internal forces, statistical methods may be used to determine the relative popularity of the various directions of easy magnetization as sampled through the peep-holes, and thus to calculate some of the magnetic properties. Historically this method is older than Kondorsky's, but all the results obtained by it may also be obtained by combining his assumptions with the hypothesis of the equivalent reversible specimen. Fig. 10 shows how well this theory predicts the dependence of magnetostriction on magnetization in polycrystalline nickel. Agreement as good as this is exceptional; in most cases small systematic deviations indicate that there are agencies at work that have not been taken into account in the theory.

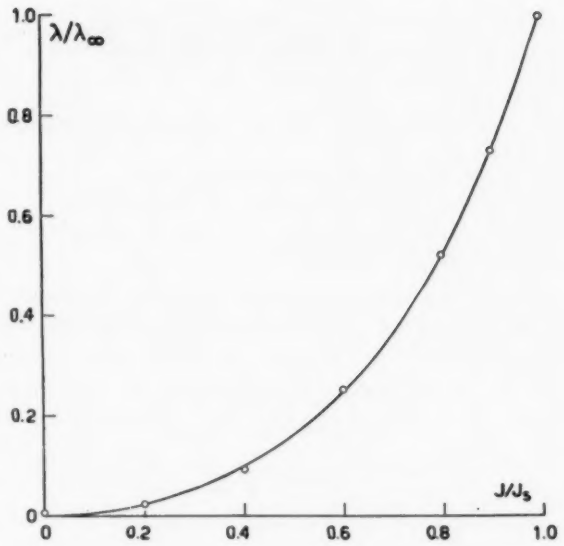

FIG. 10. Variation of magnetostriction λ with magnetization, for polycrystalline nickel at 6°C. The circles are experimental values (D. Kirkham). The curve is calculated from a formula that can be derived either by the boundary displacement theory or by a statistical method. λ_∞ is the saturation magnetostriction.

Conclusion

An attempt has been made here to outline the methods of attack that have proved useful in dealing with a very complex phenomenon. To that end, the essential ideas have been presented and some of the simpler relations derived without pretense of completeness or rigor. Unfortunately a comprehensive presentation of everything that has been done would still be sadly lacking, at certain points, in both those qualities. It seems quite certain, however, that the basic concepts are correct: though a mathematical theory of the hysteresis curve has not yet arrived, domains are here to stay.

Bibliography

I. Books that will prove generally useful.

1. E. C. Stoner, *Magnetism and Matter* (Methuen & Co., Ltd., London, Dutton, New York, 1934).
2. F. Bitter, *Introduction to Ferromagnetism* (McGraw-Hill, New York, 1937).
3. R. Becker (editor), *Probleme der technischen Magnetisierungskurve* (Springer, Berlin, 1938).
4. L. F. Bates, *Modern Magnetism* (Cambridge, and Macmillan, New York, 1939).
5. R. H. Fowler, *Statistical Mechanics*, second edition (Macmillan, New York, 1936).

II. References on specific topics.

The first few references under each heading are to specific pages (given in parentheses) of the books listed in I. The remaining references are to periodical articles. These have been selected either because they are of a general and introductory nature, or because they report results not yet to be found in the books. In the latter case, the article cited should be consulted for references to earlier articles by the same or other authors.

A. Spontaneous magnetization: 1. (114–129, 350–367, 434–435, 437); 2. (29–40, 126–143); 4. (233–241); 5. (477–501).

6. L. Pauling, Phys. Rev. **54**, 899 (1938).

B. Saturation magnetostriction and magnetic anisotropy:

(1) Crystals: 1. (385–401), 2. (176–178, 194–213, 246–255); 3. (150–163, 298–303); 4. (150–163, 298–303); 5. (503–517).

7. R. M. Bozorth, J. App. Phys. **8**, 575 (1937).
8. H. J. Williams, Phys. Rev. **52**, 1004 (1937).
9. J. H. Van Vleck, Phys. Rev. **52**, 1178 (1937).

(2) Anisotropy due to stress: 2. (243–246); 4. (305–307).

10. R. Becker, Physik. Zeits. **33**, 905 (1932).
11. L. W. McKeehan, Phys. Rev. **53**, 301 (1938).

C. Domains—experimental:

(1) Surface patterns: 2. (55–66); 4. (320–321).

12. W. C. Elmore, Phys. Rev. **53**, 757 (1938); **56**, 210 (1939).

(2) Ordinary Barkhausen effect: 1. (404, 411–413); 2. (21, 290–291); 4. (321–326).

(3) Large Barkhausen discontinuities: 1. (413–415); 3. (9–25); 4. (326–329).

13. C. W. Heaps, Phys. Rev. **50**, 176 (1936).

(4) Magnetization curves of alloys under tension: 3. (3–4); 4. (324).

14. M. Kersten, Zeits. f. tech. Physik **19**, 546 (1938) or Physik. Zeits. **39**, 860 (1938).

(5) Magnetization curves of nickel under tension: 2. (245–246); 3. (2–3); 4. (306–307); reference 10.

D. Domains—theoretical:

(1) Origin, shape, and size of domains: 2. (185–192, 293–299); first reference 12.

15. E. H. Kennard, Phys. Rev. **55**, 312 (1938).

(2) Propagation of Barkhausen discontinuities: 3. (30–41); 4. (329).

16. W. Döring and H. Haake, Zeits. f. tech. Physik **19**, 551 (1938) or Physik. Zeits. **39**, 865 (1938).
17. R. Becker, Zeits. f. tech. Physik **19**, 542 (1938) or Physik. Zeits. **39**, 856 (1938).
18. H. Schlechtweg, Ann. d. Physik **5**, 657 (1939).

(3) Reversible and irreversible boundary displacement: 1. (409–411); 3. (42–72); references 10, 14.

19. W. F. Brown, Phys. Rev. **55**, 568 (1939).

(4) Rotation theory: reference 10.

(5) Statistical theory: 1. (390–392); 2. (255–260); 5. (506–507, 517–521); reference 19.

Glass as an Electrical Insulator*

BY C. J. PHILLIPS

Corning Glass Works, Corning, New York

Introduction

IT does not seem to be generally recognized that glass is one of man's most versatile creations. In almost every phase of our modern civilization glass plays a role of ever-increasing importance. The glass windows in our homes permit a combination of light with shelter which is insensitive to the caprices of nature. The incandescent bulb has banished darkness, has given us a twenty-four-hour day and the means to double the constructive hours of our lives. We receive our milk in glass bottles; we preserve our food in glass jars. We drink from glass tumblers and snuff out our cigarettes in glass ash trays. Glass is also the tool of the scientist and makes possible his test tube and microscope, his thermometer and spectroscope. With their aid he explores the innermost fastnesses of matter and the farthest reaches of space.

Among the most important uses of glass are those in which it functions as an electrical insulator. To the incandescent lamp, as one example, can be added neon tubing, radio tubes, radio insulators, fuse plugs, lightning arrester bodies, and insulators for the transmission of electrical power over relatively long distances at high voltage. In some of these applications the virtue of transparency is added to that of insulating ability. In others, great dielectric strength or low coefficient of expansion or availability in a wide range of colors is of paramount importance. In every case, not one but several distinctive properties of glass are utilized, and to obtain these it may be necessary to employ glasses of widely differing compositions.

This last point is significant. To the layman, glass is glass. Much of his experience is with windows, bottles, or tumblers; and he naturally associates the word "glass" with those articles. Since these account for much of the total tonnage manufactured today, and since these glasses are indeed very similar in composition and characteristics, it is not surprising that one is inclined to think of all glasses as being similar. Yet, this is not the case. Corning Glass Works, for example, now melts on a commercial scale more than three hundred glasses, each different from all of the others in composition and physical characteristics. These glasses are deliberately formulated by the chemist so that each may be available for use where its particular combination of properties is most useful. It is important to have some knowledge of these properties; otherwise, a discussion of insulating ability alone would be casual and incomplete. Accordingly, the first part of this paper is devoted to a brief discussion of the chemical and physical characteristics of various glasses, with particular emphasis upon the range of values obtained from different glass compositions. The second part of the paper is concerned particularly with the electrical properties of glass, in bulk, as distinguished from fiber glass. The last section discusses the outstanding characteristics of fiber glass electrical insulation.

I. General Properties of Glass

Almost all of the glasses in use today contain silica as the primary constituent. In fact, if we could easily melt silica itself into a viscous liquid, free from bubbles, and could then fabricate articles from it, we would have an extremely useful material. Unfortunately, it is very difficult to do this. It is necessary to flux the silica with other materials. One of the more important of these is sodium oxide. So far as melting and working are concerned, a very good glass can be made from silica and soda alone, but this glass is too soluble in water to be of any commercial value. Various things can be added to overcome this defect; lime is the cheapest of these. Windows, tumblers, milk bottles, are all essentially soda-lime-silica glasses. There are many other materials which can be added as fluxes—any of the alkali metal oxides, for example.

* Modified from addresses to Pittsburgh Section, A. I. E. E., and Electrical Section, E. S. W. P., Pittsburgh, Pennsylvania, February 14, 1939, and to Wisconsin Engineering Conference, Milwaukee, Wisconsin, March 15, 1939.

After the silica has been properly fluxed, other materials may be introduced in a wide variety of proportions to change radically the properties of the simple silicate mixture. Thus, it is found that the addition of soda and lime has increased the thermal coefficient of expansion of fused silica by a factor of nearly twenty. On the other hand, borosilicate glasses often contain no lime and very little alkali, have one-third the coefficient of expansion of soda-lime glasses, and have very good resistance to water attack or attack by acids and alkalis. Other properties can be changed by a similar procedure, and the range of possible glass compositions is so large and so varied that it is frequently possible to vary one characteristic and have all others essentially unchanged. Despite the many permutations and combinations available to him, the glass chemist must at the same time contrive to keep the batch cost low, must mix materials which will melt at the lowest possible temperature, and must be sure that his glass will not crystallize upon cooling. The compositions which can be used are strictly limited by the tendency of all glasses to crystallize (devitrify), thus ceasing to be glass and losing the properties which distinguish glass from other materials. In general, glass may therefore be considered a homogeneous solution, usually obtained by melting together a large quantity of SiO_2 with smaller quantities of other alkaline oxides, alkaline earth oxides, or trivalent oxides, this solution being so cooled that devitrification does not take place.

The range of properties obtainable from various glasses is shown in Table I. A few words about some of these properties may be illuminating.

Refractive index.—Water is somewhat below the lower figure in the range 1.47 to 1.96, and the diamond is far above the higher limit. However, some glasses probably exceed the precious stone in dispersive power.

Specific gravity.—The lightest glasses have a specific gravity lower than that of fused quartz. The ordinary soda-lime glasses weigh about as much as metallic aluminum. The heaviest weigh more than gray cast iron.

Elasticity coefficient.—The resistance to distortion under stress (Young's modulus) can be varied in nearly a 2 to 1 ratio, from a value lower than that of most metals to a value higher than that of aluminum.

TABLE I. *Range of physical values obtainable from various glasses.*

PROPERTY	RANGE OF VALUES
Refractive index	1.467–1.962
Specific gravity	2.125–8.120
Elasticity coefficient	6,500,000–12,500,000 lb./in.^{2}
Compressive strength	90,000– 180,000 lb./in.^{2}
Tensile strength	4,000– 1,000,000 lb./in.^{2}
Thermal conductivity	0.0018–0.0028 cal./cm °C/sec.
Expansion coefficient	8×10^{-7}–140×10^{-7} cm/cm °C
Softening point	500°C–975°C
Annealing point	350°C–725°C
Volume resistivity	10^8–10^{18} ohms/cc
Dielectric constant	3.7–16.5
Power factor	0.000117–0.00664

Compressive strength.—The resistance to crushing possessed by glass is tremendous—greater than that of brick, concrete, or cast iron. In general, glass will maintain its shape under pressures which cause metals to flow like putty. This property can often be put to good engineering use.

Tensile strength.—The great range shown in Table I depends not so much on composition as on the condition of the exposed glass surface. The work of Griffith[1] on glass and of Joffé[2] on crystals indicates the probability that the true tensile strength of a material is determined by the molecular cohesion, and that the lower values found in practice are caused by surface imperfections, some of which may be inherent in the material. For glass, the modulus of rupture also depends upon the size and shape of the object, although both of these may be dependent variables, the kind and degree of surface imperfection being the independent variable. For example, glass in the form of threads or fibers of small diameter is tremendously strong, ranging upward from 180,000 lb./in.^{2} for fibers 0.0004″ in diameter. More is said of this in a later section of this paper.

Glass can be tempered in a manner analogous to the tempering of steel, although the physical processes occurring in the glass due to this treatment are quite different from those in the metal. By tempering, it is possible to prepare glasses which have a tensile strength of 50,000 lb./in.^{2}, about equal to the strength of wrought iron.

Expansion coefficient.—Ordinary soda-lime glass has an expansion of about 90×10^{-7} cm/cm °C, whereas the values for iron and platinum are 120×10^{-7} cm/cm °C and 90×10^{-7} cm/cm °C, respectively. "Pyrex" brand electrical glass has an expansion of 32×10^{-7} cm/cm °C. Other "Pyrex" brand glasses have expansions of $(46\text{–}50)\times10^{-7}$ cm/cm °C and seal to tungsten or molybdenum, whose values are 45×10^{-7} cm/cm °C and 52×10^{-7} cm/cm °C. The new, low expansion, 96 percent silica glass developed by Corning Glass Works has a coefficient of expansion of 8×10^{-7} cm/cm °C and compares favorably with $(5.5\text{–}5.85)\times10^{-7}$ cm/cm °C for fused quartz.

Annealing point.—The annealing temperature of glass—the temperature at which strain is relieved—is 350°C to 725°C, considerably higher than that for steel, which is between 200°C and 500°C.

A comparison of some of the electrical properties of various materials is given in Table II. These electrical properties will now be discussed in greater detail.

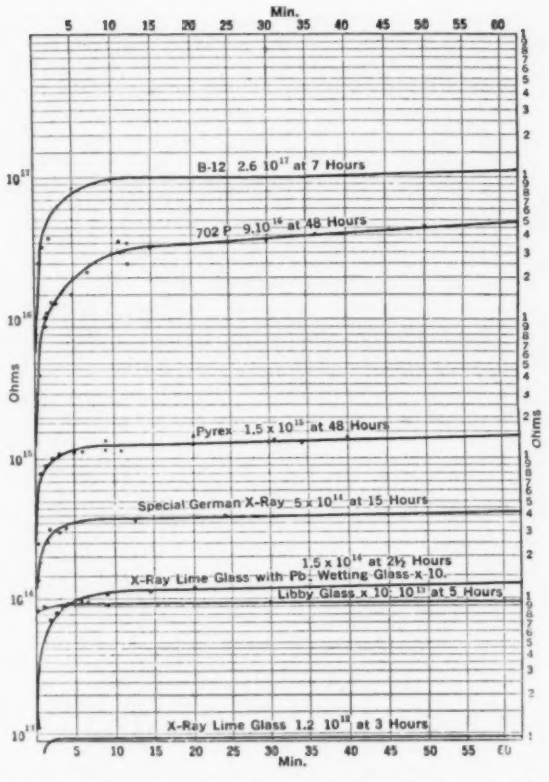
Min.
5 10 15 20 25 30 35 40 45 50 55 60
B-12 2.6 10^17 at 7 Hours
702 P 9.10^16 at 48 Hours
Pyrex 1.5 x 10^15 at 48 Hours
Special German X-Ray 5 x 10^14 at 15 Hours
1.5 x 10^14 at 2½ Hours
X-Ray Lime Glass with Pb; Wetting Glass x 10.
Libby Glass x 10; 10^13 at 5 Hours
X-Ray Lime Glass 1.2 10^12 at 3 Hours
Ohms
Min.

FIG. 1. Resistance of dry glass as a function of the time after applying voltage. (After Bronson.)

II. Electrical Properties of Glass

DIELECTRIC ABSORPTION

The electric current which flows through glass under a given impressed voltage is not a simple function of the temperature, physical dimensions, and conductivity of the sample. Instead, it requires appreciable time before the glass soaks up and becomes saturated with the electric charge. Upon discharge, the reverse may occur. The current flowing at any particular time is, therefore, an undetermined function of the total elapsed time since the initial application or removal of the voltage. This phenomenon, generally called "dielectric absorption," is not confined to glasses. It appears to be present to some degree in all solid dielectrics. Both theory and experiment show that the alternating losses in such materials are due almost entirely to this effect.

TABLE II. *Electrical properties of insulating materials.*

MATERIAL	THICKNESS (MM)	DIELECTRIC STRENGTH (KV/CM)	DIELECTRIC CONSTANT	VOLUME RESISTIVITY (OHM–CM)
1. Asbestos paper	1.2	42	—	1.6×10^{11}
2. Bakelite, Micarta—213	—	314	5.0	5.0×10^{11}
3. Cellulose acetate	0.019	480	4.0– 6.2	10^{12}–10^{14}
4. Empire cloth, muslin	0.38	480	3.5– 5.5	—
5. Ethyl cellulose	—	—	2.7– 3.3	10^{14}
6. Fiber, vulcanized	3.2	108	5.0	10^{10}
7. *Glass, various kinds*	*0.50*	*700*	*3.7–16.5*	*10^{8}–10^{18}*
8. Methyl methacrylate	—	—	3.3– 4.5	3.0×10^{13}
9. Mica	0.60	280	5.0– 7.0	2.0×10^{17}
10. Paraffine (Parowax)	—	115	2.1	10^{16}
11. Porcelain, unglazed	2.5	130	5.7– 6.8	3.0×10^{14}
12. Rubber, hard	0.50	700	2.0– 3.5	10^{18}
13. Sulphur	—	—	2.9– 3.2	10^{17}
14. Wood—maple, paraffined	15.20	46	4.1	3.0×10^{10}

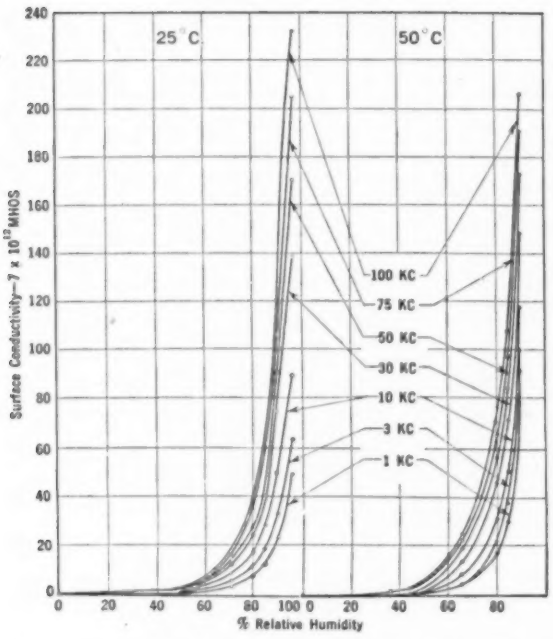

FIG. 2. The surface conductivity of Pyrex resistant glass at 25°C and at 50°C for various frequencies as a function of relative humidity. (After Yager and Morgan.)

In making measurements on the electrical resistance of glass, the dielectric absorption must be taken into account. The absorption current may predominate over the conduction current when the resistivity is high, and measurements must be taken at different time intervals until the absorption current has become negligible. The necessity for this is shown in Fig. 1.[3]

SURFACE RESISTIVITY

For many years it has been understood that part of the electrical conductivity of glass is due to a film of moisture condensed on the surface. The existence of this film was conclusively demonstrated by Warburg and Ihmori.[4] They showed that with the better glasses the film could be removed in a dry atmosphere, whereas with others it could be removed only by heating. Many other observers have shown that an increase in the alkali content is reflected in an immediate decrease in the surface resistivity. It is problematical whether the film is continuous or spotty and whether it is wholly adsorbed or partly absorbed. It appears certain, however, that the film is an aqueous, alkaline solution whose properties may vary widely. At high humidity or with glasses rich in alkali, the surface conductivity may greatly exceed the volume conductivity. On the other hand, it is entirely negligible for alkali-poor glasses with absolutely clean surfaces if the glass is properly polarized. Almost any clean glass can be used without serious surface leakage if the temperature is raised a few degrees above that of the surrounding air.

Yager and Morgan[5] made a special study of the effect of both frequency and humidity on the surface conductivity of "Pyrex" brand laboratory glass. They found that with low humidities, constant values could be obtained in two hours; but at 50°C and 95 percent humidity it was impossible even to approach equilibrium. Their results are plotted in Fig. 2.

VOLUME RESISTIVITY

The volume resistivity of glass depends upon and varies rapidly with changes in composition and temperature. At all temperatures glasses are electrolytic conductors, and most investigators ascribe all of the conduction to the sodium ion. This is probably largely, but not wholly, correct. It does not, for example, explain the role of calcium at higher temperatures, nor the mechanism of conduction in alkali-free glass. Much fundamental work remains to be done to explain these and other perplexing questions.

Curtis[6] found the volume resistivity of fused silica to be about 5×10^{18} ohm-centimeters at 22°C. At ordinary temperatures, "Pyrex" brand electrical glass has a resistivity of about 10^{16}, plate glass about 10^{12}, and certain special glasses will be as low as 10^{8}. It will be seen that at ordinary temperatures some glasses are amongst the very best insulating materials we possess.

Figure 3, reproduced from Fulda,[7] shows the change in specific resistance of a Thuringian glass with temperature. This is the only case in which the resistance has been determined from room temperature to 1200°C. Littleton[8] published data on the resistivity of several widely different glasses over a considerable range of temperatures, using data obtained by Babcock.[8] His results are shown in Fig. 4. These scattered data are sufficient to show the tremendous effect on volume resistivity of changes in glass composition and temperature.

Dielectric Constant, Power Factor, Dielectric Loss

Glasses are unique among solid dielectrics in that they possess a range of dielectric constants, K, varying by more than four to one, from about 3.7 to 16. This property is of more than purely theoretical interest. Where maximum capacity for a given size of condenser is required, a high dielectric constant is needed. Where high voltage, high frequency condensers are required, then a low dielectric constant and also a low power factor, δ, are indicated. The ordinary high voltage power insulator is another advantageous application of low dielectric constant material, because it can be shown that the smaller K is, the greater will be the voltage, V, necessary to form corona in the air in series with the insulator.

For most glasses, K decreases only slightly with increasing frequency—$4\frac{1}{2}$ percent as the frequency was varied from 500 to 10^6 cycles, according to MacLeod. K increases with increasing temperature; more so at low frequencies than at high.

The power loss per unit volume of dielectric material is directly proportional to the frequency, the square of the voltage gradient, and the product $K\delta$. For conditions of high frequency and/or high voltage, the power loss is appreciable, and $K\delta$ should be kept as small as possible. For glasses, both K and δ are to a certain extent separably alterable by changes in glass composition, and the product $K\delta$ can be varied in a ratio of more than 200 : 1. Two general classes of glass are available: (1) high K and low δ; and (2) low K and low δ. As an example, for Corning glass 707 at 10^3 cycles, McDowell, and Begeman[9] find: $K=4.1$, $\delta=0.00077$, and $K\delta\times10^4=31$.

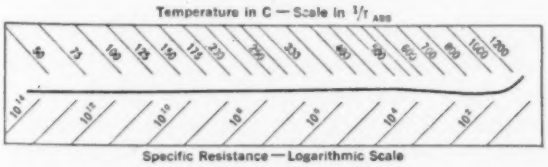

FIG. 3. The change in specific resistance of a glass with temperature. (After Fulda.)

This low loss glass is a low alkali borosilicate of low expansion and high surface stability—an ideal insulating material for most purposes.

The results on the variation of power factor with frequency present several anomalies and, therefore, are not in wholly satisfactory accord. However, it appears that for most glasses the power factor decreases with increased frequency. Power factor increases rapidly with rise in temperature. As the temperature increases, dielectric heating also increases, with eventual instability and breakdown. This condition of instability is normally reached only in the case of high field strength associated with high frequency.

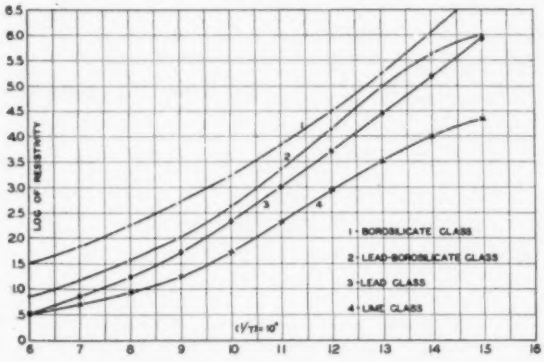

FIG. 4. The change with temperature of the resistivity of various glasses. (After Babcock.)

Dielectric Strength

The dielectric strength of any material is the voltage gradient required to puncture that material. It is usually expressed as kilovolts per mil or kilovolts per centimeter. If the dielectric strength is a true physical constant, it should be independent of the thickness of the material. Nevertheless, in most cases it is found that the greater the thickness, the lower is the measured dielectric strength. It is not known whether this effect is inherent in the material or is dependent upon the test method. The observed values of dielectric strength vary with the size and shape of the electrodes used in applying the voltage, and also vary with the frequency and duration of the voltage, the temperature, etc.

There has been very little work done on other solid materials having dielectric strengths comparable to those of most glasses. Although much attention has been paid to the elimination of electrode edge discharges, many of the other variables mentioned above have been neglected. It is probable that the true dielectric strength of glass

is even greater than it appears to be. Even so, the measured values are very high. Most of the work has been done on sections less than 0.50 mm thick. The values are usually expressed as peak values in the disruptive region with edge effects eliminated. Moscicki[10] obtained a constant value of 1360 kv/cm for various thicknesses up to 0.50 mm. Inge and Walther[11] derived a constant value of 3000 kv/cm on certain Russian apparatus glasses whose thicknesses varied from 0.05 to 0.50 mm. Rochow[12] found a flint glass to have a dielectric strength of 4000 kv/cm at 0.05 mm. Moon and Norcross[13] found values as high as 3100 kv/cm for a lead glass.

It is almost impossible to avoid electrode edge discharges at the higher voltages required to puncture thick sections of glass, and consequently few results have been published. However, there is evidence that puncture strengths above 1900 kv/cm can be reached in air on 1.0-mm sections of "Pyrex" electrical resistant glass insulators. The impulse strength of these insulators is such that one-half-inch sections have repeatedly withstood discharges of a "lightning generator" at 1500 kv.

III. Fiber Glass

Glass fibers are not new. They have been produced for many years on a small scale—first being drawn by hand, later on a large wheel: hence the name "spun glass." New methods developed in this country only a few years ago finally made it practicable to produce exceedingly fine glass fibers on a commercial scale.

Two types of fibers are of particular interest: staple fibers, 4″ to 15″ long, and perhaps 0.00025″ in diameter; and continuous fibers, which, as the name implies, are drawn as long, continuous filaments, usually about 0.0002″ in diameter. The production of these fibers is in pounds per day rather than tons. Even so, one glass marble weighing about one-third of an ounce could be melted and drawn into a continuous fiber 0.0002″ in diameter and over one hundred miles long.

Both types of fibers are equally good electrically. However, the continuous type is smoother, slightly better mechanically, and available in smaller diameters. Staple fiber products are generally better where a heavy type insulation is necessary. The continuous type has an advantage in reduced space factor and better appearance.

Fiber glass differs from ordinary lime glass in one fundamental way—it is substantially alkali-free. This freedom from alkali is essential because alkali leaches to the surface and under conditions of high humidity forms ionizable salts which decrease the surface resistivity. In a fiber 0.0002″ in diameter and 1″ long, the ratio of surface area to volume is 20,000 : 1, whereas in a piece of glass 1″ square and $\frac{1}{4}$″ thick this ratio is only 12 : 1. The effect of alkali leaching is magnified proportionally.

Glass fibers have a number of astonishing properties. In many cases these are substantially the same for both types described above. When not otherwise specified, the data given below may be assumed to apply to either type.

Tensile Strength

In discussing the tensile strength of glass fibers, one deals with figures of almost astronomical magnitude. The tensile strengths for continuous fibers are approximately as follows:

0.0002″ diameter—400,000 lb./in.^{2}
0.0003″ diameter—250,000 lb./in.^{2}
0.0004″ diameter—180,000 lb./in.^{2}

These figures should be compared with a rough figure of 70,000 lb./in.^{2} for mild steel. The reason for the high strength is closely associated with the theory of the rupture of brittle bodies, first clearly enunciated by Griffith.[1] With extremely fine fibers, carefully drawn, it is possible to reach specific tensile strengths in excess of 1,000,000 lb./in.^{2} No other textile material approaches this figure.

The flexibility of the fibers is due to their small diameter, not to any peculiarity of the glass composition. The high tensile strength allows them to be bent through a very small radius without breaking. The very fact that glass fibers can be spun, twisted, and woven on standard textile machinery into fabrics as thin as 0.0025″ is a good illustration of their flexibility.

When fibers are twisted into yarns, some of the effective strength of the fiber is lost, for several reasons: (1) lack of parallelism of fibers, (2) non-uniformity of stress distribution, (3) slip-

page of fibers, and abrasion, and (4) bending or crushing stresses, particularly in tightly woven cloths. Despite these characteristics, the finer yarns may have strengths of approximately 65,000 lb./in.^{2} and hence, weight for weight, are stronger than yarns of most organic fibers, excepting manila and linen.

When yarns are further fabricated into cloths, tapes, or braids, there is a further loss of strength. In open weaves the strength may be 80 percent

TABLE III. *Tensile strength in pounds (minimum-average-maximum) of glass tapes at room temperature.*

THICKNESS (INCHES)	STAPLE FIBER ¼" WIDE	STAPLE FIBER 1" WIDE	CONTINUOUS FIBER ¼" WIDE	CONTINUOUS FIBER 1" WIDE
0.005	—	—	133–147–172	236–258–280
.010	72– 91–110	153–178–200	229–257–285	312–452–510
.015	110–134–158	177–230–263	346	595–634–674
.020	134–158–183	213–259–305	—	—

that of the yarn, in close weaves only 50 percent. Table III shows the breaking strength of some of the staple fiber and continuous fiber glass tapes used for electrical insulation. In Table III

TABLE IV.[14] *Flexing endurance. Samples: Cloth, 0.010"×1"×17".*

TYPE	YELLOW VARNISHED COTTON	YELLOW VARNISHED GLASS
As received	2100	2700
After 280°F, 24 hr.	12,000	72,000
After 350°F, 2 hr.	4500	80,000

the values given are the minimum, average, and maximum obtained by combining the results obtained from several sources.

The effect of heat on the tensile strength of asbestos, cotton, and fiber glass is shown in Fig. 5. These curves show that fiber glass tapes are from two to twenty times stronger at room temperature than commonly used fibrous materials. Of equal importance is the fact that the strength of glass tape decreases only about 20 percent up to 600°F and after twenty-four hours at 800°F still retains half its original value.

RESISTANCE TO ABRASION AND FLEXING

No conclusive tests have been made to determine the abrasion resistance of glass tapes and fabrics because there is no unanimity of opinion as to what constitutes a proper test. In general, however, it seems that there are no outstanding differences in this respect between either treated

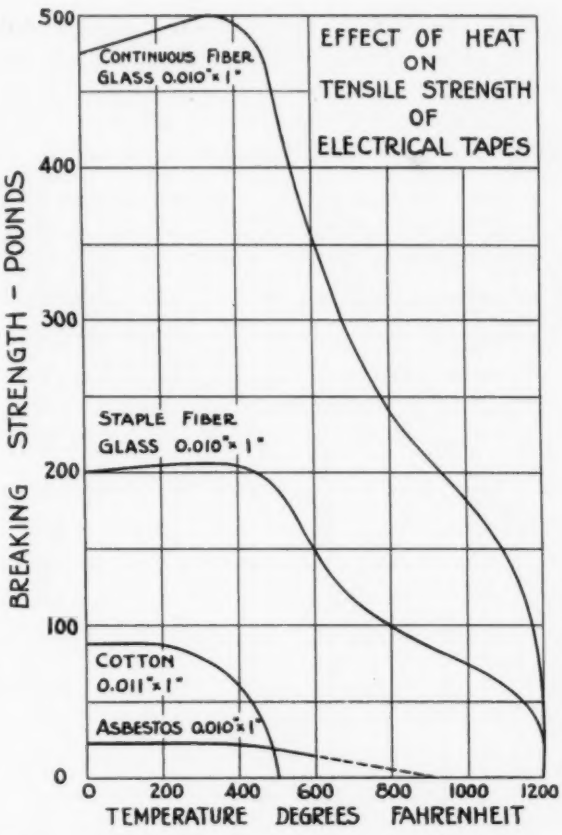

FIG. 5. Effect of heat on tensile strength of electrical tapes. (Atkinson.)

or untreated glass tapes and equivalent cotton or asbestos tapes.

In flexing endurance, glass fiber insulation seems to possess a considerable advantage, as Atkinson's[14] data shows (Table IV). These values were obtained on a machine designed to create a "whipping" motion and show the total number of flexes required to wear out each sample.

HYGROSCOPICITY

Another interesting characteristic of these fibers which makes them particularly suitable for electrical insulation is that they are practically nonhygroscopic. Their moisture absorption is lower than for any other fibrous insulating material. The moisture gain on glass fibers in passing from 0 percent to 90 percent relative humidity at room temperature will be ¼ of 1 percent by weight, or less. This small amount of moisture is probably adsorbed, rather than absorbed, and so does not change the volume

characteristics of the glass. It will have an effect on the surface characteristics, although much less than for organic materials.

Volume Resistivity

Largely because of the absence of soda and potash, the volume resistivity of alkali-free glass is very high—at 490°C (914°F) about 2×10^7 times greater than for the lime glass discussed

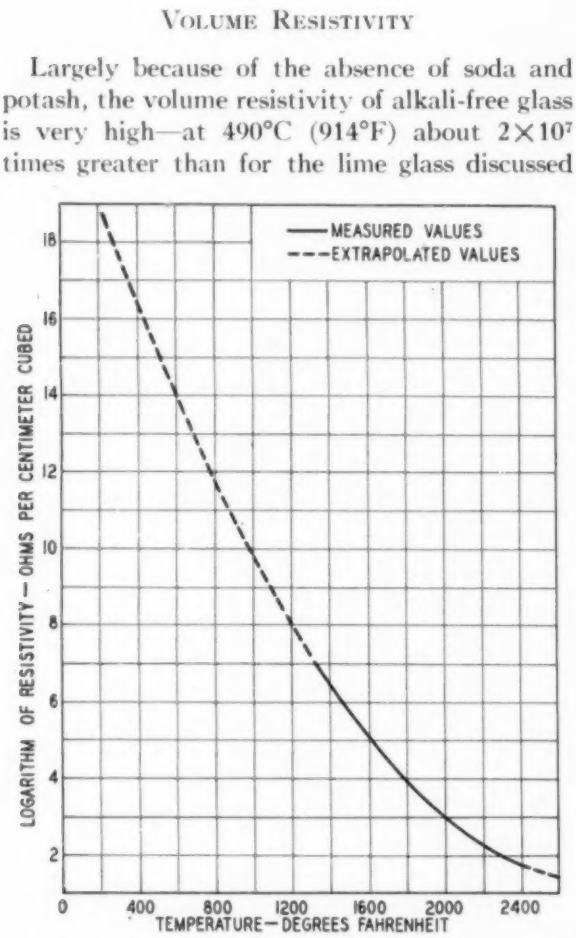

Fig. 6. Volume resistivity of alkali-free glass. (Atkinson.)

by Littleton[8] and 3×10^5 times greater than for his borosilicate glass. Fig. 6, from Atkinson,[14] shows the volume resistivity of the alkali-free glass for temperatures up to 1315°C (2400°F).

Surface Resistivity

The resistance of glass fiber insulation at ordinary temperatures can be considered almost entirely due to its surface resistance. This is because of the high ratio of surface area to volume or weight. When dry and untreated, this resistance is very high—many times greater than that of cotton or asbestos. This surface resistance is, of course, affected by the relative humidity of the atmosphere, but to a lesser extent than for most other materials. The surface resistance decreases with increased humidity, as Table V[14] shows, and also with increased time of exposure.

The resistance of treated fiber glass varies with the nature of the impregnant and the method of applying it. When dry, the glass product behaves very much like other porous, woven materials similarly treated. However, when exposed to high humidity, the glass retains a much greater part of its original insulating ability as Fig. 7[14] shows.

Dielectric Strength

The dielectric strength of fiber glass products —as is the case with any fibrous material— depends largely upon what fills the interstices of the weave. For untreated products, the dielectric breakdown is nearly the same as that of air. It is, therefore, customary to impregnate with varnishes, gums, or resins. The resulting products have dielectric strengths very nearly equal to that of the impregnant. Glass is no exception to this rule; and specific values, therefore, need not be given. Glass, however, has the advantage of being nonhygroscopic and has a higher dielectric strength than materials like asbestos after exposure to moisture.

Other Properties

Fiber glass possesses other properties which, in combination with those already described, make it outstanding. Because it is glass and inorganic, it is noninflammable and heat resistant; to a large extent the operable temperature is limited only by the impregnant. As Ferris and Moses[15] point out, higher temperatures are a means to an end: (1) reduction in size of a machine for a given rating; (2) reduction in weight; and (3) reduction in cost per unit rating. The compact-

Table V. *Insulation resistance in megohms. Standard unimpregnated tapes 1″×1″. Measurements after humidity held constant 72 hours at 100°F.*

Type	As Received		Washed	
	75% R.H.	90% R.H.	75% R.H.	90% R.H.
0.015″ asbestos	0.57	1.08	1.50	5.5
0.011″ cotton	1.03	35.	30.5	380.
0.015″ glass	12.4	200.	1400.	30,100.

ness and good thermal conductivity of fiber glass, compared to organic materials, assist in attaining the characteristics listed above. The textile itself, however, is not the complete answer. In addition, new, correlated products are required: insulating resins and compounds, insulating sheets or boards for both rotating machines and transformers, high temperature liquids for liquid-cooled transformers, and perhaps even new core plate vanishes. It is to be hoped that the advent of fiber glass will act as an incentive and a stimulant for the completion of this comprehensive program.

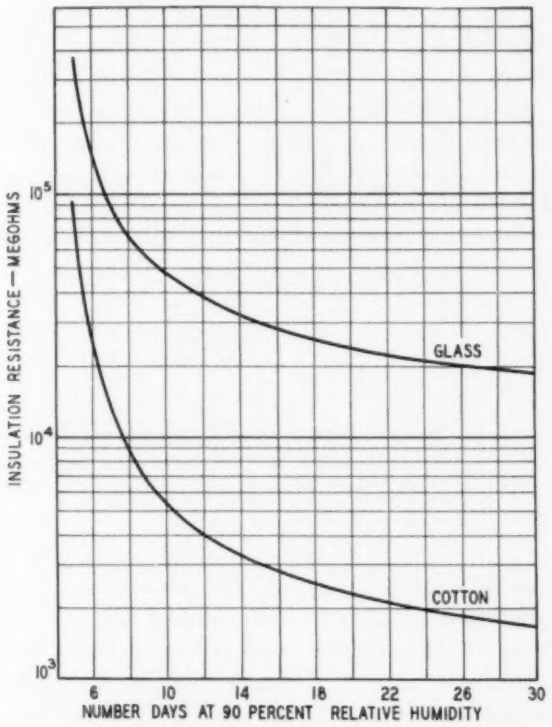

FIG. 7. Effect of humidity on resistance of black varnished cloth. (Atkinson.)

Summary

Some of the advantages of glass as an electrical insulator may be briefly summarized as follows.

(1) Glass is a homogeneous, nonporous material which is smooth, hard, and highly resistant to weathering and chemical attack.

(2) Glass has good tensile strength and is very strong in compression. If a strain member can be designed so that the glass part is in compression, very large loads are possible. Certain glass suspension insulators will support twenty-five thousand pounds.

(3) Certain kinds of glass have coefficients of expansion lower than any other ceramic substance except fused quartz. This characteristic tends to minimize the effect of severe temperature gradients and improves resistance to power arcs.

(4) Glass used for most electrical purposes has very high volume and surface resistivity.

(5) Glasses are available with a wide range of values of the dielectric constant and of power loss per unit volume.

(6) Glass has very high dielectric strength and hence great resistance to high voltage surges.

(7) Glass is available in the form of fiber glass, with the numerous advantages offered by that material.

Acknowledgments

The writer wishes to gratefully acknowledge the assistance of E. C. Sullivan and J. T. Littleton of Corning Glass Works and of F. W. Atkinson of Owens-Corning Fiberglas Corporation.

Bibliography

1. A. A. Griffith, Phil. Trans. Roy. Soc. **A221**, 163 (1920).
2. A. F. Joffé, *The Physics of Crystals* (McGraw-Hill, New York, 1928).
3. H. L. Bronson, cited by A. W. Hull, Physics **2**, 420 (1932).
4. E. Warburg and T. Ihmori, Ann. d. physik. Chemie **27**, 481 (1886).
5. W. A. Yager and S. O. Morgan, J. Phys. Chem. **35**, 2040 (1931).
6. H. L. Curtis, Bull. Nat. Bur. Stand. **11**, 359 (1914–15).
7. M. Fulda, Sprechsaal **60**, 769, 789, 810, 831, 853 (1927).
8. J. T. Littleton, Ind. Eng. Chem. **25**, 748 (1933). See also C. O. Babcock, J. Am. Ceram. Soc. **17**, 329 (1934).
9. L. S. McDowell and H. L. Begeman, Phys. Rev. **33**, 55 (1929).
10. J. Moscicki, Elektrotech. Zeits. **25**, 527 (1904).
11. L. Inge and A. Walther, Arch. Elektrotech. **24**, 88 (1930).
12. H. Rochow, Arch. Elektrotech. **14**, 361 (1925).
13. P. H. Moon and A. S. Norcross, J. Frank. Inst. **208**, 705–29 (1929).
14. F. W. Atkinson, J. A.I.E.E. **58**, 277 (1939).
15. R. E. Ferris and G. L. Moses, Elec. Eng. **57**, 480 (1938).

Resumés of Recent Research

A Hydrogen Arc for Absorption Spectroscopy

A low voltage hydrogen arc, for use in the determination of absorption spectra in the ultraviolet region was described recently by A. J. Allen and R. G. Franklin.[1] This arc emits a continuous spectrum in the ultraviolet region, compares favorably in intensity with an intense spark between iron electrodes and is easy and reliable to operate. It may be made to take the form of an approximate point or slit according to the requirements of the spectrograph used, and is, moreover, inexpensive to construct.

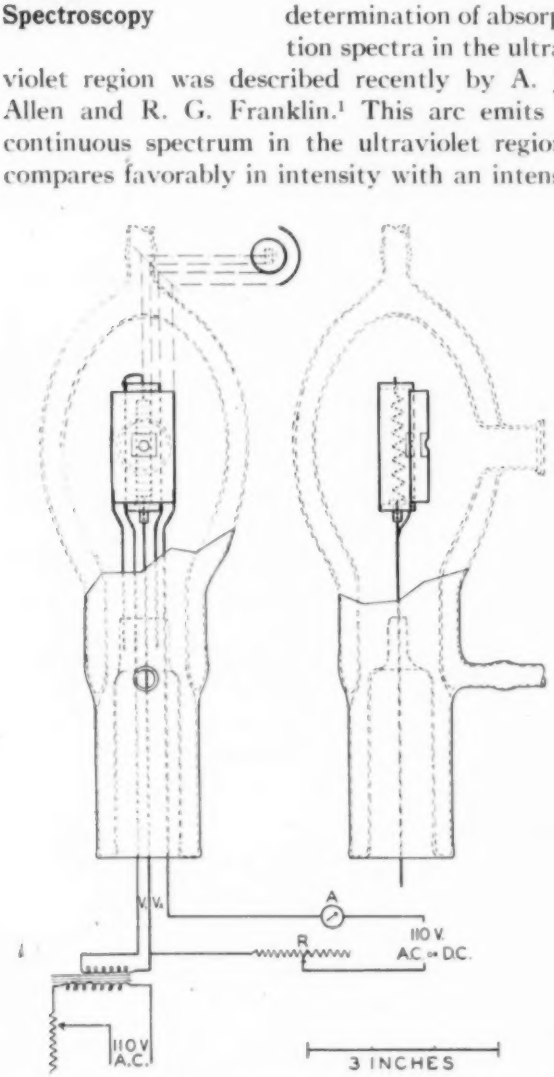

Schematic drawing of low voltage hydrogen arc. V_1—filament voltage, 3.5–4.0 volts; V_2—arc voltage, 40.0 volts; A—ammeter to measure arc current, 1.0–1.5 amperes; and R—variable resistance, 100 ohms, −2.0 amperes.

A schematic drawing of the essential elements of the arc is shown in the accompanying figure. The cathode consists of a strip of nickel screen, made into a corrugated form and dipped into an oxide coating material. The cathode is surrounded by a nickel cylinder with an orifice which can be adapted to any size or shape. The anode is a rectangular piece of molybdenum with an orifice to correspond to that of the cathode. The cathode-anode assembly is placed in a Pyrex bulb onto which a quartz window is sealed with glyptal lacquer. The bulb is completely water-jacketed for cooling. Ordinary tank hydrogen at a pressure of 4 to 6 mm of mercury has been found to be satisfactory for filling the arc. Either alternating or direct current may be used. The arc voltage is approximately 40 volts and the arc current 1.0 to 1.5 amperes. The filament carries a current of 10 to 12 amperes at 3.5 to 4.0 volts.

Complete instructions for making this arc are given in the original article. Typical spectrograms taken with the arc are also shown and data are given from which comparisons can be made with other light sources.

[1] J. Opt. Soc. Am. **29**, 1 (1939).

Identification of Aluminum Hydrate Films of Importance in Silicosis Prevention

Silicosis develops rather quickly in rabbits exposed to air containing moderate concentrations of quartz particles finer than about 5 mu, but is completely prevented if aluminum powder is also present in the air to the extent of about 1 percent by weight of the quartz powder.[1] It has been established that aluminum forms in the lungs a protective layer upon the surface of silica particles, which prevents them from dissolving and thus prevents toxic effects.[1] The nature of this layer has been studied by means of electron diffraction.[2] In these experiments electron diffraction patterns have been obtained from thin films

[1] J. J. Denny, W. D. Robson and D. A. Irwin, Canadian Medical Association J. **37**, 1–11 (1937); **40**, 213–228 (1939).

[2] L. H. Germer and K. H. Storks, Ind. Eng. Chem. Anal. **31**, 583 (1939).

of silica, about 200A thick, which had been previously exposed to aluminum and water at 38°C (approximately body temperature). A beam of high speed electrons is sent through such a treated film and the resulting diffraction pattern recorded upon a photographic plate. From studies of such patterns, and comparisons with x-ray patterns of known substances, materials composing layers upon silica surfaces have been identified.

After treatment with aluminum and water at high and medium *p*H values (6 to 9) silica films give sharp diffraction patterns which have been identified with oriented crystals of that hydrated oxide of aluminum known as aluminum alpha-monohydrate (Boehmite). At *p*H 4 monohydrate is not formed upon silica. In the presence of organic acids oriented soap crystals are formed at all *p*H values from 4 to 9, but this material appears not to be readily adsorbed upon silica.

The experiments prove that aluminum hydrate is precipitated fairly rapidly upon silica at *p*H values lying within a range in which lie also the *p*H values of body fluids of men and of animals. Since in these experiments aluminum hydrate is not formed upon silica at *p*H 4, it seems highly probable that aluminum would not afford protection from silicosis to a hypothetical animal with body fluids of *p*H 4.

Here and There

Cover Photograph

The photograph on the cover of this issue shows several sections of the 1,400,000-volt x-ray tube, constructed by General Electric for the National Bureau of Standards. A description of this tube was given in the Innovations in Instruments section of the February *Journal of Applied Physics*.

★

Research Preview

The Westinghouse Electric and Manufacturing Company held a preview of its research work in 1940 on Monday, January 29, in the Research Laboratories, East Pittsburgh, Pennsylvania. The following program was arranged:

Morning

Welcome, by Dr. L. W. Chubb
Carburization of Steel, by Dr. A. A. Bates
Hydrochloric Acid Relay, by Dr. C. F. Hill
Westinghouse "Atom Smasher," by Dr. E. U. Condon
Inspection tours of the "atom smasher," mass spectrograph, and elasticity and damping of single crystals.

Afternoon

Greeting, by M. W. Smith
Art in modern design, by D. L. Hadley
Photoelasticity, by Dr. Miklos Hetenyi
Lightning investigations, including electrical wave model and fulchronograph, by C. F. Wagner
Inspection trips to see: control devices; microchemical laboratory; exhibit room, equipped with working models; magnetic bearing tester; field balancing; creep, fatigue and relaxation; high speed tension; K-42-B demonstration; bright annealing in a new electric furnace.

★

Appointment of Dr. C. H. Kunsman, long active in research work in the U. S. Department of Agriculture, as Chief of the Physiochemical and Analytical Division of the Department's Western Regional Research Laboratory at Albany, California, was announced recently by Dr. Henry G. Knight, Chief of the Bureau of Agricultural Chemistry and Engineering.

Fellowship Fund Announced

A $25,000 trust fund to provide graduate fellowships in electrical engineering has been set up by the Westinghouse Electric and Manufacturing Company, the American Institute of Electrical Engineers announced recently. The fund is established as a memorial to Dr. Charles LeGeyt Fortescue who was associated with the Westinghouse Company for 38 years. Each award provides a minimum allowance of $500, and any student of electrical engineering who has received a bachelor's degree from an accredited college is elegible for a fellowship, provided he does not hold other fellowships which carry a stipend greater than the tuition required by the institution at which he proposes to undertake his graduate work. Professor D. F. Miner, of Carnegie Institute of Technology, is secretary of the fellowship committee.

★

Professor Ralph A. Sawyer, who has been granted a sabbatical leave from his duties at the University of Michigan for the present school semester, will spend most of that time in Ann Arbor devoting himself to study and to work on a book on experimental spectroscopy.

★

Power Conference Plans

The Annual Midwest Power Conference, to be held in Chicago's Palmer House, April 9 and 10, includes, in its tentative program, plans for sessions on the following topics: gas turbines, small power plants, electrical transmission, power-process, fuel problems of power plants, and hydro power. At the opening meeting the address of welcome will be given by Loran D. Gayton, City Engineer of Chicago; and Philip W. Swain, Editor of *Power*, will speak on "Power Fallacies." The Conference is sponsored by the Armour Institute of Technology.

Royal Society Awards

Among the awards made recently by the Royal Society of Great Britain, the following are of particular interest to physicists:

A Royal Medal was presented to Professor Paul Adrien Maurice Dirac whose work in modern theoretical physics has aided in the promotion and interpretation of observed atomic phenomena. Through careful and original mathematical treatment Professor Dirac was successful in bridging the gap between the new quantum mechanics and Newtonian, and later in reconciling quantum and relativity mechanics by making the fundamental equations of quantum mechanics invariant under a Lorentz transformation. This broadening of the field of quantum mechanics led to the revision of the theory of the hydrogen atom, gave added indication of a quantized electron spin, and hinted at the existence of the positive electron, since discovered by Anderson.

The Hughes Medal, awarded annually by the Royal Society for original discovery in the physical sciences, particularly in electricity or magnetism or their applications, was given this year to Professor George Paget Thomson, who has been able experimentally to prove de Broglie's concepts of wave mechanics, both from a qualitative and a quantitative standpoint. Professor Thomson's earlier work was concerned with research in positive rays, and he has also published a book and a number of papers on aeronautics. He collaborated with his father, Dr. J. J. Thomson, in the preparation of the third edition of the book, *Conduction of Electricity through Gases*, the most important work on that subject.

★

School Merger Planned

By September, 1940, a merger of the Armour Institute of Technology and Lewis Institute will have been completed, according to an announcement made recently by Armour Institute. The name of the new school will be Armour College of Engineering of Illinois Institute of Technology.

★

International Congress of Mathematicians

Postponement of the International Congress of Mathematicians until a more favorable time was announced by the Organizing Committee recently. The Congress was originally scheduled for September, 1940, in Cambridge, Massachusetts. The Committee further stated that due notice will be given of any arrangements to hold the Congress at a later date.

★

Science reports that Dr. Elmer O. Kraemer, formerly connected with the Experimental Station of E. I. duPont de Nemours and Company, has recently returned from Europe, where he spent a year as fellow of the Lalor Foundation, continuing his researches on the sizes and shapes of giant molecules with Professor The Svedberg at the University of Upsala, Sweden. Dr. Kraemer is now associated with the Biochemical Research Foundation of the Franklin Institute in Philadelphia.

Illinois Engineering Council

Professor Harry McCormack, Director of Chemical Engineering at Armour Institute of Technology, was recently elected President of the Illinois Engineering Council. His election took place at the annual meeting of the Council held on the campus of the Institute.

"The Illinois Engineering Council," according to President McCormack, "was founded to present a united front for the engineering professions in the State of Illinois. Actually, the Council consists of about forty representatives from the various engineering societies in this state, and the Council's function is to represent the social, economic and legal interests of the engineering profession as a whole."

The organizations thus far represented in the Council are: American Association of Engineers—Illinois Assembly; American Society of Civil Engineers, Central Illinois Section; American Institute of Chemical Engineers, Chicago Section; Illinois Association of County Superintendents of Highway; Illinois Association of Highway Engineers; and the Western Society of Engineers.

★

Mathematical Biophysics

The *Bulletin of Mathematical Biophysics*, edited by N. Rashevsky of the University of Chicago, announces the following table of contents for the March, 1940, issue:

A Neural Mechanism for Discrimination: II. Discrimination of Weights. A. S. HOUSEHOLDER
An Approach to the Mathematical Biophysics of Self Regulation and Cell Polarity. N. RASHEVSKY
Contributions to the Mathematical Biophysics of Organic Form: I. Formation of Cavities in Cellular Aggregates. N. RASHEVSKY
Discrimination between Temporally Separated Stimuli. H. D. LANDAHL
Convective Diffusion in Parallel Flow Fields. GALE YOUNG

The editorial office of the *Bulletin of Mathematical Biophysics* is located at 5822 Drexel Avenue, Chicago, Illinois.

★

Calendar of Meetings

March		
4–8	American Society for Testing Materials, Detroit, Michigan
12–14	American Railway Engineering Association, Chicago, Illinois
April		
7–13	American Ceramic Society, Toronto, Canada
8–12	American Chemical Society, Cincinnati, Ohio
17–19	American Society of Civil Engineers, Kansas City, Missouri
22–25	Society of Motion Picture Engineers, Atlantic City, New Jersey
25–27	American Physical Society, Washington, D. C.
29–30	Acoustical Society of America, Washington, D. C.
May		
1–3	American Society of Mechanical Engineers, Worcester, Massachusetts
1–4	American Geophysical Union, Washington, D. C.
6–10	American Foundrymen's Association, Chicago, Illinois
13–15	American Institute of Chemical Engineers, Buffalo, New York
June		
6–8	National Colloid Symposium, Ann Arbor, Michigan
9–14	Society of Automotive Engineers, White Sulphur Springs, West Virginia
10–14	American Medical Association, New York, New York
17–21	American Society of Mechanical Engineers, Milwaukee, Wisconsin
19–21	American Physical Society, Seattle, Washington
24–28	American Society for Testing Materials, Atlantic City, New Jersey
24–28	American Institute of Electrical Engineers, Swampscott, Massachusetts
27–29	Institute of Radio Engineers, Boston, Massachusetts

Contributors to This Issue

P. L. Hartman

Paul L. Hartman is engaged in vacuum tube work with the Bell Telephone Laboratories in New York City. He graduated in electrical engineering from the University of Nevada in 1934. Dr. Hartman received his Ph.D. degree in physics at Cornell in 1938 and held an instructorship in that department the following year.

E. C. Bingham

Eugene C. Bingham is Professor of Research at Lafayette College, Easton, Pennsylvania. He received the A.B. and D.Sc. degrees from Middlebury College and the Ph.D. from Johns Hopkins and he has studied under Sir. J. J. Thomson and W. Nernst.

P. W. Kinney

Paul W. Kinney was employed by the National Adhesives Corporation in 1936–1937 and is at present carrying on research concerning adhesive materials for the Armstrong Cork Company of Lancaster, Pennsylvania. He was awarded the Edward Hart Fellowship at Lafayette College in 1937 and received his M.S. in chemistry there in 1938.

C. J. Phillips

C. J. Phillips is the Sales Manager of the Insulation Division, Corning Glass Works, Corning, New York, with which company he has been associated since 1931. He received his training at the University of Pittsburgh (B.S., 1930), and at Oberlin College (A.M., 1931). Mr. Phillips is at present engaged in preparing a book on the technology and applications of glass.

Pictures and biographical sketches of the following contributors have appeared in previous issues of the *Journal of Applied Physics:*

F. Morgan, p. 391, Vol. 9, No. 6, 1938.
M. Muskat, p. 391, Vol. 9, No. 6, 1938.
Lloyd P. Smith, p. 415, Vol. 8, No. 6, 1937.

William Fuller Brown, Jr., received his A.B. in English at Cornell University in 1925 and his Ph.D. in physics at Columbia University in 1937. He was Lecturer in Physics at Columbia University from 1928 to 1938; at present he is Assistant Professor of Physics at Princeton University.

C. G. Brennecke

F. Breazeale

Cornelius G. Brennecke is Assistant Professor of Electrical Engineering at the University of Toledo. He is a graduate of Columbia University, from which he received his A.B. and E.E. degrees in 1926 and 1928, respectively, and of New York University, from which he received his Ph.D. degree in 1936.

W. F. Brown

Francis Breazeale has been employed with the American Enka Corporation, Enka, North Carolina, since 1936, and has divided his time between rheological studies and various other physical plant problems. He received his A.B. degree from the University of North Carolina in 1935, and his M.A. in physics from the same institution in 1936.

Innovations in Instruments

Recent Booklets

Shop and Laboratory, publication of the Mico Instrument Company, Cambridge, Massachusetts, describes a "Model G Graton-Vanderwilt Polishing Machine," in the feature article of the December, 1939, issue. The table of contents also includes articles on: "Ruling of Non-Uniform Dials," "High-Intensity Illuminators," "Microscope Counting Stage," "Refractive Index Prism," "New Instrument Lubricants," "Precision Scales," "Carriage Release for 10-inch Measuring Engine," and "Toroid Winder News."

The *Du Mont Oscillographer* for December, 1939, January, 1940, carries the second and last part of the article, "Study of Phase Displacement in Electrical Circuits from Linearly Expanded Lissajous Figures," by H. D. Brailsford, of the Underwriters' Laboratories, Inc. The *Oscillographer* is published by the Allen B. Du Mont Laboratories, Inc., 2 Main Avenue, Passaic, New Jersey.

"A Broadcast Frequency Monitor for the 20-Cycle Rule," and "One Cycle per Second from the Inverse Feedback Oscillator," are the two articles published in the January issue of the *General Radio Experimenter*, publication of the General Radio Company, 30 State Street, Cambridge A, Massachusetts.

The *Frontier*, published by the Research Foundation of Armour Institute of Technology, Chicago, Illinois, includes among the articles in the December issue the following: "Sodium in Industry," "New Safeguards in War on Rust," and "The Secret of the Lens."

The *Laboratory* devotes its feature article and its cover drawing for a recent issue to the subject of "Mendeleeff—Visionary and Prophet." The *Laboratory* is printed by the Fisher Scientific Company of Pittsburgh, Pennsylvania, "for those interested in keeping informed on the latest developments of laboratory apparatus and technique."

New Catalog

A new set of catalog sheets listing products of the Shallcross Manufacturing Company, 10 Jackson Avenue, Collingdale, Pennsylvania, has been recently issued. It is the Company's series No. 146. The items listed have been classified as follows: resistance standards and affiliated instruments, Wheatstone bridges, test sets and special apparatus, and telephone transmission test equipment and kilovoltmeters.

Varied Line of Graph Papers

Eugene Dietzgen Company, manufacturers of drafting and surveying supplies, Chicago, Illinois, announces a broad and comprehensive line of graph papers for mathematical, commercial and industrial use.

Generator for Radio Testing

For use in testing radio receivers in the ultra-high frequency range, the new Type 804-A U-H-F signal generator (see accompanying figure) has been designed by the General Radio Company, 30 State Street, Cambridge, Massachusetts. The instrument produces carrier frequencies over a wide range, extending from 7.5 to 320 megacycles. The output voltage range is 10 microvolts to 20 millivolts. This signal generator is direct-reading in both frequency and output voltage and is provided with internal 400-cycle modulation up to 60 percent. External modulation can also be used. A voltage-regulated a.c. power supply is included.

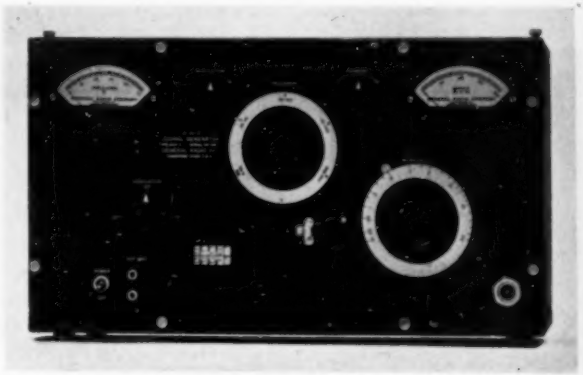

The oscillator circuit employed makes possible operation at frequencies as high as 330 megacycles. The tuning condenser is small and is driven by a worm and gear assembly. The coils are mounted on a Mycalex disk which can be rotated by means of control knob on the panel. The attenuator is capacitive and is provided with a compensating mechanism in order to present a constant capacitance to the oscillating circuit. An output cable is furnished.

Electronic Devices Announced

The Farnsworth Television and Radio Corporation of Fort Wayne, Indiana, announces the company's extensive research activities on electronic devices, including television equipment and electron multiplier tubes of various types. Many of these are now being produced commercially.

The action of the electron multiplier is based on the principle of secondary emission from a series of caesiated surfaces at successively higher potentials. The impact of each primary electron in each successive stage causes the emission of from 2 to 5 secondaries, thus amplifying the current in geometrical proportion to the number of stages. In view of the fact that electron multipliers give promise of performing many functions now performed by thermionic tubes, the producers of these multiplier tubes believe that they ultimately will have revolutionary effects on the science of radio communication and its many industrial and scientific applications.

Contributed Original Research

Remarks on the Study of Structural Viscosity in Liquids, and the Derivation of Equations for the Flux of Such Liquids Through Tubes

FRANCIS BREAZEALE
The American Enka Corporation, Enka, North Carolina
(Received April 21, 1939)

I

THE aim of this paper is briefly to indicate how the elementary flow properties of certain imperfect viscous fluids may be found; and the manner by which may be mathematically developed the expression for the flux (through a tube) of these liquids, which possess (1) structural viscosity alone, or (2) structural viscosity, changing to some thixotropic condition at high stress. It is believed that the expressions for flux of such liquids thus obtained are more accurate and more amenable to quantitative evaluation, over very considerable ranges of rates of shear, than any that have heretofore been presented.[1, 2] Comparison of experimental and theoretical results for the flux~pressure relationship is given for a typical example (cellulosic "solution").

Flux~pressure curves obtained by forcing these fluids through capillaries (or pipes), fall into two general types, namely Bingham[3] and Ostwald.[4] Fig. 1 shows these two types.

In so-called Ostwald flow, the curve is sigmoid in shape, first approaching an asymtote directed towards the pressure axis, and then rising to one directed towards the origin of the coordinates. In Bingham flow, the curve approaches an asymtote directed towards the P axis, and does not arise from it at the most elevated pressure considered. It thus appears that Ostwald flow is but a special extension of Bingham flow.

II

The possible causes for the shape of either of these two types of curves may be several; namely,

1. Existence of a yield value.
2. Creep, and not true flow. (This is also an indication of rigidity (elasticity).)
3. (a) Structural viscosity—that is, lowering of viscosity with increase of shearing stress with very rapid recovery upon release of stress.

(b) Thixotropy (slowly reversible change in liquid structure, manifested as a lowering of viscosity, from application of shear). Although the term is usually applied to sol-gel systems which show this property, we shall use it to describe the possible analogous condition in cellulose "solution."

(c) A hypothetical property which we shall call "progressive thixotropy," and define as a lowering of viscosity with shear; a process in all cases reversible, but whose time of reversibility is dependent on and increases with the magnitude of the disturbing shear. That is, at low shears, it acts as structural viscosity; at high shears as if a permanent liquid destruction had been effected.

4. Slip at the tube walls, which factor might increase faster than does the stress.

Items 1 and 2 are easily answered through use of a simple, chronophotographic method we have developed. A pigmented specimen of the liquid under study is forced through an untreated sample of the same liquid. From the displacement~time relationship of the resulting profile;

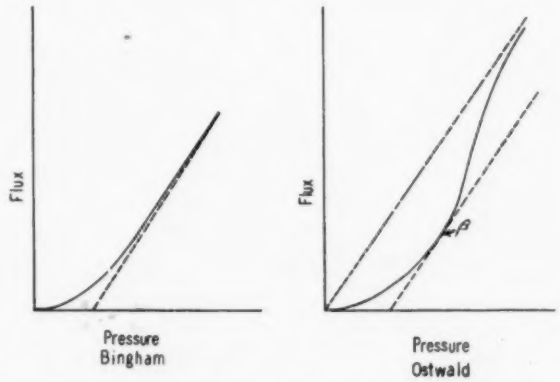

FIG. 1. Flux-pressure curves obtained by forcing certain imperfect fluids through capillaries (pipes).

[1] Farrow, Lowe, and Neal, J. Textile Institute **19**, 18 (1928).
[2] R. K. Schofield, Physics **4**, 122 (1933).
[3] E. C. Bingham and H. Green, J. Am. Soc. Testing Mat. (1919).
[4] W. Ostwald, Kolloid Zeits. **47**, 176 (1929).

and from the form of the profile itself, it is readily determined whether yield value or creep occurs.

Figure 2 is a sketch of the apparatus. The long tube with side arm, attached to glass jar with thick-walled tubing, is held in vertical position and the pigmented liquid from the jar allowed to ascend to the side arm. The main stopcock is now closed, the clear liquid poured down the tube and allowed to settle on the treated liquid. The side arm cock is now closed and the tube placed horizontally in the glass bath container, as shown. The tube has the same (or nearly same) index of refraction as the liquid understudy, and the bath likewise is of this index. Hence distortion due to refraction is not troublesome. In our case, soft glass and xylol were used for tube and bath.

The clamp is used only when disassembling, to prevent the liquid from the jar from pouring out upon removal of the main glass observation tube.

The main cock is now opened, and the profile between pigmented and unpigmented liquid photographed at regular intervals. Three typical 1/25-sec. exposures at 30-sec. intervals, the first a few seconds after the cock was opened, (to allow for kinetic energy effects) are shown in Fig. 5.

This record shows no appreciable yield value; no creep (no rigidity or elasticity), as the profile is not blunt, and the displacement ~ time relationship is linear.

To investigate Item 3 a special Couette viscometer was constructed in our instrument shop, a photograph of which is shown (Fig. 6). It is featured by its ruggedness; speed range (10–300

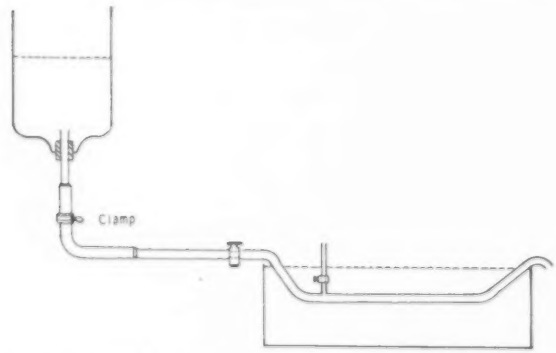

FIG. 2. Sketch of apparatus used in the chronophotographic method of determining existence of yield value and creep.

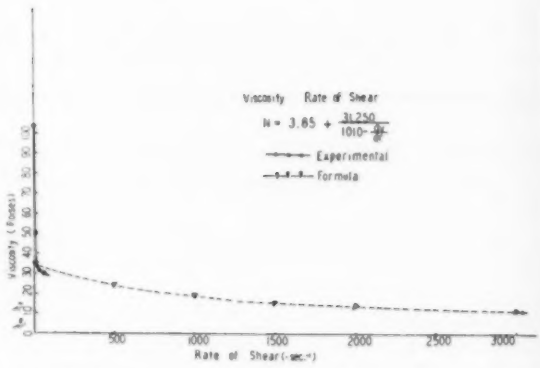

FIG. 3. Experimental and calculated curves for the relationship between viscosity and rate of shear.

r.p.m.) and small distance between cylinders in respect to their radii. This latter circumstance results in little change in rate of shear through the sample being investigated. Dimensions: inner cylinder-radius, 93.5 mm; height, 121 mm; outer cylinder-radius 99.5 mm; depth 106 mm. Clearance usually employed at bottom, 12 mm. Deflection ~ rotation speed curves thus obtained are transformed to viscosity ~ rate of shear curves by (1) assuming a perfect viscous fluid, and calculating rate of shear at inner cylinder from the familiar formula connecting this quantity and rotational speed,* and (2) dividing various points along the deflection ~ rate of shear curve by the corresponding rate of shear, and plotting the dividends as relative viscosity, in place of deflection. The determination of absolute values of viscosity, to replace relative ones is made from oil calibration curves. The assumption in the first step of a perfect viscous fluid does not defeat the purpose of the operation, inasmuch as the error thus involved can hardly be more than the change in rate of shear between inner and outer cylinders for a perfect viscous fluid, in our case, 11 percent. It will be seen that an error of this magnitude near the origin of the viscosity ~ rate of shear curve is allowable. It was found that there was no change of liquid structure under stress, for all ranges of speeds; that is, the fluid was not thixotropic in this test.

* Rate of shear at inner cylinder $= \dfrac{1/R_1}{1/R_1 - 1/R_2} \times 2\Omega$.

where:

Ω = angular velocity of outer cylinder

R_1, R_2 = radii of inner and outer cylinders, respectively.

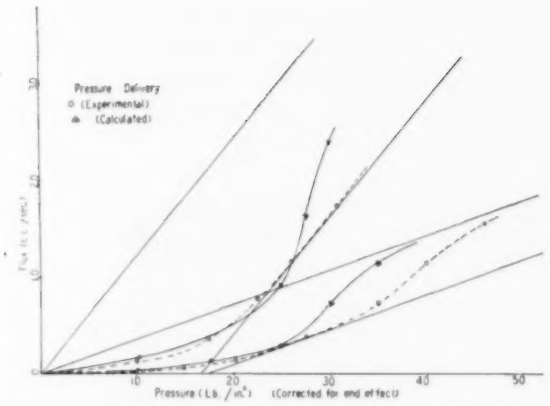

FIG. 4. Flux-pressure curves for capillaries of the same $a/21$ ratio, with the cellulosic "solution" used for Print 3.

Bottom corrections were made by filling the instrument to two different heights; top corrections (piling up) are not important under 70 r.p.m., as indicated by oil calibration curves. For this reason the speed range employed was from 10 to 60 r.p.m.

The fourth point, concerning slip at walls, is probably best answered through measurement of the Ostwald asymptotes of two capillaries of equal length but of different radii. It has been found for solutions of the type under discussion, that at any given pressure on these asymptotes, flux $(F) \sim r^4$, within small experimental error. This is an indication of parabolic velocity profile; and no slip.[5] We therefore say that in our case there is no slip in the lower region.

III

In this solution we are therefore led to believe that structural viscosity alone accounts for the lower region of both curves. Writing a general viscosity ~ rate of shear relationship from an examination of the experimental curve obtained as outlined above (Fig. 3)

$$\eta = \eta_\infty + \frac{A}{B - dV/dr},$$

where

η_∞ = viscosity at infinite rate of shear,
A, B, constants
dV/dr = rate of shear (negative in a capillary).

[5] H. Lamb, *Hydrodynamics* (Cambridge University Press, 6th Edition, 1932), p. 586.

This condition, of course, says that true flow may never be reached, as the asymptote cannot pass through the origin (Bingham flow). Then how may be expressed the circumstance that in Ostwald flow, a condition of $F \sim P$ is finally reached? Since we know from experiment at low rates of shear that the $\eta \sim dV/dr$ function is immediately reversible, it seems necessary to postulate that above a certain critical stress, S_0, corresponding to a critical rate of shear, dV/dr_c, the action is not reversible. Although a gradual transition from reversibility to irreversibility (in respect to time—therefore "progressive thixotropy") would be much more reasonable, the discontinuity is postulated for mathematical simplicity.

For Ostwald flow, then,

$$\eta = \left[\eta_\infty + \frac{A}{B - dV/dr}\right]_{dV/dr = dV/dr_c}^{dr/dr = 0}$$

and above S_0

$$\eta = \left[\eta_\infty\right]_{dV/dr = \infty}^{dV/dr = dV/dr_c}.$$

The problem of determining S_0 is now to be solved. Although this must be done to some degree intuitively, as will be apparent, it leads to results which are in fair accord with experiment. We find that in the Bingham assumption (no irreversibility) a term independent of pressure appears in the expression for the flux, and this term can easily be shown to be the ordinate distance between the Bingham asymptote and a parallel line through the origin (Ostwald asymptote for $\eta = \eta_\infty$). We may therefore suppose that when, in the Ostwald system, the curve leaves the Bingham axis, dV/dr_c has been exceeded at the wall (where rate of shear is, of course, a maximum), and that at this point, β, $S_0 = pa/2l$ (where p = pressure at β). Here we say that η has dropped to its lowest reversible value, η_r. We assume for simplicity, moreover, that the profile is parabolic here, although it is, of course, Bingham, (this assumption may be shown in most cases, *a posteriori*, to be a good one), and calculate η_r by Poiseuille's formula. η_∞ is, of course, solved exactly through Poiseuille's formula, at any point on the Ostwald asymptote. At this point (assuming parabolic flow), rate of

shear at the wall $= dV/dr_c = 4F/\pi a^3$, (where F = flux, and a = radius of tube). A and B may be solved through the simultaneous relations:

$$\eta_c = \eta_x + \frac{A}{B - dV/dr_c},$$

$$\eta_0 = \eta_x + A/B,$$

η_c, η_x, dV/dr_c, η_0 being known from above.

The values of A and B may have to be modified to some extent if the liquid exhibits an extremely rapid drop of viscosity with increased shear, at low rates of shear. In the case shown, which is an extreme one, this modification had to be made to some extent. Fig. 3 shows the experimental $\eta \sim dV/dr$ curve to be about 50 sec.$^{-1}$ (given by the viscometer); as well as η_c, and η_x. The equation which appears to fit these values best is shown in dotted line.

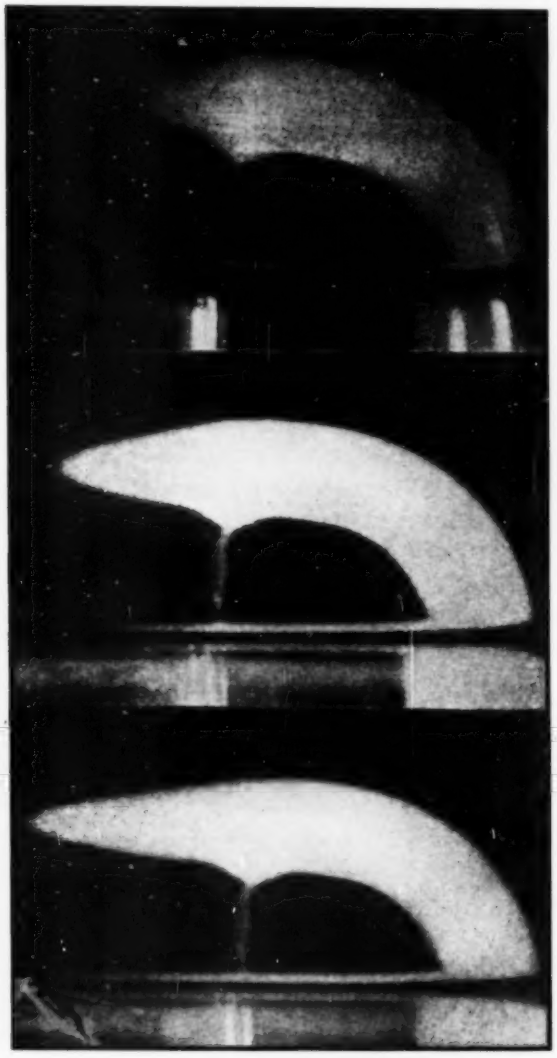

FIG. 5.

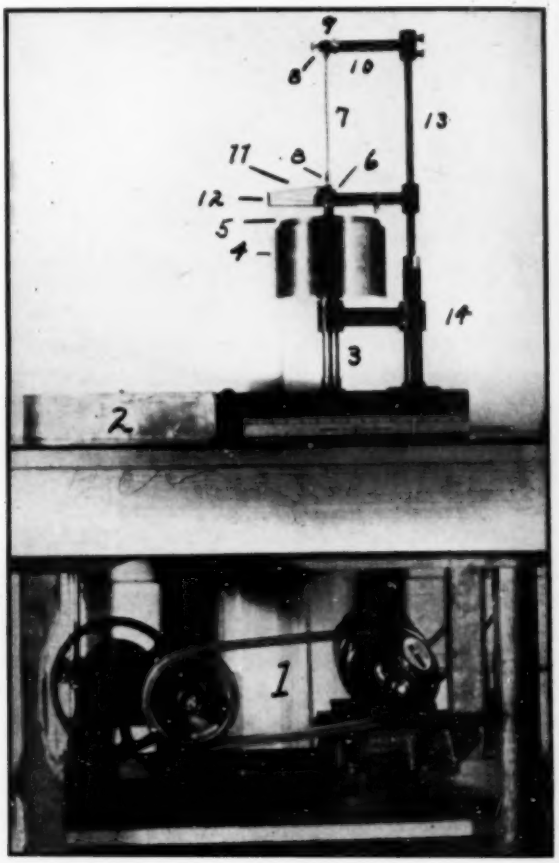

FIG. 6. Photograph of viscometer.

1. Driving mechanism powered by a ½-hp Reeves varispeed motor. Two changes of large pulley and wheel, along with two changes of drive gears gives a continuous speed variation to the rotating cylinder from about 0.2 to 5 r.p.s. This mechanism is mounted upon a separate table from that which supports the instrument, in order to prevent vibration from entering the viscometer.
2. Housing for V belt which drives viscometer. This belt connects horizontal pulley on vertical shaft of driving mechanism and one on vertical shaft which supports cylinder.
3. Shaft which supports and drives outer cylinder. Cylinder is removable.
4. Outer cylinder.
5. Inner cylinder, closed at bottom and top and weighted to sink in cellulose "solution" (sp. gr.: 1.1).
6. Ball-bearing to keep inner cylinder centered and/or supported. This bearing is engaged or disengaged (inner cylinder hanging free) at will. Its frictional resistance compared to the torque on the inner cylinder is quite negligible, however.
7. Torsion wire suspending inner cylinder.
8. Bayonet locks fastening wire to shaft of inner cylinder and centering head at top.
9. Centering head.
10. Support for torsion wire, vertically adjustable only.
11. 180° scale graduated in ½°.
12. Pointer attached to inner cylinder to measure deflection.
13. Support for inner cylinder assembly. It is removable from support (14) into which it slides, so that the whole assembly of inner cylinder, scale and suspension wire may be taken off together.

Ruler is graduated in inches.

From static considerations we obtain the two expressions for flux (Bingham and Ostwald).

For Bingham flow we have:

$$2\pi lr\left(\eta_\infty+\frac{A}{B-dV/dr}\right)\frac{dV}{dr}=-\pi r^2P,$$

where l=length of tube, P=pressure difference between ends, r=differential radius. From whence we derive a first-order, second-degree differential equation, which is solved by means of the quadratic formula, the roots of which are found to be real and unequal. This gives $V=f(r)$. By multiplying V by $2\pi r$, and integrating between $r=0$ and $r=a$, the Bingham expression for flux is obtained:

$$F=\frac{\pi Pa^4}{16\eta_\infty l}-\frac{\pi Da^3}{6}+\frac{\pi l\eta_\infty a^2}{4P}(2Qa-L)(Q^2a^2-QLa+D^2)^{\frac{1}{2}}-\frac{2\pi}{8Q}\int_{r=0}^{r=a}(2Qr-L)(Q^2r^2-QLr+D^2)^{\frac{1}{2}}rdr$$
$$+2\pi\int_{r=0}^{r=a}\left(\frac{4D^2-L^2}{16Q}\right)\ln\left\{\frac{(Q^2a^2-QLa+D^2)^{\frac{1}{2}}+Qa-L/2}{(Q^2r^2-QLr+D^2)^{\frac{1}{2}}+Qr-L/2}\right\}rdr, \quad (1)$$

where $D=A/\eta_\infty+B$; $L=2D-4B$; $A=P/2l\eta_\infty$. $-\pi Da^3/6$ is the constant term (independent of pressure) mentioned previously as the distance between Ostwald and Bingham asymptotes.

It is of interest to note that the first term is exactly $\frac{1}{2}$ of Poiseuille's value for a constant viscosity $=\eta_\infty$; and that the third and fourth terms approach this value as $P\to\infty$. The last term$\to 0$ as $P\to\infty$.

In the case of Ostwald flow, we perform a regular Poiseuille integration between $r=a$, and $r=2lS_0/P$; and then a Bingham one, as above, between $r=2lS_0/P$ and $r=0$, with the boundary condition that at $r=2lS_0/P$

$$V=\frac{P}{4l\eta_\infty}\left(a^2-\frac{4l^2S_0^2}{P^2}\right) \text{ from Poiseuille development.}$$

The results of these two are combined in one expression for Ostwald flow ($P>p$)

$$F=\frac{\pi P}{2l\eta_\infty}\left[\frac{a^4}{4}-\frac{4l^4S_0^4}{P^4}\right]+\frac{\pi l^3S_0^4}{P^3\eta_\infty}-\frac{4\pi Dl^3S_0^3}{3P^3}+\frac{\pi l^3S_0^3\eta_\infty}{P^3}\left[\frac{2QlS_0}{P}-L\right]\left[\frac{4Q^2l^2S_0^2}{P^2}-\frac{2QLS_0l}{P}+D^2\right]^{\frac{1}{2}}$$
$$-\frac{\pi}{4Q}\int_{r=0}^{r=2lS_0/P}(2Qr-L)(Q^2r^2-QLr+D^2)^{\frac{1}{2}}rdr$$
$$+\frac{\pi(4D^2-L^2)}{8Q}\int_{r=0}^{r=2lS_0/P}\ln\left\{\frac{\left(\frac{4Q^2l^2S_0^2}{P^2}-\frac{2QLS_0l}{P}+D^2\right)^{\frac{1}{2}}+\frac{2QlS_0}{P}-L/2}{(Q^2r^2-QL+D^2)^{\frac{1}{2}}+Qr-L/2}\right\}rdr. \quad (2)$$

The curves (Fig. 4) show $F\sim P$ for capillaries of the same $a/2l$ ratio, ($a=0.5$ mm, and 0.75 mm; $l=12$ mm and 18 mm) with the cellulosic "solution" used for Print 3. β is found to be at about the same pressure for both, as the theory would demand (25 lb./in.^{2}). The only correction of any importance is the entrance end one. This was effected by first obtaining $F\sim P$ curves with an orifice of capillary diameter, and then repeating the operation after attaching the capillary. The difference between the curves is probably as near the true $F\sim P$ relationship as can be obtained with reasonable effort. The value of η_ϵ and η_∞ are obtained from the lower curve (smaller capillary) as indicated previously. η_∞ is found to be 3.85 Poises; η_ϵ, 11.6 Poises. The Bingham (below β) and Ostwald (above β) curves are given by substitution of the values of A and B as found (and modified) in the preceding formulas Nos. 1 and 2. $A=31{,}250$; $B=1010$; $dV/dr_c=-3000$ sec.$^{-1}$. The curves plotted for both the large and small capillaries from these data agree with the experimental one rather well in the Bingham region; in the Ostwald region only in character. This is undoubtedly because there is no discontinuity between rever-

sibility and irreversibility in the viscosity∼rate of shear function at β, but only the quickening of a transition (in terms of time) at this point. It will be noticed that the calculated Bingham axis for the larger capillary is in fair agreement with the drawn one (parallel to the calculated Ostwald asymptote, and tangent to the curve). This offers opportunity for further mathematical work.

The graphical evaluation of the integrals in the expression for Flux (Bingham and Ostwald) is not difficult, for the $F=f(r)\cdot dr$ curves are single valued and fairly symmetrical from $r=0$ to $r=a$, and hence a few points, say at $r=\frac{1}{5}$, $\frac{2}{5}$, $\frac{3}{5}$, $\frac{4}{5}$ a, together with the known points of $f(r)dr=0$, at $r=0$, and at $r=a$, are all that are necessary to draw an accurate curve.

Summary

It is shown how the flux (through a tube) of certain fluids which show no yield value but do show structural viscosity, may be calculated with fair accuracy in the Bingham region. If we assume that the viscosity∼rate of shear relation is irreversible above S_0 (corresponding to β on the curve) the expression we derive for flux in this region agrees in character with the experimental curve obtained with the "solution" under discussion. The actual discrepancies between the two curves will, according to our theory, decrease as the transition from reversibility to irreversibility becomes more rapid (magnitude of the "progressive thixotropy"). In our case, the theory describes the transition as comparatively gradual.

Acknowledgments

It is indeed a pleasure to acknowledge thanks to: Dr. A. J. L. Moritz, Vice President and Technical Manager, for permission to publish this paper; Mr. J. J. Schilthuis, Chief Chemist, and Dr. G. I. Thurmond, Research Director, for sympathetic advice and assistance in the course of the work; Mr. E. C. Jolliff, Microscopist, for assistance in photography.

The Relation of Fluidity to Volume in Organic Liquids*

Eugene C. Bingham and Paul W. Kinney**

Department of Chemistry, Lafayette College, Easton, Pennsylvania

(Received July 12, 1939)

The Batschinski expression relating the fluidity of a compound to the specific volume at various temperatures is inadequate in the cases of associated compounds and those of high molecular weight. A modification, herein given, consists of the introduction of a correction term. The new expression, which relates linearly the fluidity and the corrected molecular free volume, has universal applicability and it holds with a high degree of precision. The constants of the new relationship are related to the complexity of the compounds in homologous series. From the constants given, the fluidity of undetermined members of the homologous series studied can be calculated if the density is known at that temperature.

Introduction

THIS paper is based on a series of investigations of the relationship existing between fluidity and molecular volume in pure organic liquids.

Using the valuable data obtained by Thorpe and Rodger in their experimental investigations, combined with experimental data of later workers including the unpublished data of Bayer,[1] and the theoretical work of Batschinski, Coombs[2] in 1934 under the direction of Professor E. C. Bingham began a thorough investigation of the relation between fluidity and volume. The work of

* Presented at the Tenth Annual Meeting of the Society of Rheology, held at Pittsburgh, Pennsylvania, December, 1938.

** Present address: Armstrong Cork Company, Lancaster, Pennsylvania.

[1] A. R. Bayer, Unpublished thesis, Lafayette College (1933).

[2] C. E. Coombs, Unpublished thesis, Lafayette College (1935).

Coombs was continued by Grant,[3] Holderith,[4] Stookey,[5] Kinney,[6] and Adams.[7]

Thorpe and Rodger,[8, 9] measured the viscosities and densities of 87 pure liquids at temperatures, ranging from 0°C to their boiling points. Their studies included a number of compounds of each of several homologous series including the aliphatic and aromatic hydrocarbons, alkyl ethers, bromides, chlorides, iodides and sulphides and aliphatic acids, acid anhydrides, alcohols, esters, ketones and aldehydes.

It was known that the fluidity increased with the temperature. Thorpe and Rodger found that the fluidities at a given temperature decreased successively as the molecular weight increased in a homologous series. This rule does not hold true in the case of the lower members of certain series, notably the aliphatic acids. Acetic acid is more fluid than formic acid; propionic acid is more fluid than acetic acid, and then butyric acid is less fluid than propionic acid, and the higher members behave in a normal fashion, that is, the fluidity decreases as the molecular weight increases.

This anomaly is attributed to association, since in other physical chemical measurements the low members of the acid series behave not as if they are simple, single molecules but as if they are associated into multi-molecular groups.

Batschinski[10, 11] indicated that the viscosity of a liquid is related to the specific volume by Eq. (1),

$$\eta = c/(v-\omega), \tag{1}$$

where η is the viscosity, v is the specific volume, i.e., the reciprocal of the density and c is the proportionality constant. The term ω is defined as the limiting volume or the value which v approaches as the viscosity approaches infinity. $(v-\omega)$ was named the "free volume." Batschinski himself, however, found that the relationship expressed by Eq. (1) did not hold in the case of associated substances, namely the lower acids and alcohols, water, etc., or even in nonassociated liquids of high molecular weight.

Equation (1) may be stated,

$$\phi = K(V-\Omega), \tag{2}$$

where ϕ is the fluidity, V is the molecular volume, K is the proportionality constant and Ω is the molecular limiting volume. Eq. (2) states that the fluidity is proportional to the molecular free volume.

When the fluidity at various temperatures is plotted against the molecular volume at the same temperature for the compounds of a homologous series, curves are obtained which are not linear at low fluidities but which instead appear to be hyperbolic.

Figure 1 shows a series of curves obtained when the fluidity ϕ is thus plotted against the molecular volume V in the case of the homologous series of n-alkyl bromides. The bromide series is typical and it is here given as an example because it is the most complete with respect to the fluidity data. It will be noted that the curves are apparently linear in the lower members of the series but as the complexity increases the curves lose their linearity. Batschinski's equation is apparently applicable to the lower members but not to the upper members. The same result has been obtained in the other series investigated.

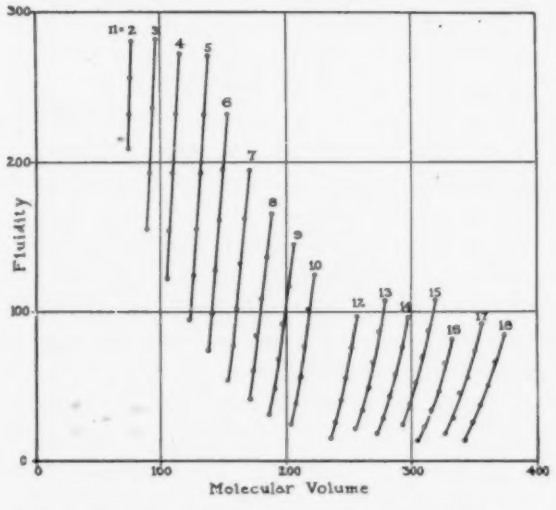

FIG. 1. Fluidity *vs.* molecular volume; bromide series.

[3] C. E. Grant, Unpublished thesis, Lafayette College (1936).
[4] A. E. Holderith, Unpublished thesis, Lafayette College (1936).
[5] D. Stookey, Unpublished thesis, Lafayette College (1937).
[6] P. W. Kinney, Unpublished thesis, Lafayette College (1938).
[7] H. Adams, Unpublished thesis, Lafayette College (1939).
[8] T. E. Thorpe and J. W. Rodger, Trans. Roy. Soc. (London) **A185**, II (1894).
[9] T. E. Thorpe and J. W. Rodger, Trans. Roy. Soc. (London) **A189** (1897).
[10] A. Batschinski, Zeits. f. physik. Chemie **84**, 643 (1913).
[11] A. Batschinski, Physik. Zeits. **13**, 1157 (1913).

New Relationship

Bingham and Coombs have developed an equation which fits the data much more accurately than Batschinski's equation. The new relationship is,

$$V = A\phi - \frac{B}{\phi} + C \tag{3}$$

where V and ϕ are, respectively, the molecular volume and fluidity, and A, B and C are constants of this hyperbolic equation.

The constants A, B and C of Eq. (3) have been calculated by use of the three-point method using the following equations:

$$A = \frac{V_2 - V_1}{\phi_2 - \phi_1} - \frac{B}{\phi_1\phi_2}, \tag{4}$$

$$B = \left(\frac{V_3 - V_2}{\phi_3 - \phi_2} - \frac{V_2 - V_1}{\phi_2 - \phi_1}\right) \Big/ \left(\frac{1}{\phi_2\phi_3} - \frac{1}{\phi_1\phi_2}\right), \tag{5}$$

$$C = -A\phi_1 + B/\phi_1 + V_1. \tag{6}$$

Each compound has a value of A, B and C. These values are given in Table I.

The hyperbolic equation (3) has been found to fit every curve. It holds for associated compounds and those of high molecular weight. The average percentage deviation between observed V and V calculated by use of the constants A, B and C for 50 compounds investigated is 0.05 percent, including associated compounds and those with chains of as high as 18 carbon atoms. As an example the observed molecular volumes and the molecular volumes calculated by use of Eq. (3) are given in Table II, for four members of the *n*-alkyl bromide series, representing 2, 6, 12 and 18 carbon atoms, respectively. The percentage deviation between observed and calculated V for the various compounds and the average percentage deviation for the various series are given in column 5 of Table I.

The fact that the Bingham-Coombs hyperbolic equation (3) requires three constants for each compound where the Batschinski equation required only two constants may at first appear cumbersome. However, it is shown later on in this paper how the three constants can be related to molecular complexity by rather simple relationships and thereby cut down the total number of constants needed in any homologous series of compounds.

The equation,

$$V - \Omega = A\phi, \tag{7}$$

where $A = 1/K$, is obtained from Eq. (2). Also by rearranging Eq. (3) it can be seen that this equation is very closely related to the rearranged Batschinski Eq. (7) and differs essentially only in the addition of a correction term to Eq. (7). Thus Eq. (8) is obtained,

$$V - C = A\phi - B/\phi. \tag{8}$$

Batschinski found his limiting volume Ω to be additive and he assigned values to several elements and to various molecular configurations. Bingham and Grant found the C term of Eq. (3) also to be additive and nearly identical to the Batschinski limiting volume Ω. The C term can be considered to be a limiting volume. The elemental values of limiting volume as calculated by Batschinski from Eq. (7) and those as calculated from Eq. (3) are given in Table III. For purposes of comparing the two equations, the limiting volume Ω as obtained by Batschinski can be applied without loss of validity. Hence Ω may be substituted for C in Eq. (8) to give,

$$V - \Omega = A\phi - B/\phi. \tag{9}$$

Eq. (9), which is the rearranged Bingham-Coombs equation, therefore differs from the Batschinski equation, as written in Eq. (7), only by the term $-B/\phi$.

In calculating C from additive Ω, no values are needed for the double bond or for the iso grouping, in the case of the new hyperbolic relationship.

The substitution of additive Ω for C in Eq. (9) is called restriction I. The average percentage deviation between observed and calculated values of V after restriction I is 0.11 percent for 98 compounds. Since there is a slight difference between C and Ω, there is a corresponding difference between the other two constants A and B of the hyperbolic equation. The values of A and B which were calculated using Ω in place of C are designated by the subscript 2. Thus A_2 and B_2 are the constants of Eq. (3) after restriction I. Eq. (3) becomes Eq. (10).

$$V = A_2\phi - B_2/\phi + \Omega. \tag{10}$$

The substitution of additive Ω for C has cut down the total number of constants needed in the calculation of molecular volume quite con-

siderably, since once the additive values of Ω have been evaluated, we do not need to calculate C for every compound. The value of Ω of Eq. (10) for any compound can be easily computed by use of the atomic limiting volumes in Table III.

The values of A_2, B_2 and Ω for the various

TABLE I. *The values of the constants A, B, C, A_2, B_2, Ω, A_3, B_3 and B_4 for various compounds studies and the percentage deviation between the observed molecular volumes and the molecular volumes calculated from the fluidity data by using the values of the constants in Eqs. (3), (10), (15) and (17), respectively.*

COMPOUND	A	B	C	% DEV.	A_2	B_2	Ω	% DEV.	A_3	B_3	% DEV.	B_4	% DEV.
n-Hydrocarbon Series													
Pentane	0.04420	0.00	96.07	—	0.04255	398.57	97.72	0.06	0.04541	890.7	0.20	719.6	0.33
Hexane	0.05505	93.65	113.67	0.01	0.05257	402.89	115.49	0.03	0.05257	407.4	0.03	543.1	0.31
Heptane	0.06067	445.71	133.53	0.01	0.06122	413.14	133.24	0.02	0.06158	454.2	0.04	428.4	0.05
Octane	0.07236	372.23	151.09	0.02	0.07241	352.50	151.00	0.02	0.07243	354.1	0.02	348.5	0.02
Nonane	0.09275	28.18	166.00	0.04	0.08619	286.75	168.76	0.04	0.08512	233.1	0.09	290.8	0.14
Decane	0.10130	204.53	185.94	0.02	0.10034	259.79	186.52	0.06	0.09966	236.8	0.06	247.1	0.05
Undecane	0.12337	124.56	202.29	0.05	0.11557	231.70	204.28	0.10	0.11604	238.9	0.10	213.3	0.14
Dodecane	0.13184	234.14	222.43	0.05	0.13392	209.67	222.04	0.05	0.13427	216.7	0.07	186.6	0.13
			Aver. =	0.03			Aver. =	0.05			0.08		0.15
n-Ether Series													
Diethyl ether	0.03368	−1,236.40	92.43	0.03	0.03672	634.00	89.61	0.05	0.03672	634.0	0.05	709.5	0.18
Ethyl propyl ether	—	—	—	—	0.04619	594.92	107.37	0.07	0.04666	656.6	0.09	586.8	0.13
Dipropyl ether	0.05573	578.23	126.43	0.05	0.05822	396.66	125.13	0.06	0.05727	329.6	0.07	502.5	0.42
Dibutyl ether	0.08399	200.16	158.95	0.03	0.08087	395.98	160.65	0.10	0.08049	375.8	0.10	393.4	0.09
Diamyl ether	0.11357	170.08	193.74	0.02	0.10575	325.98	196.17	0.09	0.10637	340.8	0.10	325.4	0.12
			Aver. =	0.03			Aver. =	0.07			0.08		0.19
n-Mercaptan Series													
Ethyl mercaptan	0.04134	−1,358.65	56.46	0.02	0.03521	−831.16	60.07	0.04	0.04113	−238.4	0.42	−305.6	0.48
Propyl mercaptan	0.04196	147.28	80.74	0.06	0.04782	−199.18	77.83	0.05	0.04782	−211.5	0.03	−145.5	0.32
Butyl mercaptan	0.06100	−404.12	93.01	0.10	0.05605	−81.92	95.59	0.04	0.05637	−47.9	0.06	−54.2	0.05
Amyl mercaptan	0.06390	109.24	114.60	0.03	0.06731	9.39	113.35	0.04	0.06677	−39.1	0.12	5.7	0.10
Hexyl mercaptan	0.07625	119.69	132.03	0.02	0.07918	58.65	131.11	0.03	0.07903	48.1	0.04	48.9	0.03
Heptyl mercaptan	0.08875	137.31	149.92	0.04	0.09429	91.63	148.87	0.06	0.09315	78.3	0.05	81.7	0.05
Octyl mercaptan	0.10763	115.63	167.04	0.02	0.11955	11.73	166.63	0.16	0.10911	193.6	(1.85)	107.5	(1.35)
Nonyl mercaptan	0.12745	97.44	184.00	0.03	0.12523	102.32	184.39	0.05	0.12694	132.0	0.11	128.6	0.10
			Aver. =	0.04			Aver. =	0.06			0.12		0.16
Thiol Series													
Propane thiol-2	—	—	—	—	0.05150	−498.76	77.83	0.07	0.04191	−1,254.6	0.79	−1,329.0	0.84
Pentane thiol-2	0.05607	431.04	117.12	0.06	0.06318	−6.31	113.35	0.09	0.06318	−29.9	0.08	−20.9	0.08
Hexane thiol-2	0.07378	77.06	131.58	0.03	0.07538	39.80	131.11	0.02	0.07567	55.5	0.05	38.8	0.05
Heptane thiol-2	0.09228	46.66	148.42	0.03	0.09000	64.80	148.87	0.03	0.08941	47.3	0.06	72.6	0.09
Octane thiol-2	0.10342	82.05	166.63	0.02	0.10350	86.45	166.63	0.02	0.10438	99.8	0.06	93.5	0.04
Nonane thiol-2	—	—	—	—	0.12176	89.82	184.39	0.02	0.12060	70.5	0.08	107.2	0.17
			Aver. =	0.04			Aver. =	0.04			0.19		0.21
n-Bromide Series													
Ethyl bromide	0.03753	340.67	67.74	0.01	0.05077	−426.38	61.33	0.05	0.05077	−426.4	0.05	−383.9	0.23
Propyl bromide	0.05090	187.18	82.21	0.01	0.05804	−128.02	79.09	0.07	0.05939	−71.9	0.13	−118.7	0.22
Butyl bromide	0.07032	0.00	96.71	0.12	0.07047	21.81	96.85	0.14	0.06942	−36.2	0.16	−16.1	0.12
Amyl bromide	0.07490	285.74	118.52	0.11	0.08492	−54.60	114.61	0.04	0.08087	−198.1	0.60	35.0	0.99
Hexyl bromide	0.09713	25.00	130.99	0.05	0.09161	102.52	132.37	0.05	0.09375	155.7	0.18	64.3	0.42
Heptyl bromide	0.10631	131.22	150.51	0.04	0.10747	102.39	150.13	0.02	0.10804	112.0	0.05	82.9	0.15
Octyl bromide	0.12319	129.16	168.15	0.08	0.12425	109.28	167.89	0.04	0.12376	88.4	0.11	95.4	0.07
Nonyl bromide	0.14584	89.02	184.70	0.05	0.13913	113.92	185.65	0.05	0.14089	129.1	0.11	104.3	0.14
Decyl bromide	0.17309	57.37	201.45	0.02	0.16154	127.46	203.41	0.12	0.15944	108.8	0.10	110.9	0.09
Dodecyl bromide	0.22520	73.79	236.34	0.06	0.19861	116.71	238.93	0.16	0.20081	125.9	0.17	119.8	0.18
Tridecyl bromide	0.21233	119.39	256.91	0.09	0.21950	126.48	256.69	0.04	0.22363	144.0	0.12	122.9	0.11
Tetradecyl bromide	0.26662	90.05	272.45	0.09	0.25358	139.47	274.45	0.11	0.24786	123.7	0.11	125.5	0.11
Pentadecyl bromide	0.26036	157.20	293.05	0.08	0.26514	134.05	292.21	0.04	0.27351	173.6	0.19	127.6	0.21
Hexadecyl bromide	0.31434	114.90	309.91	0.08	0.29491	126.85	309.97	0.16	0.30059	141.1	0.19	129.3	0.17
Heptadecyl bromide	0.33739	123.59	327.56	0.05	0.33968	146.47	327.73	0.14	0.32908	110.5	0.15	130.7	0.16
Octadecyl bromide	0.41086	79.97	341.35	0.18	0.36586	150.68	345.49	0.22	0.35900	124.6	0.19	132.0	0.22
			Aver. =	0.07			Avgr. =	0.09			0.16		0.22
n-Acid Series													
Formic acid	0.02011	35.89	37.27	0.02	0.02104	25.32	37.06	0.04	0.02104	25.4	0.04	373.1	(10.12)
Acetic acid	0.03710	90.32	55.27	0.04	0.03836	53.36	54.82	0.04	0.03154	−105.1	0.92	220.2	(3.72)
Propionic acid	0.04428	213.23	72.94	0.07	0.04560	186.37	72.58	0.06	0.04437	160.1	0.16	161.8	0.15
Butyric acid	0.06701	56.26	88.37	0.06	0.05769	140.91	90.34	0.11	0.05720	134.2	0.11	130.0	0.11
Caproic acid	0.09049	115.24	126.09	0.03	0.09254	106.37	125.86	0.03	0.08909	88.6	0.17	95.5	0.22
Heptoic acid	0.13560	51.02	140.91	—	0.10980	100.18	143.62	0.18	0.10736	89.5	0.22	84.9	0.25
Caprylic acid	—	—	—	—	0.11135	110.48	161.38	0.17	0.12720	157.3	0.64	76.7	0.99
Lauric acid	0.22001	121.00	234.58	0.11	0.24127	79.41	232.42	0.13	0.22208	22.3	0.67	56.4	0.44
Myristic acid	—	—	—	—	0.25569	79.26	267.94	0.04	0.27886	88.7	0.08	50.1	0.76
Palmitic acid	—	—	—	—	0.33531	87.25	303.46	0.07	0.34186	93.5	0.09	45.3	0.62
Stearic acid	0.37731	377.31	382.44	—	0.41927	49.68	338.98	0.21	0.41109	28.6	0.34	41.4	0.26
			Aver. =	0.06			Aver. =	0.10			0.31		0.42
n-Alcohol Series													
Methyl alcohol	0.01278	190.20	39.46	0.01	0.02107	−88.78	36.33	0.16	0.02641	103.4	(1.09)	−236.0	(4.50)
Ethyl alcohol	0.02407	109.67	57.40	0.01	0.03662	−84.20	54.09	0.26	0.03662	−84.2	0.26	−103.4	0.33
Propyl alcohol	0.02970	92.50	75.59	0.13	0.04798	−50.79	71.85	0.46	0.04710	−61.6	0.53	−48.2	0.56
Butyl alcohol	0.04348	65.36	92.15	—	0.05815	−5.22	89.61	0.59	0.05784	−8.6	0.65	−16.4	0.67
Heptyl alcohol	0.08214	50.98	142.98	0.14	0.08641	56.85	142.89	0.16	0.09163	79.9	0.60	31.6	0.78
Octyl alcohol	0.13105	23.58	158.58	0.14	0.10248	43.78	160.65	0.39	0.10342	46.1	0.41	40.8	0.39
Octadecyl alcohol	—	—	—	—	0.23811	78.79	302.73	0.07	0.23563	77.6	0.09	83.3	0.11
			Aver. =	0.08			Aver. =	0.30			0.42		0.47

compounds studied are given in Table I, together with the percentage deviation between observed molecular volumes and those calculated by use of Eq. (10). In Table II are given four typical members of the *n*-alkyl bromide series, showing the observed and calculated molecular volume, calculated from the fluidity at various temperatures, after restriction I.

Study of Constants A and B

The constants A_2 and B_2 of Eq. (10) were investigated to determine how they varied from compound to compound in a homologous series. Eq. (7) and Eq. (9) both show that the fluidity is proportional to the free volume. In the first case it has been shown that the Batschinski expression is only an approximation and that in reality the fluidity is proportional to a "corrected free volume." This corrected free volume expression, since it holds true in every case, may be considered a fundamental property and may be designated by the term F. Eq. (11) expresses the foregoing statement.

$$F = A_2\phi, \tag{11}$$

where $(V-\Omega)+B_2/\phi$ is the corrected free volume F. The proportionality factor A_2 of Eq. (11) is a very important constant. It has been designated by Stookey as the "rheolar free volume" and is theoretically defined as the free volume necessary to give unit fluidity to a liquid. Eq. (12) may further clarify the rheolar free volume relationship.

$$A_2 = F/\phi. \tag{12}$$

A_2 has a different value for each compound. The value of A_2 for the various members of a homologous series becomes larger as we increase the molecular complexity of the compounds of the series. That is, in the larger molecules more free volume is needed to give the same fluidity. Fig. 2 gives the curve obtained when the values of A_2 are plotted against the number of carbon atoms in the case of the *n*-alkyl bromides. Similar curves are obtained in the cases of the other

Table I (*Continued*).

Compound	A	B	C	% Dev.	A_2	B_2	Ω	% Dev.	A_3	B_3	% Dev.	B_4	% Dev.
Ester Series													
Methyl formate	0.04460	−916.35	45.57	—	0.02802	355.6	54.82	0.06	0.02802	355.7	0.06	1,068.0	(4.30)
Ethyl formate	0.04552	−256.56	67.93	—	0.03697	356.5	72.58	0.05	0.03663	332.0	0.04	787.3	(2.20)
n-propyl formate	0.05037	74.13	87.81	—	0.04544	365.7	90.34	0.06	0.04584	391.9	0.09	634.0	(1.09)
n-butyl formate	0.06117	86.62	107.51	—	0.05963	131.9	108.10	0.01	0.05564	20.7	0.26	535.9	(2.86)
n-butyl acetate	0.06987	167.73	123.58	—	0.06448	363.1	125.86	0.10	0.06602	428.1	0.19	467.2	0.28
n-butyl *n*-propionate	0.08367	174.26	140.06	—	0.07404	439.6	143.62	0.13	0.07700	535.0	0.31	416.0	0.38
Ethyl *n*-valerate	—	—	—	—	0.07461	430.05	143.62	0.15	0.07700	507.1	0.23	416.0	0.34
n-butyl *n*-butyrate	0.09595	186.88	157.45	—	0.08343	431.22	161.38	0.17	0.08857	552.1	0.40	376.3	0.64
n-butyl *n*-valerate	0.11272	137.38	174.97	—	0.09699	353.8	179.14	0.15	0.10073	417.7	0.25	344.3	0.32
Ethyl *n*-heptylate	—	—	—	—	0.09578	361.99	179.14	0.18	0.10073	444.6	0.33	344.3	0.43
n-heptyl acetate	—	—	—	—	0.10733	286.98	179.14	0.22	0.10073	207.2	0.42	344.3	0.74
n-amyl *n*-butyrate	0.10878	178.21	176.06	—	0.09800	343.79	179.14	0.14	0.10073	392.2	0.20	344.3	0.23
n-hexadecyl acetate	0.36388	90.94	332.12	—	0.26169	174.09	338.98	0.18	0.23674	135.9	0.38	204.4	0.63
							Aver.	=0.12			0.24		0.44
Miscellaneous Hydrocarbons													
Benzene	0.03260	404.88	86.47	—	0.05016	−200.70	79.80	0.03	—	—	—	—	—
Toluene	0.05337	−59.18	96.90	—	0.05182	9.88	97.56	0.05	—	—	—	—	—
o-xylene	0.06010	101.03	114.40	—	0.05767	175.71	115.32	0.06	—	—	—	—	—
m-xylene	0.05989	−32.63	112.79	—	0.05456	233.07	115.32	0.07	—	—	—	—	—
p-xylene	0.05615	142.06	115.11	—	0.05586	176.43	115.32	0.03	—	—	—	—	—
Isoprene	0.04514	−1,537.37	77.17	—	0.04247	−855.12	79.88	0.02	—	—	—	—	—
Diallyl	0.04261	161.41	104.09	—	0.05108	−1,029.14	97.64	0.07	—	—	—	—	—
Isopentane	0.04831	−661.14	93.64	—	0.04308	278.5	97.72	0.04	—	—	—	—	—
Isohexane	0.04715	954.48	118.01	—	0.05106	286.42	115.49	0.52	—	—	—	—	—
Isoheptane	0.06014	432.39	133.08	—	0.05724	498.74	133.24	0.65	—	—	—	—	—
Miscellaneous Halides													
Allyl chloride	0.03765	114.75	70.80	—	0.04297	−351.69	67.61	0.03	—	—	—	—	—
Propyl chloride	0.04500	−33.10	75.59	—	0.04349	110.22	76.53	0.02	—	—	—	—	—
Isopropyl chloride	0.05188	−714.39	73.18	—	0.04618	−229.11	76.53	0.02	—	—	—	—	—
Isobutyl chloride	0.05430	−64.15	93.69	—	0.05307	28.25	94.29	0.08	—	—	—	—	—
Carbon tetrachloride	0.06702	115.17	90.76	—	0.09171	−305.03	84.00	0.27	—	—	—	—	—
Isopropyl bromide	0.04988	245.62	85.02	—	0.06327	−391.0	79.09	0.06	—	—	—	—	—
Isobutyl bromide	0.06484	171.43	103.19	—	0.08046	−423.04	96.85	0.24	—	—	—	—	—
Methyl iodide	0.04224	−84.67	53.20	—	0.04037	−9.40	53.96	0.01	—	—	—	—	—
Ethyl iodide	0.05123	112.37	72.49	—	0.05319	41.18	71.72	0.02	—	—	—	—	—
Propyl iodide	0.06408	102.66	89.45	—	0.06460	115.58	89.48	0.07	—	—	—	—	—
Isopropyl iodide	0.06726	35.54	90.17	—	0.06902	−22.64	89.48	0.04	—	—	—	—	—
Isobutyl iodide	0.07142	230.53	108.62	—	0.07502	108.50	107.24	0.06	—	—	—	—	—
Acid Anhydrides													
Acetic anhydride	0.05799	124.67	89.75	—	0.05418	218.11	91.07	0.13	—	—	—	—	—
Propionic anhydride	0.07654	183.92	123.84	—	0.06767	358.81	126.59	0.20	—	—	—	—	—

series investigated. The curve of A_2 *vs.* n is found to be parabolic, obeying the equation,

$$A_2 = a + bn + cn^2 \qquad (13)$$

where n represents the number of methylene groups in the molecule. The validity of Eq. (13) can be shown by taking the first derivative of Eq. (13) to give,

$$dA_2/dn = b + 2cn. \qquad (14)$$

In Fig. 2, $\Delta A_2/\Delta n$ is plotted against n. The resulting straight line proves the validity of Eq. 14.

The various terms of the parabolic equation all have theoretical justification. The "a" term is not dependent upon the number of carbon atoms and is the free volume which must be supplied by the residue, i.e., the H_2, HBr, HS, etc.; the "b" of the "bn" term must be the rheolar free volume value of a single CH_2 group and therefore in a chain, the value of a single CH_2 group is multiplied by the number of carbon atoms. These two terms alone would satisfy the straight line relationship $A_2 = a + bn$, which is what would be expected when a number of CH_2 groups and a residue are involved. There is still another term, the "cn^2" term for which we must account. The fact that the length of the chain is squared suggests that an area is involved. If the chain may be considered to be rotating in propellor fashion, then the effective volume, or volume of influence, of the molecule is not alone that of the actual molecule itself. The influence of the area of rotation must be taken into account.

We find an illustrative parallel to this n-squared relationship in the work of Staudinger[12] on the viscosity of solutions of long chain molecules. He finds that the range of action in solution of the thread molecules does not increase

[12] H. Staudinger, *Die hochmolekülaren organischen Verbindungen Kautschuk und Cellulose* (J. Springer, Berlin, 1932).

TABLE II. *Example of calculation of molecular volumes at various temperatures from the fluidities at the same temperatures by use of the Bingham-Coombs equation and after restrictions I, II and III, respectively.*

T°C	ϕ	$\frac{V \text{ (OBS.) MOL. WT.}}{\text{SP. GR.}}$	V (CALC.) EQ. (3)	% DEV.	V (CALC.) AFTER REST. I	% DEV.	V (CALC.) AFTER REST. II	% DEV.	V (CALC.) AFTER REST. III	% DEV.
					Ethyl Bromide					
0	209.2	73.96	73.96	0.00	73.99	0.04	73.99	0.04	73.79	0.23
10	231.7	74.96	74.97	0.01	74.93	0.04	74.93	0.04	74.75	0.28
20	255.1	76.00	75.97	0.04	75.95	0.07	75.95	0.07	75.78	0.29
30	280.1	77.03	77.03	0.00	77.07	0.05	77.07	0.05	76.92	0.14
			Aver. = 0.01			0.05		0.05		0.23
					Hexyl Bromide					
0	73.4	137.79	137.78	0.01	137.69	0.07	137.13	0.48	138.37	0.42
20	99.1	140.43	140.37	0.04	140.42	0.01	140.07	0.26	141.01	0.41
40	128.4	143.27	143.27	0.00	143.33	0.04	143.20	0.05	143.91	0.45
60	161.0	146.45	146.44	0.01	146.43	0.02	146.49	0.03	147.06	0.42
80	195.5	149.85	149.85	0.00	149.76	0.06	149.90	0.03	150.37	0.35
100	231.5	153.01	153.37	0.24	153.14	0.08	153.40	0.25	153.79	0.51
			Aver. = 0.05			0.05		0.18		0.43
					Dodecyl Bromide					
0	15.0	235.34	234.80	0.23	234.13	0.51	233.55	0.76	233.95	0.59
20	26.2	239.35	239.42	0.03	239.68	0.14	239.38	0.01	239.62	0.11
40	40.4	243.61	243.61	0.00	244.06	0.18	243.92	0.13	244.07	0.19
60	57.1	247.97	247.91	0.02	248.23	0.10	248.20	0.10	248.30	0.13
80	76.4	252.58	252.58	0.00	252.57	0.00	252.62	0.02	252.70	0.05
100	97.0	257.14	257.42	0.11	257.00	0.05	257.11	0.01	257.17	0.01
			Aver. = 0.06			0.16		0.17		0.18
					Octadecyl Bromide					
40	13.0	342.72	340.54	0.64	338.66	1.18	340.58	0.62	340.01	0.79
60	26.6	349.28	349.27	0.00	349.55	0.08	350.36	0.31	350.08	0.23
80	37.5	355.15	354.63	0.15	355.19	0.01	355.63	0.14	355.43	0.08
100	50.7	361.21	360.60	0.17	361.25	0.01	361.23	0.01	361.09	0.03
120	67.2	367.77	367.77	0.00	367.84	0.02	367.76	0.00	367.65	0.03
140	84.2	374.47	374.99	0.14	374.50	0.01	374.24	0.06	374.15	0.19
			Aver. = 0.18			0.22		0.19		0.22

proportionally to the length of the molecule but to the square of the length. In the case of very long molecules the effect of the "a" and "bn" terms of our parabolic equation would be negligible with respect to the effect of the "cn^2" term. At the limiting viscosity the volume of the solvent available is just equal to the effective volume of the dissolved thread molecules, so that the molecules no longer possess freedom of movement. In our considerations a rough parallel might be drawn between Staudinger's volume of solvent and our free volume; between his volume of limiting viscosity, i.e., the volume of solvent plus volume of molecules and our molecular volume; between his volume of molecules and our limiting volume; and between his range of action in solution and our effective volume. The comparison cannot be carried beyond the qualitative stage, however. The fact that the n squared relationship occurs in both realms is the significant relationship.

The values of a, b and c of parabolic equation (13) for the various series studied are given in Table IV. The values of A calculated by use of Eq. (13) were given the subscript 3. Restriction II comprises the substitution of A_3 in the hyperbolic equation (3) to give,

$$V=(a+bn+cn^2)\phi-B_3/\phi+\Omega. \qquad (15)$$

The average percentage deviation between observed values of volume and those calculated using Eq. (15) is 0.20 percent for 72 compounds. The values of A_3 and B_3 for the various compounds studied are given in Table I, together with the percentage deviation between observed molecular volumes and those calculated by use of Eq. (15). In Table II are given four typical members of the n-alkyl bromide series, showing the observed and calculated molecular volume, calculated from the fluidity at various temperatures, after restriction II.

TABLE III. *Values of limiting volume from Batschinski and from Bingham-Coombs equation.*

Element or Group	Batschinski Values	Grant's Bingham-Coombs Values
C	8.8	8.84
H	4.3	4.46
CH_2	17.4	17.76
O	8.6	9.65
S	19.0	15.63
Cl	19.2	18.79
Br	24.8	21.35
I	32.0	31.74
Double Bond	3.3	0
iso-	0.7	0

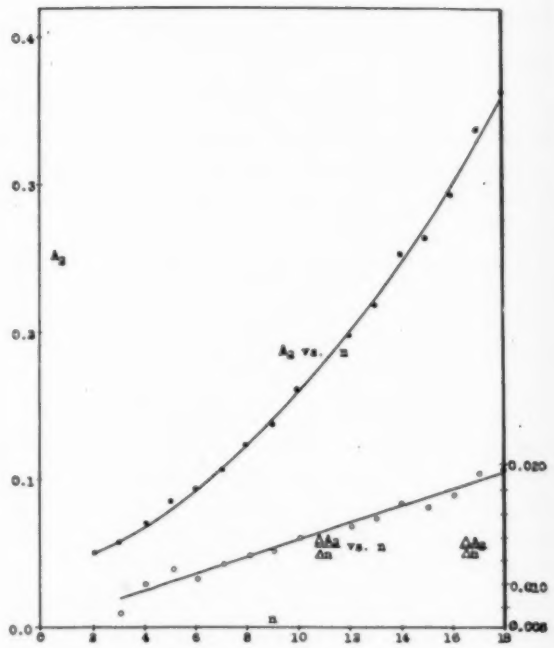

FIG. 2. Parabolic relationship between A_3 and n for bromide series. Also linear relationship between $\Delta A_3/\Delta n$ and n.

TABLE IV. *Values of constants of Eq. (13) and of Eq. (16).*

Series	a	b	c	d	f	E
Bromides	0.03780	0.00506	0.00071	−3.2406	−1.7211	144
Hydrocarbons	0.03727	−0.00298	0.00092	3.9350	−1.5421	0
Mercaptans	0.03331	0.00205	0.00093	−3.0399	−0.6354	400
Thiols	0.01930	0.00567	0.00062	−3.8789	−2.3551	150
Alcohols	0.01645	0.00983	0.00013	−2.5866	−0.6071	150
Esters	0.01256	0.00714	0.00030	3.2554	−0.7529	0
Acids	0.01210	0.00816	0.00078	2.5718	−0.7607	0
Ethers	0.00361	0.00694	0.00033	3.3630	−0.8505	0

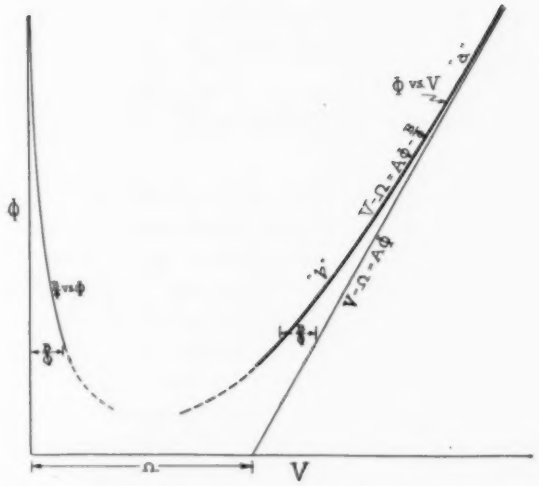

FIG. 3. Interrelations of the functions of Φ and V. "a"—Batschinski region. "b"—Hyperbolic region.

Consideration of the significance of the B/ϕ term and the B_3 constant now follows. The B/ϕ term is the difference between the Batschinski equation and the Bingham-Coombs equation and is therefore the most significant part of these researches involving the new relationship. The difference between the two equations is better understood by the graphical illustration given in Fig. 3. The straight line corresponding to the equation $V-\Omega=A\phi$ is the Batschinski relationship. The hyperbolic equation is defined by the equation $V-\Omega=A\phi-B/\phi$. In other words the B/ϕ term indicates, and is a measure of, the departure of the hyperbola from the straight line. It is possible to make the degree of deviation more clear by plotting ϕ against B/ϕ. It will be noted that as ϕ increases B/ϕ decreases and the hyperbola approaches the straight line. In this fact lies the reason why Batschinski made his relationship one of a straight line. He worked in the region of high fluidity. The fluidity in the case of the lower members of a given series is, at the temperature of measurement (0°C to the boiling point), rather high and therefore in such compounds as pentane, hexane, diethyl ether, etc. Batschinski did obtain straight lines. These straight lines are in reality the asymptotes of the true hyperbolas.

As shown by Volkman and Petrokubi,[13] who studied the fluidity of pentane at temperatures as low as −70°C, the straight line obtained by Batschinski becomes the characteristic hyperbola at low fluidities. This observation emphasizes the importance of the magnitude of the fluidity at which the comparisons are made.

The need for the correction term B/ϕ has been attributed to the effect of intermolecular attraction. Nearly all the values of B/ϕ are positive. Certain compounds, especially those of high fluidity, have negative values of B. Inaccuracies in application of the three-point method for the calculation of B probably accounts for these negative values.

When the values of B_3, calculated after restriction II, are plotted against the number of carbon atoms, curves are obtained similar to those shown in Fig. 4. These curves appear to be hyperbolic and obey roughly the equation

$$B_3=E\pm dn^f, \tag{16}$$

where E is the horizontal asymptote and d and f are constants. The sign of the dn^f term is positive for curves of which that of the hydrocarbons is typical and negative for curves of which the curve of the bromides is typical.

The curves obtained above appear, at first consideration, to be poor but it must be pointed out that the B_3/ϕ term of the hyperbolic equation is never more than 3 percent of the molecular volume V and is usually much less than 3 percent, so that quite a variation in the value of B_3 will not greatly effect the value of V.

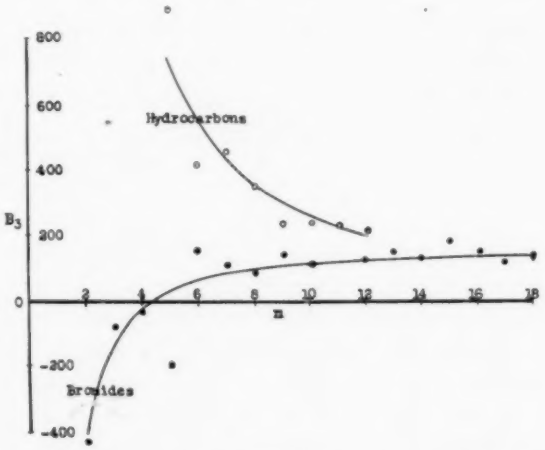

FIG. 4. Hyperbolic relationship between B_3 and n. The open-circle curve is for hydrocarbons and the closed-circle curve for bromides.

[13] R. G. Volkman and J. L. Petrokubi, Unpublished thesis, Lafayette College (1936).

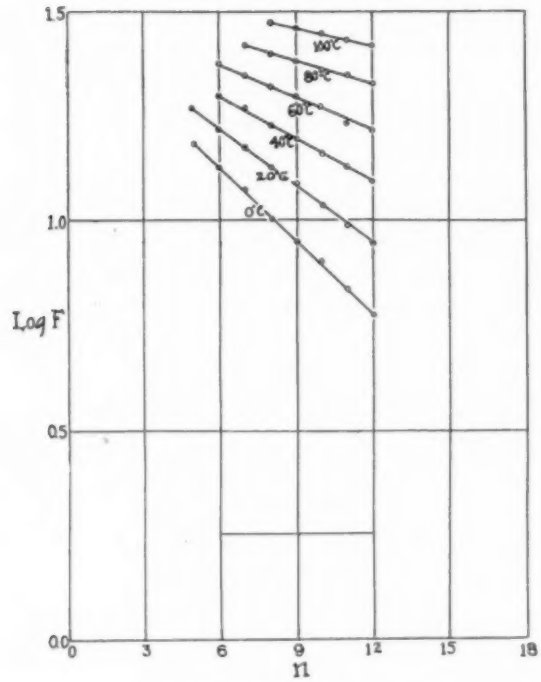

FIG. 5. Log F *vs.* n-hydrocarbons.

The values of B_3 calculated by use of Eq. (16) are given the subscript 4. Restriction III comprises the substitution of B_4 into the Bingham-Coombs hyperbolic equation to give equation

$$V=(a+bn+cn^2)\phi-\frac{E\pm dn^f}{\phi}+\Omega. \qquad (17)$$

The average percentage deviation between calculated values of V after restriction III is 0.2 percent for unassociated series. Association appears to affect the calculated values of B_3 although due to the possibilities for accumulated error in B_3 the degree of association cannot be calculated. For the "associated" series, if we do not consider the highly associated formic acid, acetic acid, methanol and the lower esters, we have an average percentage deviation of 0.4 percent.

The values of B_4 for the various compounds studied are given in Table I, together with the percentage deviation between observed molecular volumes and those calculated by use of Eq. (17). In Table II are given four typical members of the n-alkyl bromide series, showing the observed and calculated molecular volume, calculated from the fluidity at various temperatures, after restriction III.

TABLE V. *Corrected free volume F at various temperatures, observed and calculated for aliphatic n-hydrocarbons.*

Number of C atoms	0°C		20°C		40°C		60°C		80°C		100°C	
	Obs.	Calc.	Obs.	Calc.	Obs.	Calc.	Obs.	Calc.	Obs.	Calc.	Obs.	Calc.
5	15.13	15.17	18.32	18.32	—	—	—	—	—	—	—	—
6	13.32	13.32	16.38	16.50	19.86	19.83	23.83	23.57	—	—	—	—
7	11.83	11.69	14.93	14.86	18.35	18.32	22.14	22.20	26.37	26.23	—	—
8	10.16	10.26	13.44	13.38	16.91	16.92	20.74	20.91	24.95	25.08	29.57	29.67
9	9.09	9.00	12.15	12.06	15.58	15.63	19.68	19.69	23.96	23.96	28.86	28.76
10	7.95	7.90	10.88	10.85	14.42	14.44	18.46	18.55	22.81	22.91	27.89	27.87
11	6.91	6.93	9.73	9.78	13.36	13.34	16.90	17.47	21.96	21.90	27.00	26.99
12	6.01	6.09	8.76	8.81	12.32	12.33	16.54	16.45	20.96	20.93	26.14	26.17

TABLE VI. *Corrected free volume F at various temperatures, observed and calculated for aliphatic n-acids, along with calculated apparent associations of lower members.*

No. of C atoms	60°C			80°C			100°C			Average Association
	Obs.	Calc.	Ratio Calc./Obs.	Obs.	Calc.	Ratio Calc./Obs.	Obs.	Calc.	Ratio Calc./Obs.	
1	2.39	7.99	3.34	3.09	10.17	3.19	3.85	12.02	3.12	3.22
2	5.50	7.52	1.37	6.86	9.74	1.42	8.31	11.74	1.41	1.40
3	6.85	7.08	1.03	8.42	9.32	1.11	9.99	11.47	1.15	1.10
4	6.74	6.66	0.99	8.61	8.92	1.04	10.66	11.20	1.05	1.03
6	6.18	5.90	0.96	8.31	8.18	0.98	10.61	10.67	1.01	0.98
7	5.55	5.55	1.00	7.87	7.83	1.00	10.73	10.43	0.97	0.99
8	4.99	5.23	1.05	7.35	7.50	1.02	9.95	10.18	1.02	1.03
12	4.16	4.10	0.99	6.62	6.31	0.95	10.22	9.26	0.91	0.95
14	3.58	3.63	1.01	5.36	5.78	1.08	8.38	8.83	1.05	1.05
16	—	—	—	5.44	5.30	0.97	8.04	8.42	1.05	1.01

Calculation of Fluidity from Volume Data

If it is desired to calculate the fluidity when the volume is known, this can be done by use of the equation

$$\phi=\frac{V-\Omega}{2A_3}+\left(\frac{B_4}{A_3}+\left(\frac{V-\Omega}{2A_3}\right)^2\right)^{\frac{1}{2}}. \qquad (18)$$

A value of this research, aside from theoretical interest, is that we can calculate very accurately the fluidity of any member of the series investigated at any temperature if we know the density of the material at that temperature. The normal straight-chain series of aliphatic hydrocarbons, ethers, bromides, acids, alcohols, esters, mercaptans and thiols have been investigated.

The values of A_3 and B_4 for any member of these series can be calculated by use of Eqs. (13) and (16), using constants given in Table IV. The value of Ω for the member can be obtained by using the additive values of limiting volume given in Table III.

Free Volume *Versus* Chain Length

The results of our investigations lead us to believe that the corrected free volume is a fundamental property and therefore should have a definite relation to the complexity of the members of a homologous series. The corrected free volume F has been found to be related exponentially to the number of carbon atoms in the various series at any chosen temperature. This relationship is expressed

$$F=De^{-Kn}, \qquad (18)$$

where D and K are constants.

Figure 5 shows the linear curves obtained when the logarithm of the corrected free volume F is plotted against the number of carbon atoms at the various temperatures for the hydrocarbon series. Similar sets of curves are obtained in the cases of bromides, ethers, thiols and mercaptans series. Table V gives the values of F observed and calculated by Eq. (18). The "observed" values are $(V-\Omega)+B/\phi$.

In the case of series in which the lower members are associated, the results shown in Fig. 6 are obtained. This acid series may be regarded as typical. The deviation of the lower members from the straight line drawn through the upper members of the series gives us a method for the calculation of the degree of association. Thus it has been found that the ratio of the calculated free volume to the observed free volume is equal to the apparent molecular association. The values of observed and calculated F are given in Table VI, along with the degree of association. The associations calculated in this manner compare favorably with those calculated by other workers. Similar curves were obtained for the esters series but no good curves could be obtained for the alcohols.

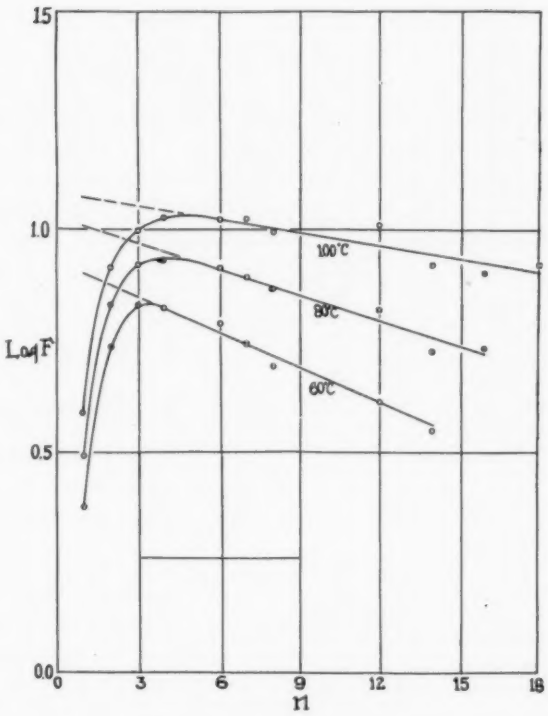

Fig. 6. Log F *vs.* n-acids.

The authors wish to acknowledge indebtedness to Coombs, Grant, Holderith and Stookey for liberal use of their calculations and results.

Summary

1. A new relationship between fluidity and volume is given. In it a correction term is applied to the Batschinski equation which states that the fluidity is proportional to the free volume. The Batschinski equation is limited in its application. The new equation is universal.

2. The three constants necessary in the new equation are studied. C is found to be additive and closely related to the Batschinski limiting volume. The limiting volume is regarded as the volume of the atoms themselves.

3. The other two constants of the new equation are related to the number of carbon atoms of the members of homologous series.

4. The need for the B/ϕ correction term is attributed to intermolecular attraction at low temperatures (and low fluidities).

5. The corrected free volume is a fundamental property. The fluidity is proportional to the corrected free volume.

6. In a given series and at any chosen temperature, the corrected free volume is related exponentially to the number of carbon atoms in the chain.

Conductivity Measurements on Potassium Halides

CORNELIUS G. BRENNECKE
University of Toledo, Toledo, Ohio.

(Received August 18, 1939)

The electrical conductivities of flat crystal plates of KBr and KCl were measured over a temperature range of from 25°C to 600°C, at stresses of from 0.05 to 0.90 kv/cm. Ohm's law was found to hold, when cold conductivities were measured after preliminary heating. Current-time data indicated an exponential decay of current with time at the lower temperatures, and a current constant with time at the higher temperatures. An exponential relation between conductivity and temperature was found to hold for both KBr and KCl, but in the latter case an abrupt change in the slope of the curve was found to take place at a temperature between 200°C and 250°C.

INTRODUCTION

WHILE much work has been done on the electrical characteristics of dielectric materials, the complexity of the subject seems to justify additional research, since only sufficient data will make it possible finally to correlate all the phenomena involved with a relatively simple theory.

In simple ionic crystals such as the alkali halides, at normal temperatures and low field strengths, metallic conduction is absent because of the closed configuration of the ions.[1] The current observed under such conditions is now ascribed by many[1–4] to a "lattice conductivity"; that is, to the presence of points in the crystal lattice from which the ions are missing, and to a resultant ionic migration under the influence of the field. The current furthermore seems to be a linear function of the field;[5] i.e., to obey Ohm's law. When, however, still at normal temperatures, potential differences approaching the order of magnitude of the breakdown potential are applied across the crystals, Ohm's law no longer holds,[6] and the relation between current and voltage becomes exponential, somewhat in the manner first predicted by Poole.[7] The equation proposed by Poole is

$$\kappa = ae^{bx} \qquad (1)$$

where κ is the conductivity, x the field strength, and a and b arbitrary constants, but it gives only a first approximation to experimental data. On the basis of much work[8] in this field, von Hippel concludes that the phenomena in the region of breakdown are chiefly electronic in nature: Electrons locally bound to the lattice points become first excited and then conducting, moving in preferential lattice directions. If sufficiently accelerated by the field, these electrons ionize by impact. The ionization becomes cumulative,

[1] N. F. Mott, Trans. Faraday Soc. **34**, 822 (1938).
[2] W. Schottky, Zeits. f. physik. Chemie **29**, 335 (1935).
[3] A. Smekal, Physik. Zeits. **37**, 150 (1936).
[4] E. Koch and C. Wagner, Zeits. f. physik. Chemie **38**, 295 (1937).
[5] A. Wenderowitsch and R. Drisina, Zeits. f. Physik **98**, 108 (1935).
[6] F. Quittner, Physik. Zeits. Sowjetunion **11**, 359 (1937).
[7] H. H. Poole, Phil. Mag. **32**, 112 (1916); **34**, 195 (1917); **42**, 488 (1921).
[8] A. von Hippel, Zeits. f. Physik **75**, 145 (1932); J. App. Phys. **8**, 815 (1937); Phys. Rev. **54**, 1096 (1938).

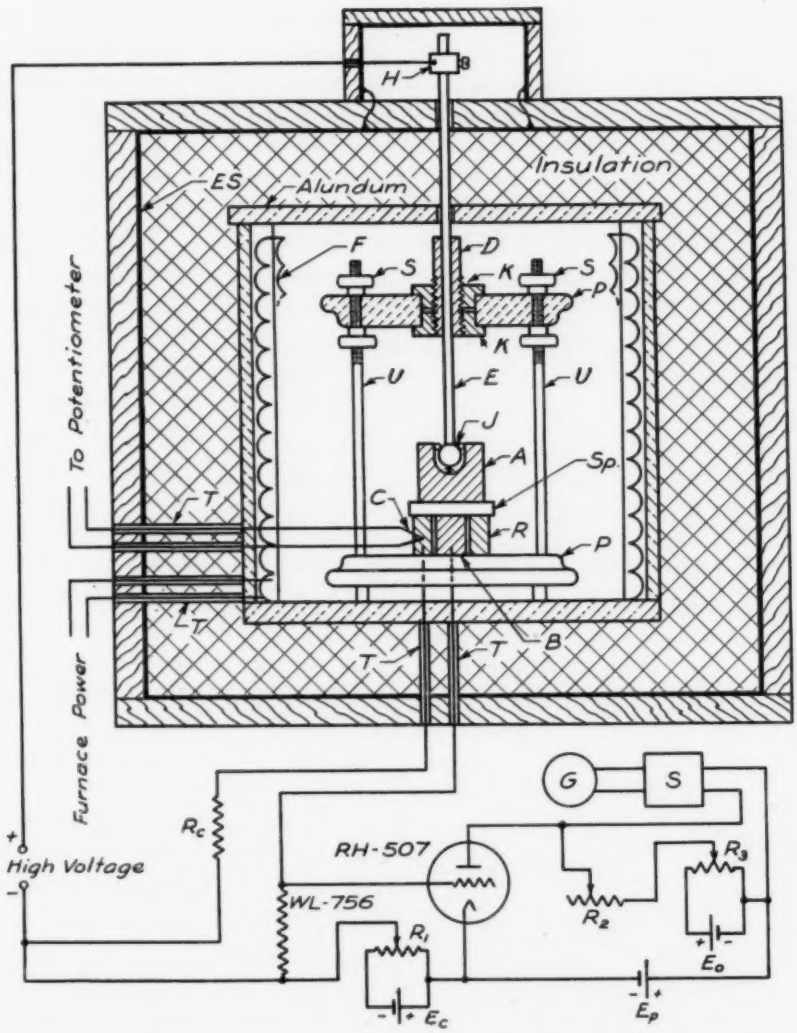

FIG. 1. Specimen-holder, electric furnace, and electrometer circuit.

the resulting space charges distort the field, the material is weakened, and breakdown occurs. This theory, of course, denies the older one of Joffé[9] and his co-workers, who maintained that ions loosened from the lattice produce the impact ionization which leads to breakdown.

Again, when at low field strengths the temperature of the crystal is raised, the conductivity rises sharply. The relation

$$\kappa = Ae^{-B/T} \tag{2}$$

where κ is the conductivity, T the Kelvin temperature, and A and B constants, was proposed by Rasch and Hinrichsen[10] to describe this phenomenon, but it has been found to hold exactly, over the entire temperature range, for very few of the solid salts which have been investigated. The whole question is complicated further by the presence of the so-called anomalous charging current first noted by the Curies[11] in 1888, and variously explained as polarization, a space-charge effect, or the like. The current, in most cases observed,[12–14] appears to follow an empirical law of the form

$$I = kt^{-m} \tag{3}$$

[9] A. F. Joffé, *The Physics of Crystals* (McGraw-Hill Book Co., New York, 1928).
[10] A. Rasch and H. Hinrichsen, Zeits. f. Elektrochem. **14**, 41 (1908).
[11] J. and P. Curie, Ann. chim. phys. **17**, 385; **18**, 203 (1889).
[12] A. D. Goldhammer, Physik. Zeits. Sowjetunion **5**, 523 (1934).
[13] E. Hippauf and R. Stein, Physik. Zeits. **39**, 90 (1938).
[14] F. Seidl, Physik. Zeits. **39**, 714 (1938).

where t is the time in seconds and k and m are constants.

In the present work the current passed by pure crystal plates of KBr and KCl was measured over a wide range of temperatures. At each temperature a number of rather low voltages (well below breakdown potential) were applied, and current-time data were taken at each voltage.

Description of Apparatus

Figure 1 shows the specimen-holder, the furnace in which it was placed, and the electrometer circuit used for measurement. Upper electrode A, lower electrode B, guard ring R, and connecting rod E were all made of Chromel, to withstand the temperatures used. Rod E slides freely in the Chromel bushing D, which is fastened by two Chromel nuts K to the upper porcelain plate P. The entire upper assembly, including electrode A, is removable for insertion of the specimen Sp. With the specimen in place, the upper assembly may be set on the three guide rods U (two only are shown) and fastened in place with the leveling nuts S, whereupon rod E is moved through bushing D until contact is established with the specimen. The ball and socket joint J ensures even contact between electrode A and the specimen. To provide electrical connection, Chromel wires were hammered into holes drilled in electrode B and guard-ring R, and a third wire was fastened by collar H to rod E. The Chromel-Alumel couple C, by means of which the specimen temperature was measured, was fastened in contact with guard-ring R. Electrode B and guard-ring R were accurately centered and permanently fastened with Chromel screws to the lower porcelain plate P. The separation thus achieved was considered sufficient insulation for the guard-ring, since the compensating resistor R_c was used to maintain it at the same potential as the electrode B. The conductivity of the entire specimen-holder was measured with no specimen in place and the electrodes separated by about the thickness of a specimen, and was found negligible in comparison with the specimen conductivities later measured.

The specimen-holder was mounted in an electric furnace with Alundum walls, roughly cubical in shape, with the inside edge measuring eight inches. Approximately a foot of mineral wool was used to separate the furnace from its outer container. This container was lined with a grounded electrostatic shield ES, with only the specimen connections, furnace power wires, and thermocouple leads emerging, through thin Alundum tubes T.

The specimen leads were carried directly to the electrometer circuit, the source of potential, and the calibrating circuit (not shown in Fig. 1). A Westinghouse RH-507 electrometer tube[15] was used in the simple arrangement shown, with Westinghouse WL-756 special resistors (sputtered and mounted in evacuated glass tubes) in the input circuit. A sufficient selection of input resistors to cover the range of currents measured (10^{-16} to 10^{-5} ampere) was provided, although it was found that at the higher currents the galvanometer G, having a sensitivity of 10^8 mm per ampere, could be used directly with almost as great an accuracy. Battery E_0 and resistors R_2 and R_3 were used to balance out the normal plate current of the RH-507, so that the galvanometer read only increments due to currents passing through the specimens. The universal shunt S provided a number of changes of range with the same input resistor. Linear amplification was achieved on each range by adjustment of the tube voltages.

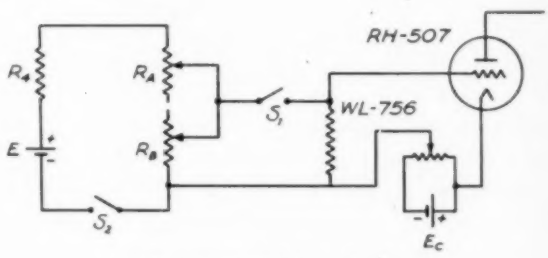

Fig. 2. Calibrating circuit.

In using the RH-507 for the measurement of very low currents, it is important that the grid bias voltage be so adjusted that no grid current flows. A check on this was furnished by the calibrating circuit shown in Fig. 2. Resistor R_B was less than 10^4 ohms: of much lower value than the WL-756 input resistor, which for the smallest current readings was 10^{12} ohms. Thus, if grid

[15] Bulletin TD 83 (1937), Westinghouse Electric and Manufacturing Company.

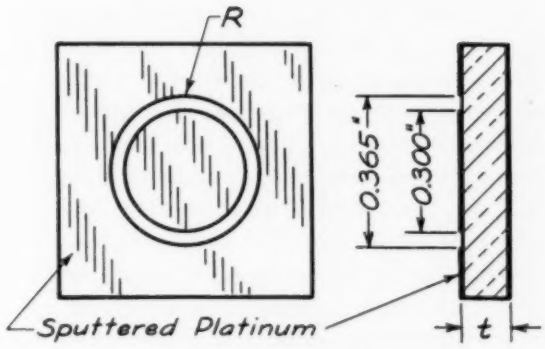

FIG. 3. Detail of specimen.

current was flowing and switch S_1 was closed (S_2 remaining open), the grid potential would change, producing a deflection of the galvanometer in the plate circuit. Accordingly, the potentiometer across battery E_c was adjusted until no deflection was noted upon the closing of S_1.

For calibration, switch S_2 was closed, S_1 remaining closed after the grid bias adjustment. R_A and R_B were decade resistance boxes, so used that the total resistance $R_4+R_A+R_B$ in series with battery E was 2×10^4 ohms. Thus the calibrating potential applied to the RH-507 grid was $0.5\times10^{-4}\times R_B\times E$. The voltage of battery E was checked, with the circuit in operation, by means of a thermionic voltmeter, also used to check the potential applied to the specimens.

As a source of adjustable potential, a heavily filtered transformer-rectifier circuit was used, with a General Radio Company "Variac" controlling the input voltage. Batteries were substituted for several check readings, but no appreciable difference in the readings was noted. The potential source, the calibrating circuit, the electrometer circuit, and the furnace control circuits were all thoroughly shielded and bonded to the furnace shield, such precautions proving quite necessary for proper operation of the electrometer tube.

EXPERIMENTAL TECHNIQUE

Four specimens were tested, two of KBr and two of KCl. All were flat plates two cm square, with thicknesses as follows: KBr I, 3.64 ± 0.02 mm; KBr II, 2.78 ± 0.02 mm; KCl I, 4.62 ± 0.02 mm; and KCl II, 4.14 ± 0.02 mm. After grinding to the tolerance indicated, the specimens were uniformly sputtered with platinum. As shown in Fig. 3, the sputtering was then removed from the ring R separating the contact areas of lower electrode and guard-ring, and from the four faces of width t.

By taking some care to reach thermal equilibrium, it was found easily possible to hold the temperature constant to within 0.5°C (=0.02 mv on the precision potentiometer used for measurement) during a run. After constant temperature was achieved, one operator adjusted, measured, and applied the potential, and signaled time intervals. A second operator noted the electrometer readings at intervals of a few seconds. This procedure, while somewhat crude, was found sufficiently accurate for the determination of the first-throw current, and for current-time plots from which the value of the constant m in Eq. (3) could be deduced. After taking readings over a period of several minutes, the potential was removed and the specimen short-circuited. Readings at the next voltage were not taken until the residual (reversed) charging current was reduced to a negligible proportion of the recorded currents. These precautions became less necessary at the higher temperatures, where the current was essentially constant with time.

Readings were taken on each specimen at a number of temperatures between 25°C and 600°C. At the lower temperatures potentials between 20 and 250 volts were applied, but at the higher temperatures the maximum voltage was 100, to avoid the possibility of breakdown.

RESULTS

a. Reduction in cold conductivity

Measurements in the range 25°C–50°C were taken on all crystals, before heating to the higher temperatures, after heating to the highest temperature, and after several reheatings. In two cases the cold conductivity seemed to rise sharply after heating, but this was found due to poor original contact between specimen and electrodes. With this difficulty remedied, it was found in all cases that the first heating (taking from 36 to 48 hours) reduced the cold conductivity by 15 to 25 percent, room temperature conductivity being reduced in greatest degree.

No reduction in the conductivity at temperatures above 50°C was noted, and a second heating produced no further change in the cold conductivity. This effect seems similar to that reported by Smekal[3] for rocksalt, and by Rahimi[16] for both rocksalt and quartz. The reduced conductivities are those used in the curves discussed below.

b. Current-voltage relation

No appreciable departure from Ohm's law was noted for any of the specimens tested. In Fig. 4 first-throw galvanometer deflection (=constant×current) is plotted against voltage for five typical cases. Only in the case of specimen KBr II, measured at 29°C, are deviations from the linear relation at all prominent, and even there they are small enough to be ascribed to experimental error.

c. Current-time relation

In Figs. 5 and 6, where the logarithm of the resistivity in ohm-cm is plotted against the reciprocal of the absolute temperature for KBr and KCl, respectively, small curves are superimposed upon the main graphs to show the approximate current-time relations for the various regions. Eq. (3) describes the dependence of current on time rather closely. In fact, it appears from the data that the effect of increasing temperature is to reduce the value of the exponent m in Eq. (3) from about unity at the lowest temperatures to successively lower values, until (at about 200°C in all cases) m is so small that current decay with time was no longer measureable. The current-time curves can only be considered a first approximation, however, and it is planned to use a more accurate experimental method for a thorough investigation of the current-time relationship for these and other crystals at various temperatures.

d. Resistivity-temperature relation

Since Ohm's law seemed to hold, a resistivity-temperature curve for one voltage only was plotted for each of the four specimens tested. The voltage chosen was 100, for convenience in calculation. A great variation in resistivity with temperature was found, as was to be expected: from nearly 10^{17} ohm-cm at room temperatures it fell to less than 10^{7} ohm-cm for KBr and less than 10^{6} ohm-cm for KCl at the highest temperatures used.

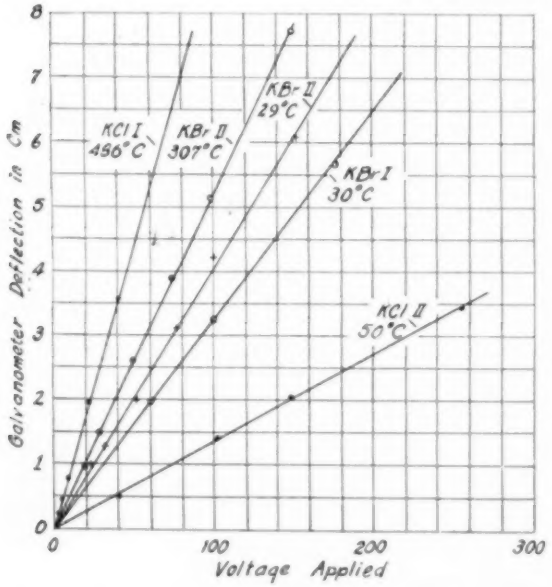

FIG. 4. Current-voltage relation for all specimens. The ordinates must be multiplied by a different constant in each case, to obtain the conduction current in amperes.

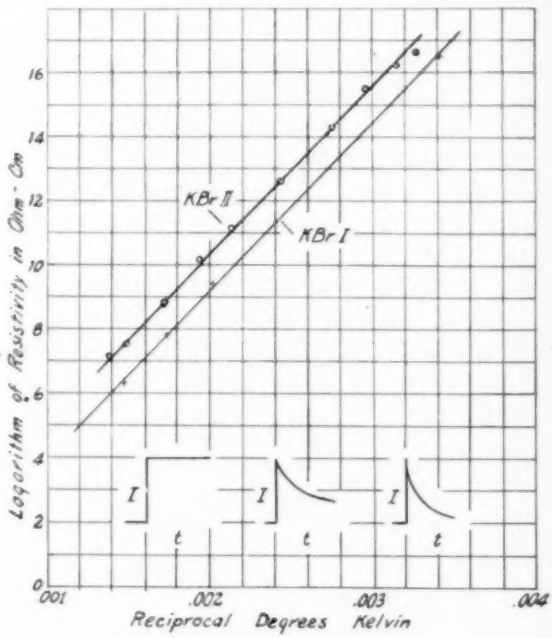

FIG. 5. Resistivity-temperature relation for KBr, with approximate current-time curves.

[16] M. G. Rahimi, J. de phys. et rad. **9**, 291 (1938).

Figure 5 shows the results for KBr. Both specimens obey the exponential law of Eq. (2), and the curves have, within experimental error, the same slope, although the intercepts are quite different, constant A of Eq. (2) having the value 20.0 for KBr I and 2.24 for KBr II. Constant B, on the other hand, is 12,200 for KBr I and 12,300 for KBr II, a difference of only 0.82 percent. The activation energy deducible from these constants is 24.5±0.2 kcal. per mole.

The curves for KCl, shown in Fig. 6, are not so simple. Eq. (2) might be said to hold on either side of a critical temperature (235°C for KCl I and 208°C for KCl II), at which an abrupt change of slope occurs. Similar, though smaller, deviations from the Rasch and Hinrichsen equation have been reported for sodium,[17] potassium,[18] and lithium[19] halides by Phipps and his coworkers, and may be explainable by the assumption that at the lower temperatures only the potassium cations take part in the conduction, while at the higher temperatures the chlorine anions become active. On this assumption, Smekal[20] has proposed as a modification of Eq. (2) the form

$$\kappa = A_1 e^{-B_1/T} + A_2 e^{-B_2/T} \qquad (4)$$

where B_1 and B_2 are constants whose respective values depend on the activation energies of the two kinds of conducting ions present, but this form seems inadequate to describe the conductivity-temperature relation found for KCl in the present work. Furthermore, while at the higher temperatures; i.e., to the left of the critical point in Fig. 6, the slopes for KCl I and KCl II agree quite well, this is not the case at the lower temperatures. This may indicate that in the low temperature region the conductivity is more a function of the particular specimen tested than of the material of which it consists. In the higher temperature region the slope of the resistivity

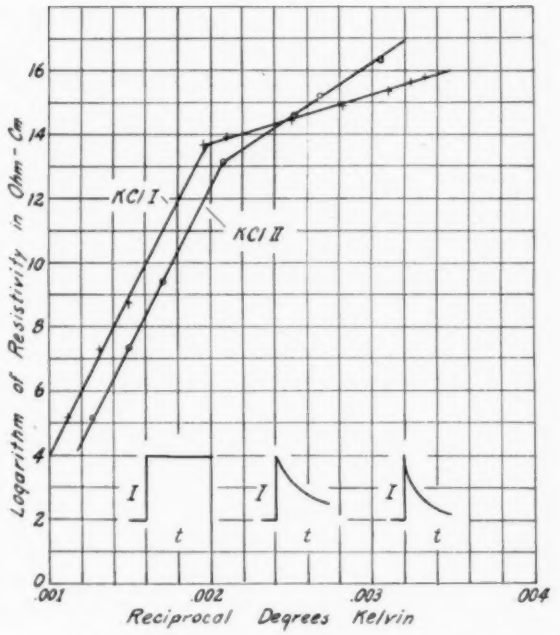

FIG. 6. Resistivity-temperature relation for KCl, with approximate current-time curves.

curve is 10,050 for KCl I and 9900 for KCl II, corresponding to an over-all activation energy of 45.8±0.2 kcal. per mole.

e. Summary of results

From the data taken, it may be concluded that: (1) Ohm's law holds for KBr and KCl, at temperatures between 25°C and 600°C, and at fields of from 0.05 to 0.90 kv/cm. (2) There is an exponential relation, most prominent at lower temperatures, between current and time, for KBr and KCl. (3) An exponential relation holds for KBr between conductivity and temperature in the range tested. (4) There is an exponential relation between conductivity and temperature for KCl, but the value of the exponential constant changes at a critical temperature between 200°C and 250°C.

The author wishes to acknowledge the valuable assistance of Professor M. F. Manning, who collaborated in planning and beginning this work, and of Mr. Fred Willard, who assisted in construction of apparatus and the taking of data. The specimens used were obtained through the courtesy of Professor H. M. Randall.

[17] Phipps, Lansing and Cooke, J. Am. Chem. Soc. **48**, 112 (1926).
[18] T. E. Phipps and E. G. Partridge, J. Am. Chem. Soc. **51**, 1331 (1929).
[19] D. C. Ginnings and T. E. Phipps, J. Am. Chem. Soc. **52**, 1340 (1930).
[20] A. Smekal, Zeits. f. tech. Physik **8**, 561 (1927); Zeits. f. Elektrochem. **34**, 472 (1928).

Studies in Lubrication

VII. The Lubrication of Plane Sliders of Finite Width

M. Muskat, F. Morgan and M. W. Meres
Gulf Research & Development Company, Pittsburgh, Pennsylvania
(Received August 30, 1939)

The theory of the lubrication of plane sliders of finite width—thrust block bearings—has been developed by a method that is more convenient for numerical calculations than that of Michell and Boswall. Whereas previously all the derived properties of such systems have had to be obtained by direct graphical and numerical procedures, explicit analytical expressions have been obtained in the present theory for the friction coefficients, the inclination of the wedges, the load-carrying capacities, the minimum film thickness, and the lubricant flow. The theory has been applied numerically to a much wider range of conditions than has been done before. In particular, with respect to self-aligning thrust bearings or sliders, numerical results have been obtained so as to cover both the range where the pivot is very near the center of the slider and where it is set within short distances of the trailing edge. With such extended ranges it has been possible to construct complete curves for the variation of the important derived properties of the slider system as functions of the pivot position.

Introduction

THE theory of the viscous lubrication of plane sliders of finite width, as based upon the Reynolds equation, was first given by A. G. M. Michell in 1905.[1] Except for some additional numerical calculations carried out by means of Michell's formulas by Martin,[2] and Boswall,[3] no extensions or improvements have been made in the theory. Duffing[4] has developed a solution for the mathematically simpler case where the film viscosity is proportional to the film thickness, and has pointed out that in some cases, at least, the first derivative term in the Reynolds equation does not greatly affect the final solution. However, no advance was made in the solution of Michell's original problem.

The main disadvantage of Michell's theory is that it not only reduces to an inherently numerical method, but moreover requires independent numerical or graphical integrations for the determination of every feature derivable from the solutions for the pressure distribution, such as the load-carrying capacity, friction coefficients, the center of pressure, and the lubricant flow. As a consequence, the only calculations heretofore made on sliders of finite width have referred to the two cases where the ratios of inlet to outlet film thicknesses have been either 3.0 or 2.0. The results so obtained, for various length to width ratios, have been summarized by Boswall.

Because the plane slider of finite width is essentially nothing else than the thrust block bearing so widely used in industry, it is desirable to have a more comprehensive treatment of its lubrication properties. In the following we shall therefore develop solutions of the Reynolds equation for such sliders which are more convenient for numerical calculation than those of Michell. In principle they do not differ greatly from Michell's solution. However, they give explicit

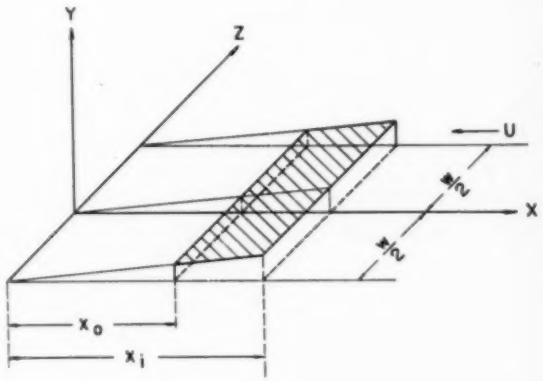

Fig. 1.

[1] A. G. M. Michell, Zeits. f. Math. Physik **52**, 123 (1905).
[2] H. M. Martin, Eng. **109**, 233 (1920).
[3] R. O. Boswall, *The Theory of Film Lubrication* (Longmans, Green and Co., 1928).
[4] G. Duffing, *Handbuch der Physik Tech. Mech.*, Vol. 5 (1931), p. 839.

series representations of the resultant pressure distribution in terms of Bessel functions which have been completely listed in standard tabulations. The one troublesome step in the solution is the determination of the roots of certain transcendental Bessel function equations which must be calculated separately for each ratio of the inlet to outlet film thickness. However, once these have been found, the subsequent calculations for variable slider widths can be made very simply.

The Solution of the Reynolds Equation

The Reynolds equation appropriate to the lubricant film between plane sliders may be written as:

$$\frac{\partial}{\partial x}\left(\frac{h^3}{\mu}\frac{\partial p}{\partial x}\right)+\frac{\partial}{\partial z}\left(\frac{h^3}{\mu}\frac{\partial p}{\partial z}\right)=-6U\frac{\partial h}{\partial x}, \qquad (1)$$

where (cf. Fig. 1) p is the pressure distribution in the film, x is the coordinate in the direction of motion of the slider, h is the film thickness, μ its viscosity, z the transverse coordinate, and U is the velocity of the sliding plate, which is assumed to be moving in the direction of the negative x axis.

Assuming a constant viscosity, and a film thickness given by:

$$h=mx, \qquad (2)$$

Eq. (1) reduces to:

$$\frac{\partial^2 p}{\partial x^2}+\frac{3}{x}\frac{\partial p}{\partial x}+\frac{\partial^2 p}{\partial z^2}=-\frac{6\mu U}{m^2x^3}. \qquad (3)$$

Michell's method consisted essentially in expanding both p and the right side of Eq. (3) as Fourier series in z, thereby obtaining a series of ordinary inhomogeneous equations in x. While the homogeneous solutions of these equations were the first-order Bessel functions of the third kind, the particular integrals were expressed simply as power or Laurent series. The coefficients of the various terms of the solutions were then determined numerically so as to give vanishing pressures at the leading and trailing edges of the film, the Fourier series terms being so adjusted initially that the pressure distribution automatically vanished at the lateral edges of the film. In this way solutions were obtained in the form of a series of functions known only numerically, and which had to be computed separately for each different set of physical parameters specifying the lubrication system.

Here we shall formally eliminate the inhomogeneity of Eq. (3) by first subtracting off from the solution that corresponding to the slider of infinite width, that is by making the substitution:

$$p=\bar{p}+\frac{6\mu U}{m^2(x_i+x_0)}\cdot\frac{(x_i-x)(x-x_0)}{x^2}, \qquad (4)$$

where x_i represents the inflow or leading edge of the film and x_0 the outflow or trailing edge. The equation for $\bar{p}$ is clearly the homogeneous equation corresponding to Eq. (3). We take its solution to be of the form:

$$\bar{p}=\frac{6\mu U}{m^2}\sum\frac{C_nU_n(x)}{x}\frac{\cosh\alpha_n z}{\cosh\alpha_n w/2}, \qquad (5)$$

where

$$U_n(x)=J_1(\alpha_n x_0)Y_1(\alpha_n x)-Y_1(\alpha_n x_0)J_1(\alpha_n x), \qquad (6)$$

J_1 and Y_1 being first-order Bessel functions of the first and second kind, respectively.[5] The slider width is taken as w and the x axis is assumed to lie in the plane of symmetry.

The constants α_n and the coefficients C_n must now be chosen so that the resultant series of Eq. (5) will satisfy the boundary conditions of the problem. Since p itself must vanish on all four sides of the film, $\bar{p}$ must vanish on the leading and trailing edges, and must cancel off the distribution in the infinitely wide slider at the lateral edges. These conditions will be satisfied if the α_n are chosen so that:

$$U_n(x_i)=0, \qquad (7)$$

and if the C_n are determined so that:

$$\sum C_nU_n(x)=\frac{(x_i-x)(x_0-x)}{(x_i+x_0)x}. \qquad (8)$$

[5] The Bessel functions appearing here are those of the first and second kind, rather than of the third kind appearing in Michell's analysis, because of the use of hyperbolic functions in the terms involving z rather than trigonometric. This difference is introduced here to accelerate the convergence of the series from the numerical point of view.

By carrying out the standard manipulations for the determination of the coefficients of orthogonal expansions, it is finally found that the pressure distribution can be expressed as:

$$p=\frac{6\mu U}{m^2}\left[\frac{(x_i-x)(x-x_0)}{(x_i+x_0)x^2}-\frac{\pi^2}{2}\sum\frac{\gamma_n\alpha_n J_1^2(\alpha_n x_i)}{J_1^2(\alpha_n x_0)-J_1^2(\alpha_n x_i)}\frac{U_n(x)}{x}\frac{\cosh\alpha_n z}{\cosh\alpha_n w/2}\right]. \tag{9}$$

where

$$\gamma_n=J_1(\alpha_n x_0)\int_{x_0}^{x_i}Y_0(\alpha_n x)dx-Y_1(\alpha_n x_0)\int_{x_0}^{x_i}J_0(\alpha_n x)dx. \tag{10}$$

By applying Eq. (8) to the first term in Eq. (9) the pressure distribution can also be expressed as:

$$p=\frac{3\pi^2\mu U}{m^2}\left[\sum\frac{\gamma_n\alpha_n J_1^2(\alpha_n x_i)}{J_1^2(\alpha_n x_0)-J_1^2(\alpha_n x_i)}\frac{U_n(x)}{x}\left\{1-\frac{\cosh\alpha_n z}{\cosh\alpha_n w/2}\right\}\right]. \tag{11}$$

The Derived Properties of the Plane Slider

Once the pressure distribution has been determined, the other properties of the system can be obtained by integration processes. First, however, it is convenient to introduce the following additional notation:[6]

$$\rho=\frac{x_i}{x_0};\quad \alpha_n x_0=\beta_n;\quad \bar{w}=\frac{w}{L};\quad S=\frac{\mu U w}{W};\quad \delta_n=\frac{\pi}{2}\alpha_n\gamma_n J_1(\beta_n\rho), \tag{12}$$

where L is the length of the slider in the direction of motion and W is the total load supported by it. From these definitions it will be clear that $\bar{w}$ represents the dimensionless width of the slider, $\bar{w}=\infty$ corresponding to the infinitely wide slider, and $\bar{w}=1$ to the square slider. The dimensionless parameter S characterizes the physical conditions to which the lubricant film is subjected, since it includes the relative speed of the slider, the load which the film must support, and the viscosity of the film, all of which are to be considered as being externally imposed on the system.

With this notation the load supported by the film will be given by:

$$W=\int_{-w/2}^{w/2}\int_{x_0}^{x_i}p\,dx\,dz=\frac{6\mu U w}{m^2}\left[\log\rho-\frac{2(\rho-1)}{\rho+1}-\frac{4}{\bar{w}(\rho-1)}\sum\frac{\delta_n^2\tanh\beta_n(\rho-1)\bar{w}/2}{\beta_n\{J_1^2(\beta_n)-J_1^2(\beta_n\rho)\}}\right], \tag{13}$$

so that

$$\frac{S}{m^2}=\frac{1/6}{\log\rho-\dfrac{2(\rho-1)}{\rho+1}-\dfrac{4}{\bar{w}(\rho-1)}\displaystyle\sum\frac{\delta_n^2\tanh\beta_n(\rho-1)\bar{w}/2}{\beta_n\{J_1^2(\beta_n)-J_1^2(\beta_n\rho)\}}}. \tag{14}$$

It will be noted that here as well as in Eqs. (9) and (13) the series terms represent the effect of the finiteness of the slider width. Because of the factor $1/\bar{w}$, its contribution will vanish as the slider becomes infinitely wide, as indeed it should.

The frictional forces may be obtained by integrating over the bounding surfaces the stress components

$$\sigma=\frac{\mu U}{h}\mp\frac{h}{2}\frac{\partial p}{\partial x}, \tag{15}$$

where the upper sign refers to the moving plate and the lower to the stationary slider. These components are essentially nothing more than the surface tractions in the lubricant film at the bounding surfaces, with the signs adjusted so as to take account of the direction of motion of

[6] The parameter ρ, which is also equal to the ratio of the inlet to outlet film thickness, is equivalent to 1 plus the parameter b introduced by Boswall. From the manner in which it enters the subsequent analysis it will be clear that it is more convenient for our purposes than would be the parameter b.

the moving slider and to give directly the numerical magnitude of the individual external forces required to keep the moving slider moving and the fixed plate stationary. Carrying out these integrations formally, evaluating the second terms by integrations by parts, and introducing the above notation, it is found that the friction coefficients for the moving slider will be given by

$$\frac{f}{m}=\frac{1}{2}+\frac{S}{m^2}\log\rho, \tag{16}$$

and that on the stationary slider by:

$$\frac{\bar{f}}{m}=-\frac{1}{2}+\frac{S}{m^2}\log\rho. \tag{17}$$

It should be noted that the latter refers to the frictional force as measured *parallel to the stationary slider*. Defined in this way its numerical value will become negative for those values of S/m^2 where f/m is less than 1, since the difference between f/m and $\bar{f}/m$ will always equal 1. Such negative values of the friction coefficient imply physically that the stationary slider tends to be pushed back by the viscous film in the direction opposite to the moving slider. This apparently paradoxical behavior may be readily understood by a closer analysis of the velocity distribution in the film under such conditions where the negative values of $\bar{f}$ are obtained. At the same time, however, it should be pointed out that because the normal stresses on the slider, which provide the load-supporting power equal to W, are also inclined to the vertical by the angle between the sliders, they provide a horizontal component which counterbalances the negative contribution due to $\bar{f}$. Moreover they leave a resultant friction coefficient *parallel to the moving slider* which is not only positive, but is, in addition, exactly equal to that on the moving slider.

Another property of interest of the lubricant film between the plane sliders is the center of pressure. By symmetry it obviously must lie midway between the lateral ends. Its position along the central traverse in the direction of motion is given by:

$$\frac{\Delta x}{L}=\frac{1}{WL}\int_{-w/2}^{w/2}\int_{x_0}^{x_i}(x-x_0)p\,dx\,dz=-\frac{1}{\rho-1}+\frac{6S}{m^2}\left[\frac{1}{2}-\frac{\rho}{\rho^2-1}\log\rho\right.$$
$$\left.+\frac{4}{\bar{w}\rho(\rho-1)^2}\sum\frac{\delta_n\{J_1(\beta_n)-\rho J_1(\beta_n\rho)\}\tanh\beta_n(\rho-1)\bar{w}/2}{\beta_n^3\{J_1^2(\beta_n)-J_1^2(\beta_n\rho)\}}\right]. \tag{18}$$

where again the series term[7] represents the effect of the finiteness of the width of the slider and vanishes as the slider becomes infinitely wide ($\bar{w}\to\infty$).

Finally it is of interest to derive the expressions for the lubricant flow between the sliders. From the basic hydrodynamic expressions for the average flow between parallel plates, and from which Eq. (1) is derived, it is readily found that the total lubricant inflow at the leading edge will be given by:

$$Q=\int_{-w/2}^{w/2}\left(\frac{h^3}{12\mu}\frac{\partial p}{\partial x}+\frac{Uh}{2}\right)_{x=x_i}dz=\frac{UmwL\rho}{\rho^2-1}\left[1-\frac{2(\rho+1)}{\bar{w}(\rho-1)}\sum\frac{\delta_n J_1(\beta_n)\tanh\beta_n(\rho-1)\bar{w}/2}{\beta_n\{J_1^2(\beta_n)-J_1^2(\beta_n\rho)\}}\right]. \tag{19}$$

While the outflow at the trailing edge will be given by evaluating the integral of Eq. (19) with the integrand taken at $x=x_0$, it is more convenient to consider directly the side leakage, which may be calculated from the equations:

$$Q_z=-2\int_{x_0}^{x_i}\left(\frac{h^3}{12\mu}\frac{\partial p}{\partial z}\right)_{z=w/2}dx=\frac{2UmwL}{\bar{w}(\rho-1)^2}\sum\frac{\delta_n\{J_1(\beta_n\rho)-\rho J_1(\beta_n)\}\tanh\beta_n(\rho-1)\bar{w}/2}{\beta_n\{J_1^2(\beta_n)-J_1^2(\beta_n\rho)\}}. \tag{20}$$

[7] The terms outside the series, here, and in Eqs. (14), (19) and (20), which represent the values for the infinitely wide slider, could be included in the series merely by replacing $\tanh\beta_n(\rho-1)\bar{w}/2$ by: $\tanh\beta_n(\rho-1)\bar{w}/2-\beta_n(\rho-1)\bar{w}/2$. However, this change would slow up the convergence of the series and would mask the effect of the side leakage as a correction factor for the corresponding systems of infinite width.

TABLE I. *Values of* β_n.

ρ \ n:	1	2	3	4	5	6	7	8
1.2	15.7277	31.4259	47.1305	62.8368	78.5438	94.2511		
1.5	6.3218	12.5861	18.8628	25.1427	31.4239	37.7057		
2.0	3.1917	6.3116	9.4446	12.5812	15.7199	18.8595		
3.0	1.6356	3.1789	4.7381	6.3028	7.8696	9.4375		
5.0	0.84715	1.61105	2.38532	3.1642	3.9454	4.7279	5.5112	
10.0	0.394094	0.733057	1.074838	1.418864	1.764331	2.110731	2.457757	2.80522

As it should, the whole of this term vanishes as the slider width is made indefinitely large. Moreover, if Q_z be subtracted from the total inflow, as given by Eq. (19), the flow out of the trailing edge will be obtained.

These complete the formal derivations of the expressions for the significant physical properties of plane slider lubrication systems. We shall now proceed with the problem of evaluating these expressions numerically and with the interpretation of the final results.

PLANE SLIDERS WITH FIXED WEDGE ANGLE

As already indicated, the main problem involved in the evaluation of the analytical expressions derived in the last section lies in the determination of the roots β_n of Eq. (7). In terms of the notation of Eq. (12) this equation may be rewritten as:

$$J_1(\beta_n)Y_1(\beta_n\rho)-Y_1(\beta_n)J_1(\beta_n\rho)=0. \quad (21)$$

As these roots are not given in the standard texts on Bessel functions, and as this type of equation appears in other physical problems, those that were used in the present investigation are reproduced in Table I. The values for $\rho=1.2$, 1.5, and 2.0 were taken from a paper by A. Kalahne,[8] after correcting Kalahne's first three roots for $\rho=2.0$. The roots for the other values of ρ were calculated explicitly for the purpose of the present problem. It should be emphasized that these roots, especially the lower ones and those for large values of ρ, must be known with a high degree of accuracy. In fact, for $\rho=10$, even the seventh decimal places in the lower β_n, as determined by graphical interpolation, had some noticeable effect upon the left side of Eq. (21). Moreover all the subsequent calculations, and in particular those of the functions δ_n, must be carried out to a high degree of accuracy or else the final results will be quite meaningless. While this is a rather tedious problem, it can fortunately be carried out with satisfactory precision by making use of the Bessel function tables given in Watson's treatise[9] and in the *British Association Tables*.[10]

The functions γ_n defined by Eq. (10), and appearing in δ_n, were obtained by expressing the integrals of Eq. (10) in terms of Struve functions, i.e., as:

$$\gamma_n=\frac{2x_0}{\pi\beta_n J_1(\beta_n\rho)}\left[J_1(\beta_n)\left\{1-\frac{\pi}{2}H_1(\beta_n\rho)\right\}-J_1(\beta_n\rho)\left\{1-\frac{\pi}{2}H_1(\beta_n)\right\}\right], \quad (22)$$

the H_1 being the Struve functions of the first order. Account was taken of the fact that the β_n are roots of Eq. (21). These Struve functions, up to arguments equal to 16, were taken from the tables of Watson. For higher values asymptotic expansions were used. For such values where both of the Struve functions in Eq. (22) permitted the use of asymptotic expansions the resultant values of δ_n took the form:

$$\delta_n=\frac{1}{{\beta_n}^2}\left[J_1(\beta_n\rho)-\frac{J_1(\beta_n)}{\rho^2}-\frac{3}{{\beta_n}^2}\left\{J_1(\beta_n\rho)-\frac{J_1(\beta_n)}{\rho^4}\right\}+\frac{45}{{\beta_n}^4}\left\{J_1(\beta_n\rho)-\frac{J_1(\beta_n)}{\rho^6}\right\}+0\left(\frac{1}{{\beta_n}^6}\right)\right]. \quad (23)$$

Once the β_n and δ_n are calculated, it is a rela-

[8] A. Kalahne, Zeits. f. Math. Physik **44**, 55 (1907).

[9] G. N. Watson, *Theory of Bessel Functions* (Cambridge University Press, 1922).

[10] *British Association Mathematical Tables*, Vol. 6, *Bessel Functions*, Part I, 1937.

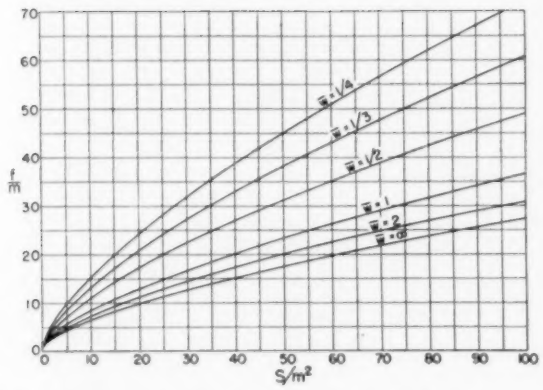

FIG. 2. The variation of the friction coefficient, f, with S, for sliders of finite width. $S = \mu U w / W$; μ = film viscosity; U = slider speed; w = slider width; L = slider length, in the direction of motion; W = total load; m = slope of slider inclination; $\bar{w} = w/L$.

tively simple matter to carry through the evaluation of the final physical quantities of interest such as the load carried by the film, the friction coefficients, center of pressure, etc. Moreover the major elements in the terms of the various series remain the same for the calculation of different slider widths, as these can be taken care of merely by changing the arguments in the hyperbolic tangent terms.

For the slider systems of fixed wedge angle the final parameter used for plotting the various physical properties of the system was S/m^2 as given by Eq. (14), although this in itself is determined by the dimensionless slider width $\bar{w}$, and the ratio of the maximum to minimum film thicknesses, ρ.

In Fig. 2 is plotted a series of curves showing the variation of the friction coefficient *vs.* S/m^2 as calculated by Eqs. (14) and (16). The curve for $\bar{w} = \infty$ corresponds to the infinitely wide slider as given by the Reynolds theory. It will be seen that for fixed values of S/m^2 the friction coefficient (divided by m) increases with decreasing slider width. The magnitude of this increase becomes more pronounced for larger values of S/m^2. This effect is caused, of course, by the side leakage, which in turn tends to lower the average film pressure and thus necessitates that the surfaces come closer together in order to support the external load.

As in the case of the infinitely wide slider, the friction coefficient increases with S/m^2 more slowly than linearly. In fact, except at very small values of S/m^2, the various curves are essentially parallel on double logarithmic paper, so that the magnitudes of the friction coefficient may be approximately expressed as a function of the width times a function of S/m^2 corresponding to the infinitely wide slider. Thus taking the values for the infinitely wide slider as unity, the values of f/m at $S/m^2 = 50$ are 1.14, 1.33, 1.77, 2.16, and 2.56 for $\bar{w} = 2$, 1, $\frac{1}{2}$, $\frac{1}{3}$, and $\frac{1}{4}$, respectively. That is, a square slider will have a friction coefficient roughly 4/3 as great as that of the infinitely wide slider, and one whose width is only $\frac{1}{4}$ as great as its length—but with the same value of m—will have coefficients about $2\frac{1}{2}$ times as great as the slider of infinite width. These ratios break down at very low values of S/m^2, and in the limit of vanishing S/m^2, f/m approaches the value $\frac{2}{3}$ regardless of the slider width.

The effect of the slider width on the minimum film thickness is shown in Fig. 3. Here, as would be expected, the minimum film thickness uniformly decreases with decreasing slider width, this effect being the consequence of the side leakage. Moreover, as in the case of the friction coefficients, the curves are approximately parallel on double logarithmic paper, so that the values of h_0/mL may also be roughly expressed as a function of the width times a function of S/m^2 corresponding to the infinitely wide slider. At $S/m^2 = 50$ these width factors are 0.86, 0.70, 0.48, 0.37, and 0.29 for $\bar{w} = 2$, 1, $\frac{1}{2}$, $\frac{1}{3}$, and $\frac{1}{4}$, respectively. For vanishing values of S/m^2 the minimum film thickness will in all cases go to zero.

The variation of the center of pressure with

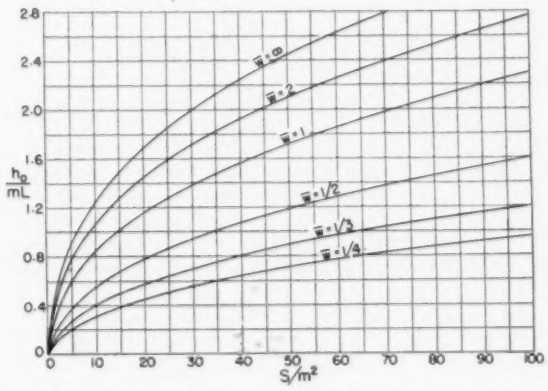

FIG. 3. The variation of the minimum film thickness, h_0, with S, for sliders of finite width. Notation same as in Fig. 2.

S/m^2 is plotted in Fig. 4. The ordinates are the distances of the center of pressure from the trailing edge divided by the slider length in the direction of motion. It will be seen that the center of pressure is shifted closer and closer toward the trailing edge as the slider width decreases. Here the curves are roughly parallel on the Cartesian scale, so that the various curves are related to each other by differences which are approximately constant, rather than uniform factors. For very small values of S/m^2, however, the steepness of the curves completely vitiates the parallelism obtaining for large values of S/m^2.

For fixed large values of S/m^2 the total lubricant flow into the slider decreases with decreasing slider width (cf. Fig. 5). For small values of S/m^2 there is a crossing of the curves and a reversal of the variation with the slider width. That is, for large values of S/m^2, Q decreases monotonically with decreasing slider width. For $S/m^2 \lesssim 10$, Q increases first as the slider width decreases, reaches a maximum, and then decreases as the width decreases still further. Moreover the maximum becomes shifted to decreasing widths as S/m^2 is made to approach 0.

As would be expected, the side leakage increases with decreasing slider width for all values of S/m^2. Moreover within the errors of the calculations the magnitude of the side leakage is essentially independent of S/m^2, for large values of the latter. However, as S/m^2 approaches 0 the curves develop maxima and ultimately fall off again before the Q_s axis is reached.

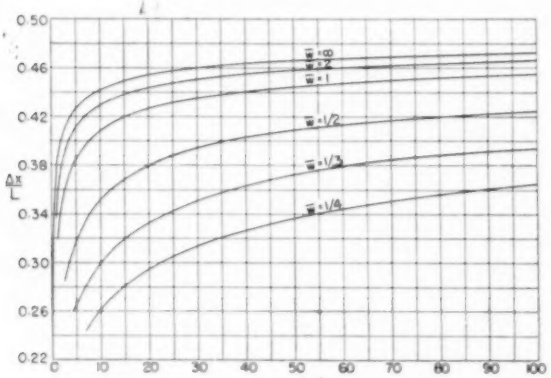

FIG. 4. The variation of the center of pressure with S, for sliders of finite width. Δx = distance of center of pressure from trailing edge. Rest of notation same as in Fig. 2.

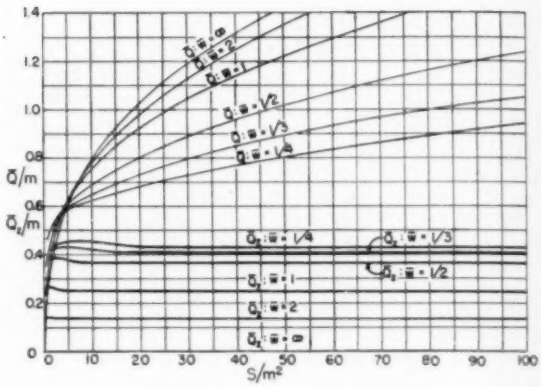

FIG. 5. The variation of the lubricant flow with S for sliders of finite width. $\bar{Q} = Q/UwL$; $\bar{Q}_s = Q_s/UwL$; Q = total lubricant inflow at leading edge; Q_s = total side leakage. Rest of notation same as in Fig. 2.

SELF-ALIGNING SLIDERS OF FINITE TRANSVERSE WIDTH

It will be clear that the results just presented may be given a direct physical interpretation only when the slope of the inclined surfaces, as represented by m, is considered to be fixed or known. As under the conditions of practical operation the value of m will be extremely small, it is not convenient to achieve fixed and predetermined wedge angles in practice. A much more practical procedure is to permit the sliders to be self-adjusting and to take up whatever mutual inclination is necessary to support the externally applied load. As originally pointed out by Michell and Kingsbury, this can be attained by pivoting the load supporting slider and permitting it to rotate about the pivot line. Since the external load must act through the pivot line, the supporting film pressures will also have to have their center of pressure along this line, and, depending upon the magnitudes of the speed, load, and lubricant viscosity, will force an inclination of the pivoted sliders so that the center of pressure will fall under the pivot line.[11]

This is the principle of the pivoted slider block. By its definition the system is essentially determined by the position of the pivot, which must coincide with the center of pressure, the inclination of the surfaces being merely a second-

[11] To obtain exact equilibrium of the moments about the pivot line the actual center of pressure would have to be displaced somewhat from the pivot line because of the moments arising from the friction forces on the slider. In practice, however, where the height of the pivot above the sliding surface is not large, this effect will be quite negligible.

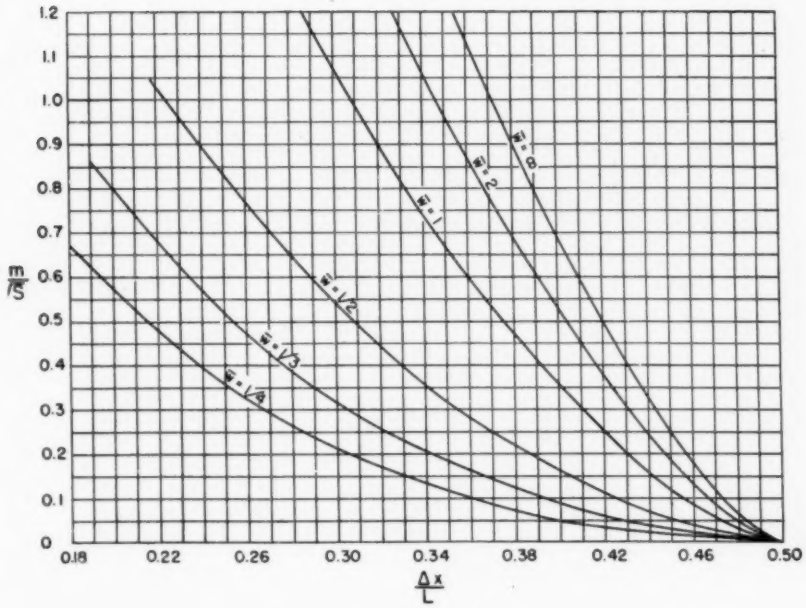

FIG. 6. The variation of the slider inclination, m, with the pivot position for pivoted sliders of finite width. $\Delta x/L$ = (distance of pivot from trailing edge)/(slider length, L). Rest of notation same as in Fig. 2.

ary parameter. For such systems therefore the fundamental independent variable is the quantity $\Delta x/L$, which gives the position of the center of pressure or the distance of the pivot line from the trailing edge, although from an analytical point of view the fundamental parameter is ρ, which determines $\Delta x/L$ through Eqs. (14) and (18). In fact, if we define the function $D(\rho)$ by:

$$D^2(\rho)=6\log\rho-\frac{12(\rho-1)}{\rho+1}-\frac{24}{\bar{w}(\rho-1)}\sum\frac{\delta_n^2\tanh\beta_n(\rho-1)\bar{w}/2}{\beta_n\{J_1^2(\beta_n)-J_1^2(\beta_n\rho)\}}\equiv D^2\left(\frac{\Delta x}{L}\right), \tag{24}$$

we will have directly from Eqs. (14), (16), (17), (19), and (20);

$$m=D\sqrt{S};\quad \frac{h_0}{L}=\frac{D}{\rho-1}\sqrt{S}; \tag{25}$$

$$f=\left(\frac{D}{2}+\frac{\log\rho}{D}\right)\sqrt{S};\quad \bar{f}=\left(-\frac{D}{2}+\frac{\log\rho}{D}\right)\sqrt{S}; \tag{26}$$

$$\bar{Q}=\frac{Q}{ULw}=\frac{D\rho}{\rho^2-1}\left[1-\frac{2(\rho+1)}{\bar{w}(\rho-1)}\sum\frac{\delta_n J_1(\beta_n)\tanh\beta_n(\rho-1)\bar{w}/2}{\beta_n\{J_1^2(\beta_n)-J_1^2(\beta_n\rho)\}}\right]\sqrt{S}; \tag{27}$$

$$\bar{Q}_z=\frac{Q_z}{ULw}=\frac{2D}{\bar{w}(\rho-1)^2}\left[\sum\frac{\delta_n\{J_1(\beta_n\rho)-\rho J_1(\beta_n)\}\tanh\beta_n(\rho-1)\bar{w}/2}{\beta_n\{J_1^2(\beta_n)-J_1^2(\beta_n\rho)\}}\right]\sqrt{S}. \tag{28}$$

These relations show that all the fundamental characteristics of the pivoted sliders including the slope m, the friction coefficients f and $\bar{f}$, the minimum film thickness h_0, and both the total lubricant flow Q and side leakage Q_z, are proportional to $\sqrt{S}$ for a fixed-pivot position. The effect of the pivot position and the slider width enter only in the coefficients of Eqs. (25)–(28). These are plotted in Figs. 6–11.

It will be seen from Fig. 6 that for all values of the slider width the sliders will adjust themselves to greater wedge angles as the pivot is moved closer to the trailing edge.[12] Thus for a square

[12] The ending of the various curves in Figs. 6–11 at

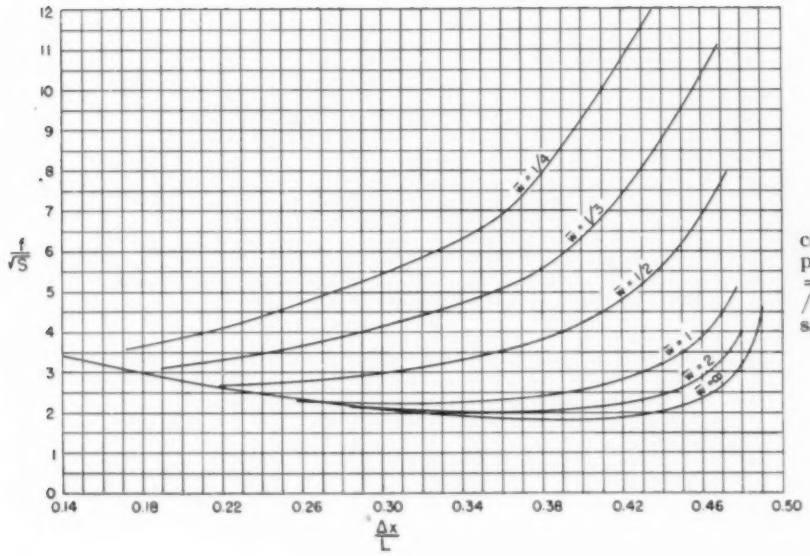

FIG. 7. The variation of the friction coefficient, f, with the pivot position for pivoted sliders of finite width. $\Delta x/L$ = (distance of pivot from trailing edge) /(slider length, L). Rest of notation same as in Fig. 2.

slider a shift of the pivot position from 0.45 to 0.40—measured as fractions of the total length from the trailing edge—will increase the wedge slope, for the same values of S, by a factor of 3.

The wedge angle will also increase for a fixed-pivot position with increasing slider width. In particular, for the fixed-pivot position of 0.40, cutting the width of the square slider by two will decrease the slope of the wedge by a factor of 2.1 for the same load or speed, that is, S. This behavior is clearly due to the fact that the higher film pressures obtaining in the sliders of greater width permit the load to be carried with the greater wedge angles. As indicated directly by Eq. (13), if the pivot position (ρ) and width are kept fixed the load-carrying power will vary inversely as the square of the slope of the wedge angle.

The variation of $f/\sqrt{S}$ is shown in Fig. 7, as a function of the pivot position. The general behavior of all the curves indicates a sharp fall in $f/\sqrt{S}$ as the pivot position is moved away from the center of the slider, very flat minima in the curves for pivot positions less than 0.39 of the slider length, and rather moderate rises to higher values of $f/\sqrt{S}$ as the pivot is moved still further toward the trailing edge. In the case of the slider of infinite width, the minimum in the curve lies at $\Delta x/L = 0.39$. For the sliders of finite width the minima are shifted to smaller values of $\Delta x/L$, and for $\bar{w} < 1$, the curves are still falling over the range of $\Delta x/L$ covered by the calculations. The absolute values of $f/\sqrt{S}$ uniformly increase with decreasing slider width for large values of $\Delta x/L$. Thus for the square slider the friction coefficient with fixed S for a pivot position of 0.40 will be 41 percent greater than for the infinitely wide slider, and for a slider width equal to $\frac{1}{3}$ of the length the coefficient will be 3.48 times as great as for the infinitely wide slider. However, for small values of $\Delta x/L$ the curves tend to merge and ultimately cross. In fact, the infinitely wide slider curve is crossed by those for $\bar{w} = 2$ and 1 at $\Delta x/L > 0.26$, and even that for $\bar{w} = \frac{1}{4}$ should cross after a small extrapolation.

Figure 8 gives the corresponding variations of the minimum film thickness which is, of course, that at the trailing edge. Here, regardless of the slider width, the minimum film thickness first rises as the pivot position is moved away from the center of the slider, reaches a maximum, and then falls rather slowly as the pivot position approaches the trailing edge. For large values of $\Delta x/L$ the minimum film thickness decreases with decreasing slider width, but as $\Delta x/L$ is decreased the curves for finite width ultimately cross that for $\bar{w} = \infty$. Moreover, the maxima of the curves

different values of $\Delta x/L$ is due to the fact that the values of $\Delta x/L$ for the individual values of ρ—and in particular for the largest value, $\rho = 10$—decrease with increasing $\bar{w}$. As previously indicated, the calculations were made by assuming ρ and computing the $\Delta x/L$ corresponding to it by Eq. (18).

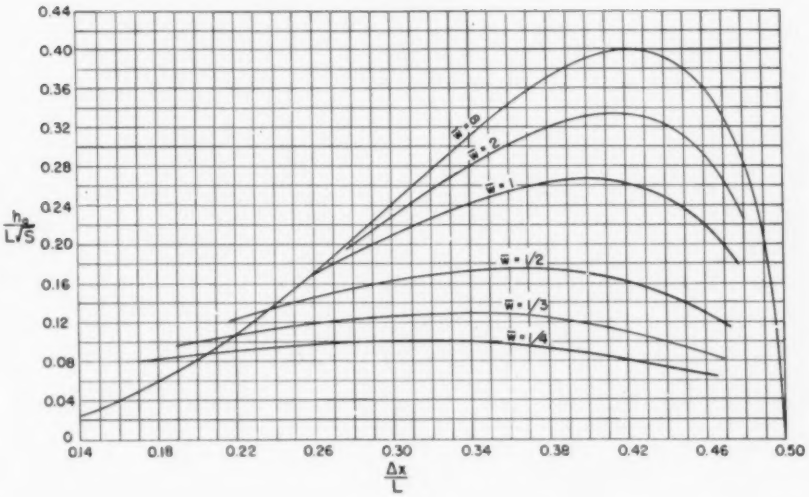

FIG. 8. The variation of the minimum film thickness, h_0, with the pivot position for pivoted sliders of finite width. $\Delta x/L$ = (distance of pivot from trailing edge)/(slider length, L). Rest of notation same as in Fig. 2.

shift to smaller values of $\Delta x/L$ with decreasing slider width, and the rise to and fall from the maxima become increasingly more gradual as the slider width decreases. Hence both from the point of view of obtaining minimum friction and maximum values of the trailing edge film thickness the pivot positions in the finite width sliders should be shifted closer to the trailing edge than is indicated by the theory of the infinitely wide slider. Even so, the absolute values of the minimum film thickness will be materially less in the sliders of finite width near their maximum values. Thus the maximum value of the trailing edge thickness in the square slider will be only 67 percent of that for the infinitely wide slider with the same value of S, while sliders twice as long as they are wide will have maximum trailing edge thicknesses only 44 percent of those of the infinitely wide slider.

At first thought, the result that a slider of finite width could operate with higher trailing edge thickness and lower friction coefficient than the infinitely wide slider with the same pivot position and value of S is indeed surprising. For the pressures in a film open at the sides must certainly be lower than in one of the same geometry except for its infinite width. And indeed this is also directly supported by Fig. 3,

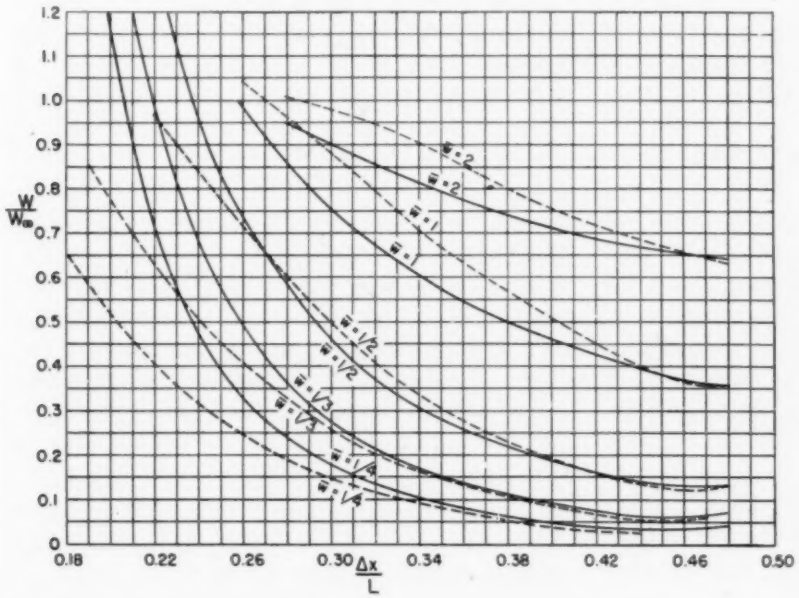

FIG. 9. Relative load-carrying capacities of pivoted sliders of finite width. W/W_∞ = (load per unit width carried by slider of finite width)/(load per unit width carried by slider of infinite width); $\Delta x/L$ = (distance of pivot from trailing edge)/(slider length, L); w = slider width; $\bar{w} = w/L$; solid curves: load-carrying capacities for sliders of equal minimum film thickness; dotted curves: load-carrying capacities for sliders of equal frictional force per unit width.

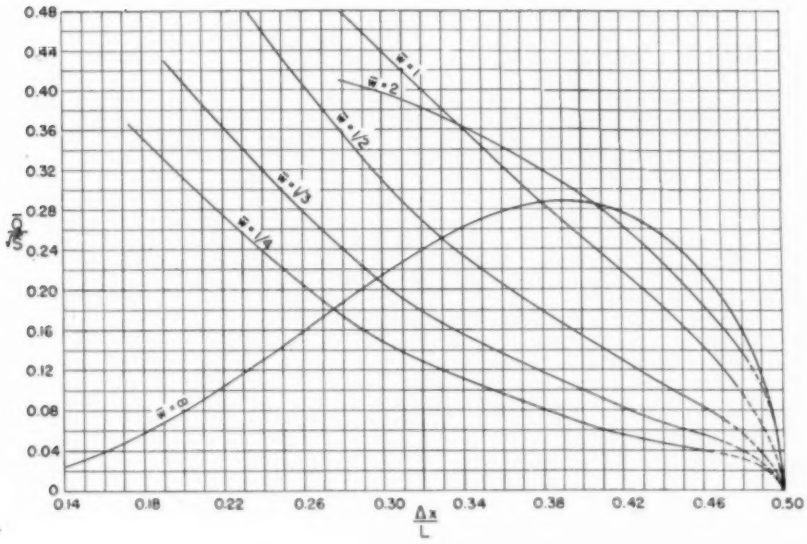

FIG. 10. The variation of the total lubricant flow with the pivot position for pivoted sliders of finite width. $\bar{Q}=Q/UwL$; Q=total lubricant inflow at leading edge; $\Delta x/L$ =(distance of pivot from trailing edge)/(slider length, L). Rest of notation same as in Fig. 2.

which shows that for fixed values of m and h_0 the load-carrying powers of the finite width films will be less than those of the infinite width film. However, it must be noted that in Figs. 7 and 8 the films compared are for sliders with the same pivot position, or center of pressure. The actual geometry of the film will then be materially different for the sliders of different width. In particular, as Fig. 6 shows, the slopes m will be much smaller for the finite width sliders than for the infinitely wide slider, and this drop in m will be especially large for small values of $\Delta x/L$. Since the smaller values of m inherently lead to larger load-carrying capacities, this factor will ultimately counterbalance the direct end effect of the open sides of the finite width slider and enable the latter to carry the applied load with a minimum film thickness that is even higher than that required for the infinitely wide slider. And associated with the higher values of the minimum film thicknesses, is the tendency of the friction coefficients to fall below that of the infinitely wide slider. However, the actual crossing of the friction coefficient curves does not develop as soon as in the case of the minimum film thickness because the friction forces depend on the average film thickness as well as on the minimum thickness.

A somewhat more practical way of expressing the results shown in Figs. 7 and 8 may be had by considering the relative load-carrying capacities of the sliders of finite width as compared to those of infinite width. Thus supposing that the sliders are of the same length, have the same pivot position, and operate at the same speed with lubricants of the same viscosity, the ratios of the loads per unit width carried by the finite and infinite width sliders for equal trailing edge film thicknesses will be given by the reciprocals of the squares of the ordinates of Fig. 8. These ratios are plotted as the solid curves in Fig. 9. While these curves are subject to some error because of the graphical interpolations required for their calculation, there can be little question with regard to their main features. Thus, except for the shallow minima in the region of large $\Delta x/L$, the relative load-carrying capacities will be seen to increase monotonically as the pivot line approaches the trailing edge. And for the smaller values of $\bar{w}$ this increase is so marked that the value unity is exceeded even within the range of the calculations. This corresponds, of course, to the crossing of the curves of Fig. 8, previously discussed. In particular, if $\Delta x/L=0.40$ the square slider will be able to carry a load, per unit width, only 46 percent as great as the infinitely wide slider, for the same speed, film viscosity, and minimum film thickness. And if the slider width is cut to $\frac{1}{4}$ its length the load-carrying capacity will be reduced to only 5 percent of the infinitely wide slider. However, if $\Delta x/L=0.23$ or less, the load-carrying capacities of all sliders whose widths are not less than $\frac{1}{4}$ of their length will even exceed that of the infinitely wide slider.

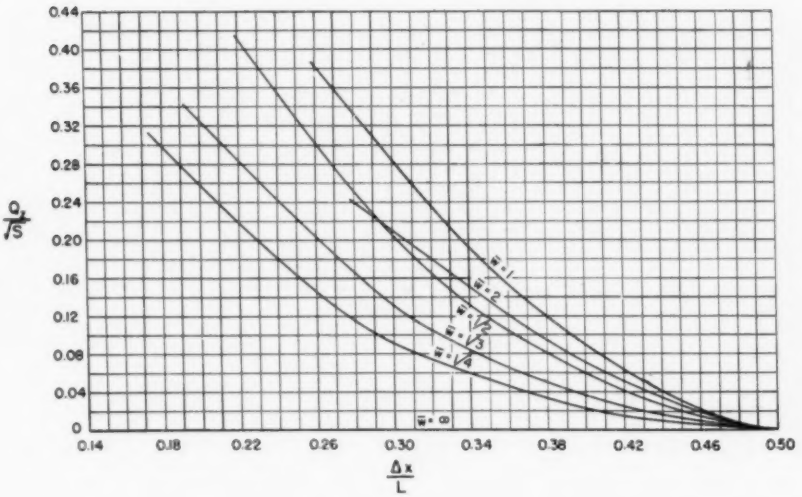

FIG. 11. The variation of the total side leakage with the pivot position for pivoted sliders of finite width. $\bar{Q}_z = Q_z/UwL$; Q_z = total side leakage; $\Delta x/L$ = (distance of pivot from trailing edge)/(slider length, L). Rest of notation same as in Fig. 2.

Considering sliders having the same total frictional force per unit width, the relative load-carrying capacities will be as indicated by the dotted curves of Fig. 9. These were obtained from the ratios of the reciprocals of the squares of the ordinates of Fig. 7 rather than Fig. 8. It will be seen that for practical purposes these relative load-carrying capacities are pretty much the same as those for which the minimum film thickness is kept fixed, although the rise for the sliders of small widths at small values of $\Delta x/L$ is not at all as sharp as in the case of the solid curves.

In Fig. 10 are shown the ratios of $\bar{Q}/\sqrt{S}$ for different slider widths as functions of $\Delta x/L$. The quantities $\bar{Q}$ are the dimensionless total lubricant flows, as defined by Eq. (27). Here it will be seen that the details of the curves depend markedly upon the geometry of the slider. Thus the value of $\bar{Q}$ for the infinitely wide slider increases to a maximum at $\Delta x/L = 0.39$ as the pivot position is moved away from the center of the slider and then decreases as the pivot approaches the trailing edge. For sliders of relatively great width the general behavior is rather similar, although the maxima in the curves are shifted toward considerably lower values of $\Delta x/L$. For narrow sliders, however, the curves show inflections and continue to rise with decreasing values of $\Delta x/L$ even up to values as low as 0.20. As functions of the slider width, for fixed values of $\Delta x/L$, the quantities $\bar{Q}/\sqrt{S}$ will therefore show monotonic increases with increasing width when $\Delta x/L$ is high, but will reach maxima at finite values of the width and fall back again to lower values as the width is made indefinitely large, when the pivot position is appreciably shifted from the center of the slider.

The corresponding results for the dimensionless side leakage, $\bar{Q}_z$, are shown in Fig. 11. Here there appears to be a monotonic increase in side leakage as the pivot position is moved over toward the trailing edge, the side leakage always being zero when the pivot is at the center of the slider. In its variation with the slider width, however, it again increases first as the slider width is diminished, reaches a maximum, and ultimately falls again as the sliders are made still narrower. With respect to the absolute magnitude of the side leakage, it may be noted that while it is necessarily smaller than the total lubricant inflow $\bar{Q}$, it becomes of the same order of magnitude as $\bar{Q}$ except when the pivot position is very close to the centers of the sliders.

The authors are indebted to Dr. Paul D. Foote, Executive Vice President, Gulf Research & Development Company, for permission to publish this paper.

The Formation and Maintenance of Electron and Ion Beams

LLOYD P. SMITH AND PAUL L. HARTMAN
Department of Physics, Cornell University, Ithaca, New York
(Received September 1, 1939)

The radial potential distribution in an ionic beam of circular cross section is calculated and the maximum beam current which can be obtained in a beam of given radius and boundary conditions is computed. In the case of ions the maximum beam currents may be quite small. The ions in such beams have a considerable velocity distribution which in turn leads to a greater beam divergence than former calculations indicate. In Section 3 a method is worked out for holding the beam together during the initial accelerations. A disadvantage of cylindrical lenses is pointed out in this connection. The use of electrostatic lenses for holding together a beam composed of high energy particles is discussed in some detail. Calculations show the special arrangements of the lenses necessary for producing convergence of the beam. A few other arrangements to prevent divergence which were tried experimentally are described.

INTRODUCTION

BEAMS of electrons and positive ions have assumed a place of great importance in modern electronic devices and in researches in physics and biology. In these fields it has become more and more important to increase the current density in the beam. Considerable difficulty has been experienced in obtaining positive ion beams of high intensity and in some cases even with electron beams. In fact, the following analysis will show that there is a definite upper limit to the current that can be obtained in a beam of given cross section under specified voltage conditions. For positive ions this current is quite small.

The problem of beam formation divides itself naturally into five parts: (1) that of keeping the ions together during the period of initial acceleration; (2) the space charge divergence throughout the remainder of the beam length; (3) that of preventing divergence over the high velocity region; (4) the radial potential or velocity distribution in the beam and (5) the maximum beam current that can be realized. These aspects of the problem will be considered in detail in the following sections and various practical methods of holding the beam together will be discussed.

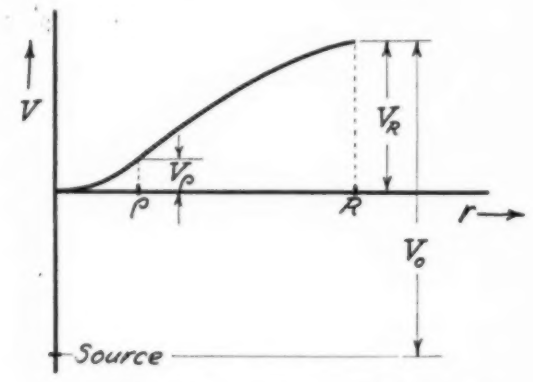

FIG. 1. Key for the designation of the various beam potentials.

1. RADIAL POTENTIAL DISTRIBUTION AND MAXIMUM CURRENT IN BEAM*

In a beam of electrons whose center lies on the axis of a cylindrical surface of definite potential, the potential distribution will in general depend on the distance r from the axis and the distance z along the beam. This general case will not be treated here but it will be assumed that the potential is a function of the radius only. In practice this would correspond to a case where the spreading of the beam was small or to a situation in which the electrons or ions were made to travel parallel to the axis of the beam by the application of an intense magnetic field parallel to the beam axis. Under these circumstances Haeff [1] has determined the potential distribution through a two-dimensionally infinite lamina of finite thickness.

Consider a beam of electrons of radius ρ coaxial with a cylindrical conductor of radius R. The potential at the center of the beam will be taken as zero and the potential of the cylindrical

* The calculations in the first two sections were completed by the first author while temporarily associated with the Research and Engineering Department, RCA Manufacturing Company, Harrison, New Jersey.

[1] A. V. Haeff, Proc. I. R. E. **27**, 586 (1939).

surface as V_R while the potential difference between cylinder and source of electrons will be denoted by V_0 as shown in Fig. 1. The velocity of an electron or ion of mass M at a distance r from the axis is

$$v=(m/M)^{\frac{1}{2}}\{(2e/m)[V_0-V_R+V(r)]\}^{\frac{1}{2}}$$

and the charge density is $\sigma=-i/v$ where i is the constant current density. In cylindrical coordinates, Poisson's equation for the resulting potential distribution is

$$\frac{1}{r}\frac{d}{dr}\left(r\frac{dV}{dr}\right)=\left(\frac{M}{m}\right)^{\frac{1}{2}}\times\frac{4\pi i}{([2e/m][V_0-V_R+V(r)])^{\frac{1}{2}}}.$$

The above equation may conveniently be expressed in terms of the dimensionless variables s and φ where

$$r=as \quad \text{and} \quad \varphi=V(r)/(V_0-V_R) \tag{1}$$

and

$$a^2=\frac{(m/M)^{\frac{1}{2}}(2e/m)^{\frac{1}{2}}}{4\pi i}(V_0-V_R)^{\frac{3}{2}}. \tag{2}$$

In these variables the differential equation becomes

$$\frac{1}{s}\frac{d}{ds}\left(s\frac{d\varphi}{ds}\right)=\frac{1}{(1+\varphi)^{\frac{1}{2}}}. \tag{3}$$

Before discussing the actual solution of this equation, it is advantageous to discuss the conditions at the boundary of the beam and their relation to the total beam current. In the region $\rho<r\leq R$ the charge density is zero and it is readily found that the potential in this region is given by

$$V'=\frac{(V_R-V_\rho)\log r/\rho+V_\rho\log R/\rho}{\log R/\rho}, \tag{4}$$

$$\rho\leq r\leq R,$$

where V_ρ is the potential at the beam boundary. This potential must smoothly join the potential for $r<\rho$ at $r=\rho$ which requires that

$$dV'/dr\}_{r=\rho}=dV/dr\}_{r=\rho}.$$

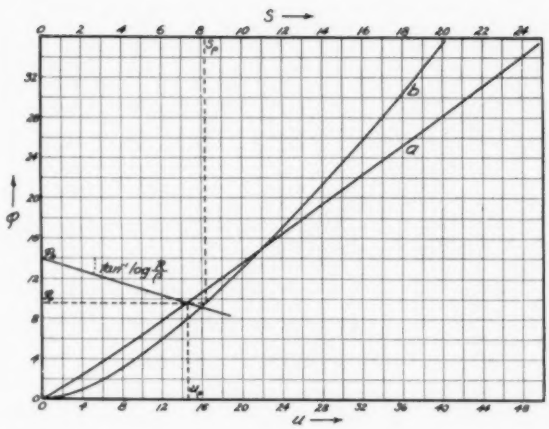

FIG. 2. Curve a shows φ as a function of u. Curve b shows φ as a function of s. Heavy straight line is a plot of Eq. (5). Dashed line indicates procedure for determining s_ρ.

In terms of the variables φ and s, this relation becomes

$$\frac{(V_0-V_R)}{a}\left(\frac{d\varphi}{ds}\right)_{s_\rho}=\frac{V_R-V_\rho}{\log R/\rho}\frac{1}{\rho}$$

or

$$\varphi_\rho=\varphi_R-\log\frac{R}{\rho}s_\rho\left(\frac{d\varphi}{ds}\right)_{s_\rho}, \tag{5}$$

where

$$\varphi_\rho=V_\rho/(V_0-V_R) \quad \text{and} \quad s_\rho=\rho/a. \tag{6}$$

Eq. (5) may be regarded as an equation for the determination of the value of s corresponding to the beam boundary for proper matching. This together with Eq. (2) then determines the total beam current in terms of V_0 and V_R. The form of Eq. (5) suggests the following procedure for determining s_ρ. Assuming that the solution of Eq. (3) is known and letting $sd\varphi/ds=u$, $\varphi(s)$ is plotted as a function of u as shown by curve a in Fig. 2. Eq. (5) may be written

$$\varphi=\varphi_R-\log R/\rho\cdot u$$

and is represented by the straight line in Fig. 2 whose slope is $-\log R/\rho$. The intersection of this line and curve a determines the values of φ and u at the beam boundary, namely φ_ρ and u_ρ. By plotting φ as a function of s in the same figure, curve b, the value of s corresponding to φ_ρ can be found as indicated by the dotted line in Fig. 2.

With the value of s_ρ thus determined, the value of the total beam current I as a function of V_R/V_0 can be found, since $a=\rho/s$ and the

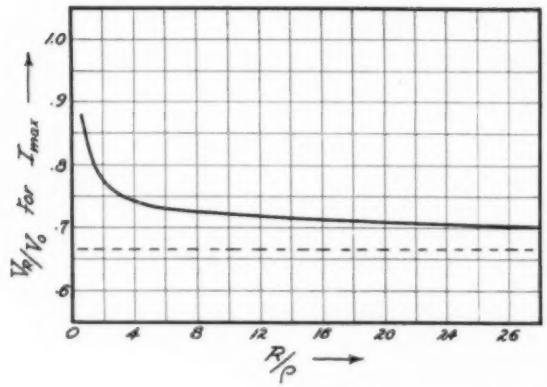

FIG. 3. V_R/V_0 for maximum beam current as a function of R/ρ.

relation (2) give

$$w=\frac{6.07\times10^{4}(M/m)^{\frac{1}{2}}I(\text{amp.})}{\{V_0(\text{volts})\}^{\frac{3}{2}}}=\left(1-\frac{V_R}{V_0}\right)^{\frac{3}{2}}s_\rho^2. \quad (7)$$

The solution of Eq. (3) cannot be given in terms of elementary functions. For values of s not too large a useful series solution satisfying the conditions $\varphi=d\varphi/ds=0$ at $s=0$ may be found in the usual way. The first three terms in this series give

$$\varphi=\frac{s^2}{4}\left(1-\frac{s^2}{2\cdot4^2}+\frac{7s^4}{4^3\cdot6^2}\cdots\right). \quad (8)$$

This gives values of φ accurate to less than 1 percent even at $s=2$. For large values of s the equation was integrated numerically to provide the curves plotted in Fig. 2.

In order to calculate s_ρ analytically, (when s_ρ is not too large) Eq. (8) is substituted in Eq. (5), which after some rearrangement gives

$$s_\rho^2=\frac{1}{1+2\log R/\rho}\left[\frac{4x}{1-x}+\frac{1+4\log R/\rho}{2\cdot4^2}s_\rho^4-\frac{7}{4^3\cdot6^2}\left(1+6\log\frac{R}{\rho}\right)s_\rho^6\right].$$

The value of s_ρ can be obtained by solving this equation by the method of successive approximations starting with

$$(s_\rho^2)_1=\frac{1}{1+2\log R/\rho}\,\frac{4x}{1-x}$$

as the first approximation, where $x=V_R/V_0$. Three approximations are warranted here and the third approximation yields

$$s_\rho^2=A\frac{x}{1-x}\left\{1+B\frac{x}{1-x}+C\left(\frac{x}{1-x}\right)^2\cdots\right\}, \quad (9)$$

where

$$A=\frac{1}{4}\,\frac{1}{1+2\log R/\rho},$$

$$B=\frac{1+4\log R/\rho}{8(1+2\log R/\rho)^2}, \quad (10)$$

$$C=\frac{1}{16}\left[\frac{(1+4\log R/\rho)^2}{2(1+2\log R/\rho)^4}-\frac{7}{9}\,\frac{1+6\log R/\rho}{(1+2\log R/\rho)^3}\right].$$

From Eq. (7) the total beam current is proportional to $(1-x)^{\frac{3}{2}}s_\rho^2=w$. When $Cx/(1-x)\ll1$ the value of x which makes w a maximum can be determined in the usual way and its value is readily found to be

$$(x=V_R/V_0)_{\max I}=\frac{2}{3}\left[1+\frac{1}{4}\,\frac{1+4\log R/\rho}{(1+2\log R/\rho)^2}\right]. \quad (11)$$

The slowly varying function of R/ρ on the right is plotted in Fig. 3. Eq. (11) furnishes the rather surprising result that the maximum beam current does not occur when $V_R=V_0$ but $V_R\approx\frac{2}{3}V_0$. By comparing the analytical values of x for maximum I with those found by the graphical method, it has been established that the values computed from Eq. (11) are very accurate for the entire range $1\leq R/\rho<\infty$.

In Fig. 4, w has been plotted as a function of V_R/V_0 for several values of R/ρ including the interesting case when $R/\rho=1$. The beam current for any given value of V_0 can then be calculated by means of relation (7). It is interesting to note that for $R/\rho=10$ and $V_0=1000$ volts, the maximum beam current of molecular hydrogen ions is only 2.6 ma.

The radial voltage distribution in the beam is of very great practical importance. On account of it, the electrons or ions have a considerable range of velocities. It is more useful to express the potential at any point in the beam with respect to the source of electrons or ions. This potential will be denoted by V_s and may be

expressed in terms of the potentials already used by writing

$$V_s = V_0 - V_R + V(r) = V_0 - V_R + (V_0 - V_R)\varphi \quad (12)$$

or $V_s/V_0 = (1 - V_R/V_0)(1+\varphi)$. φ may be expressed in terms of r/ρ by replacing s in (8) by $s = r/a = (r/\rho)s_\rho$, which gives

$$V_s/V_0 = \left(1 - \frac{V_R}{V_0}\right)\left[1 + \frac{s_\rho^2}{4}(r/\rho)^2\left\{1 - \frac{1}{8}\frac{s_\rho^2}{4}(r/\rho)^2 + \frac{7}{4\cdot 6^2}(s_\rho^2/4)^2(r/\rho)^4 \cdots\right\}\right], \quad r/\rho \leq 1. \quad (13)$$

The function of r contained in the brackets $\{\ \}$ is normally a rather slowly varying function of r especially for $R/\rho \gg 1$, so that the voltage distribution in the beam is rather closely represented by

$$V_s/V_0 \cong \left(1 - \frac{V_R}{V_0}\right)\left(1 + \frac{s_\rho^2}{4}\frac{r^2}{\rho^2}\right), \quad r/\rho \leq 1. \quad (14)$$

The voltage distribution outside of the beam

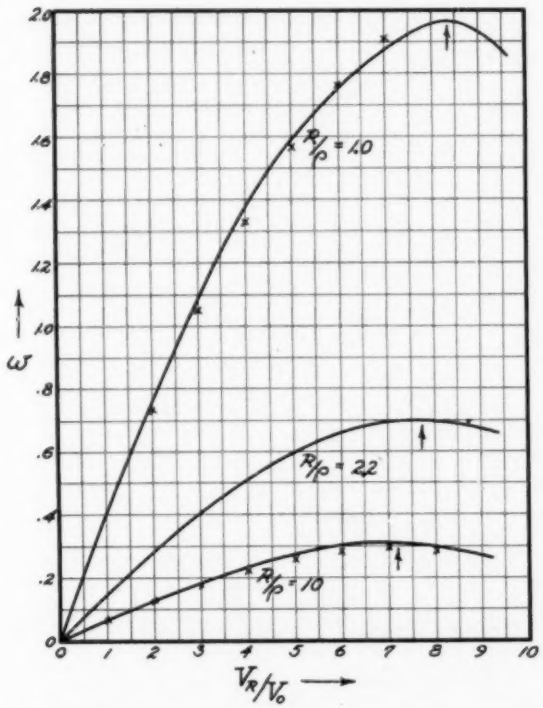

FIG. 4. w, which is proportional to beam current I, plotted as a function of V_R/V_0. Arrows indicate value of V_R/V_0 for maximum w as computed by Eq. (11). Crosses indicate values of w computed from Eqs. (7) and (9).

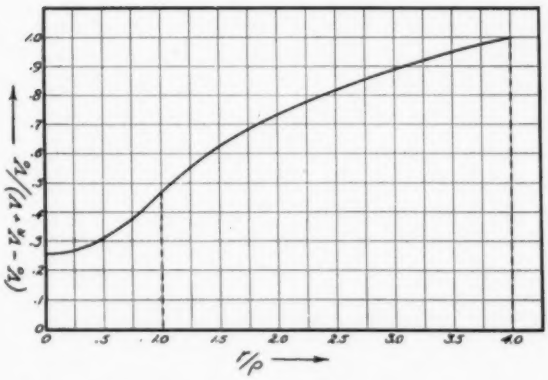

FIG. 5. Potential distribution from center of beam to boundary cylinder for $R/\rho = 4$ and maximum beam current.

$1 \leq r/\rho \leq R/\rho$ is readily found from (4) so that

$$V_s/V_0 = (1 - V_R/V_0) + \frac{(V_R/V_0 - V_\rho/V_0)\log r/\rho + (V_\rho/V_0)\log R/\rho}{\log R/\rho}, \quad (15)$$

$$1 \leq r/\rho \leq R/\rho.$$

The voltage distribution for maximum beam current for $R/\rho = 4$ as computed from expressions (13) and (15) is shown in Fig. 5. This clearly brings out the fact that all of the electrons in the beam are traveling with velocities very much different than that corresponding to the applied voltage V_0. This is an extremely important matter in certain uses of electron and ion beams. In particular when the confining magnetic field is removed the beam diverges faster than one would expect. This is shown in the next section.

2. Divergence of the Beam

The divergence of an electron or ion beam produced by the mutual repulsion of the charged particles in the beam has been computed by several people.[2] In these computations it has been assumed that all of the electrons or ions in the beam are traveling with the same velocity. The analysis of the preceding section shows that this will not be the case except for extremely low beam currents. The velocity distribution of the

[2] E. E. Watson, Phil. Mag. **3**, 849 (1924). M. Knoll and E. Ruska, Ann. d. Physik **12**, 604 (1932). F. D. Fowler and G. F. Gibson, Phys. Rev. **46**, 1075 (1934).

electrons in the beam will cause the beam to diverge more rapidly than the above-mentioned computations would indicate. In calculating the divergence, it will be assumed that the electrons retain the velocity distribution characteristic of the initially confined beam. This is justified provided the divergence is not large.

The radial force acting on an electron initially at the outside edge of the beam may be found by differentiating expression (15) with respect to r. This gives

$$E_r = \frac{V_R - V_\rho}{\log R/\rho}\frac{1}{r} = \frac{(V_0 - V_R)u_\rho}{r}. \tag{16}$$

The term on the right was obtained with the help of Eq. (5). The equation of motion in the radial direction is

$$M\frac{d^2r}{dt^2} = \frac{(V_0 - V_R)u_\rho e}{r}. \tag{17}$$

The equation of the path may be obtained by writing $v_\rho = dz/dt$ where z is the coordinate along the beam axis and v_ρ is the velocity of the electron initially at the beam edge. Then

$$\frac{d^2r}{dz^2} = \frac{e}{M}\frac{(V_0 - V_R)u_\rho}{v_\rho^2 r} = \frac{u_\rho}{2(1+\varphi_\rho)r}.$$

Integrating this equation twice gives

$$z = 2\rho\left(\frac{1+\varphi_\rho}{u_\rho}\right)^{\frac{1}{2}}\int_0^{(\log r/\rho)^{\frac{1}{2}}} e^{\xi^2}d\xi. \tag{18}$$

The expression for z obtained by Fowler and Gibson[2] may be written

$$z' = 2\rho(2/w)^{\frac{1}{2}}\int_0^{(\log r/\rho)^{\frac{1}{2}}} e^{\xi^2}d\xi, \tag{19}$$

where w is defined by (7). The ratio of the distances required for the beam to diverge the same amount in the two cases is

$$z/z' = \frac{((1+\varphi_\rho)w)^{\frac{1}{2}}}{2u_\rho}. \tag{20}$$

This ratio is plotted as a function of w in Fig. 6 for the case $R/\rho = 10$. The ratio is less than unity for all values of w up to its maximum value except at $w = 0$ where the ratio is unity. Thus the two computations are in agreement only for extremely small beam currents. At maximum beam current ($w \leqq 0.3$ in this case) the beam will diverge a given amount in about one-half the distance computed by Fowler and Gibson.

3. Prevention of Beam Divergence During Acceleration

In the early stages of beam formation the electrons or ions start with a relatively low velocity and are accelerated. The natural divergence computed in the last section is especially marked at low velocities and must be prevented. It will be shown in this section that it is always possible in principle to hold the beam together during acceleration. It is only necessary to produce a radial force toward the center of the beam which is somewhat greater than that produced by the charge in the beam. Such a radial field arises whenever the gradient of the electric field in the beam direction increases with distance along the beam.

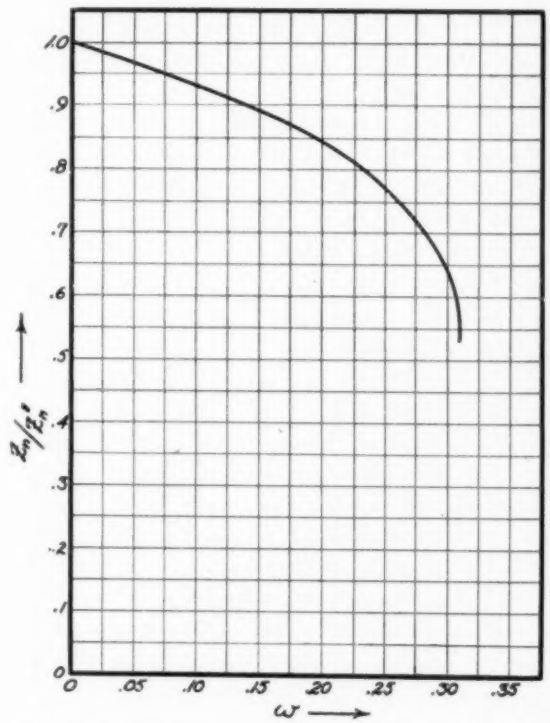

Fig. 6. Ratio of distances for beam to diverge a given amount taking into account and not taking into account the voltage distribution through the beam. $R/\rho = 10$.

When Gauss' theorem is applied to a cylindrical surface of length Δz coaxial with the beam of not too large a radius, it is readily found that the radial component of electric field is given by

$$E_r=\tfrac{1}{2}(4\pi\sigma-\partial E_z/\partial z)r,$$

where $\sigma=i/v$ is the charge density and v is the velocity of the particles in the beam and E_z is the component of electrical field along the axis of the beam. Expressing E_z and v in terms of the potential at a given point we arrive at the following differential equation for the way in which V must vary in order that $E_r=0$:

$$\frac{d^2V}{dz^2}+\frac{4\pi i}{(2Ve/m)^{\frac{1}{2}}}=0.$$

The signs are to be so chosen that $Ve>0$ and $id V/dz<0$. The solution of this equation subject to the boundary conditions $V=dV/dz=0$ at $z=0$ is

$$V=\frac{3^{4/3}}{(2e/m)^{1/3}}\left(\frac{\pi}{|i|}\right)^{2/3}z^{4/3}.$$

This may conveniently be written

$$V(\text{volts})=5680|i(\text{amp.})|^{2/3}(M/m)^{1/3}z^{4/3}, \quad (21)$$

where M/m is the ratio of the mass of the particle considered to that of an electron. It is of interest to note that this is the potential variation given by the Child-Langmuir equation for the case of a diode with infinite parallel plane electrodes.

A convenient practical way of obtaining this variation of potential along the axis is to pass the beam through holes in a succession of closely spaced disk electrodes the potential of which increases so as to produce the proper variation along the axis. If the potential increases faster than the $\frac{4}{3}$ power of z then the beam will be confined to a smaller cross section. It should be noticed that for beams of not too large a radius the space charge force is compensated throughout the entire cross section of the beam.

It is of considerable practical importance to realize that the use of cylindrical electrodes for rapidly increasing the velocity of relatively slow electrons or ions may result in the loss of a large number of particles from the beam by over-focusing. In order to obtain some idea of the order of magnitude of this effect the path of an electron or ion was computed for a particular case neglecting space charge but using the otherwise exact equation[3]

$$\frac{2U}{1+(dr/dz)^2}\frac{d^2r}{dz^2}-\frac{\partial V}{\partial z}\frac{dr}{dz}+\frac{\partial V}{\partial r}=0, \quad (22)$$

where $Ue>0$ is the energy of the particle and V is the potential within two adjacent coaxial cylinders of radius R separated by a plane. Since this equation is invariant under a transformation of the unit of length, the unit will be taken as the radius R of the cylinder. For convenience the initial energy Ue in this case will be taken to be $Ue=V_0-V(r_0,z_0)$ where $2V_0$ is the potential difference between the two cylinders and $r_0=0.9$ and $z_0=-1$, z being measured from the plane of separation of the electrodes.

The potential within the cylinders in the neighborhood of the plane of separation for long cylinders and for electron acceleration is given by

$$\begin{aligned}
V/V_0&=-\frac{1}{\pi}\int_{-\infty}^{+\infty}\frac{J_0(i\mu r)}{J_0(i\mu)}\frac{\sin\mu z}{\mu}d\mu\\
&=\frac{z}{|z|}\left[1-2\sum_{n=1}^{\infty}\frac{J_0(y_nr)e^{-y_n|z|}}{J_1(y_n)y_n}\right],\\
\frac{1}{V_0}\frac{\partial V}{\partial r}&=-\frac{i}{\pi}\int_{-\infty}^{+\infty}\frac{J_1(i\mu r)}{J_0(i\mu)}\sin\mu z d\mu\\
&=\frac{z}{|z|}2\sum_{n=1}^{\infty}\frac{J_1(y_nr)e^{-y_n|z|}}{J_1(y_n)}, \qquad (23)\\
\frac{1}{V_0}\frac{\partial V}{\partial z}&=-\frac{1}{\pi}\int_{-\infty}^{+\infty}\frac{J_0(i\mu r)}{J_0(i\mu)}\cos\mu z d\mu\\
&=+2\sum_{n=1}^{\infty}\frac{J_0(y_nr)e^{-y_n|z|}}{J_1(y_n)},
\end{aligned}$$

where $J(r)$ denotes the Bessel's function of the first kind and y_n denotes the zeros of $J_0(y)$. The convergence of the above series is sufficiently rapid to use them in the numerical integration of Eq. (22). This was done for the initial conditions $dr/dz=0$ at $r_0=0.9$ and $z_0=-1$ and

[3] E. g., see I. G. Maloff and D. W. Epstein, *Electron Optics in Television* (McGraw-Hill, 1938), p. 80.

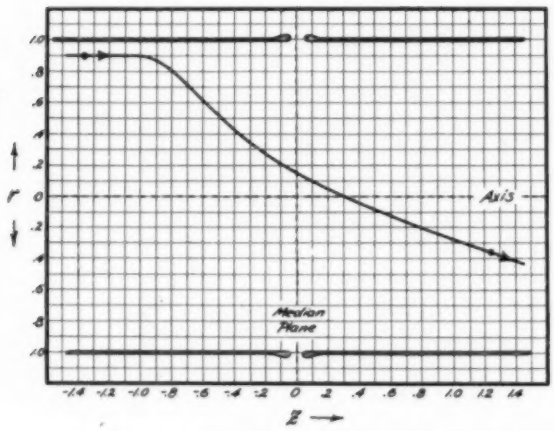

FIG. 7. Trajectory showing overfocusing when a relatively slow charged particle is appreciably accelerated through cylindrical electrodes.

initial energy

$$U/V_0=1-\frac{V(r_0,z_0)}{V_0}=1-\frac{V(0.9,-1)}{V_0}\leqq 0.02.$$

This means that for 100,000 volts across the cylinders the initial energy corresponds to $U=1000$ volts. The resulting path is shown in Fig. 7. It is readily seen that an electron or ion attains a considerable radial component of velocity which it tends to retain. As a result the ion strikes the cylinder wall about two and one-half radii from the gap. This shows the overfocusing characteristic of cylindrical lenses for slow particles rather far from the center of the beam and indicates that for large initial accelerations such cylindrical electrodes should be avoided.

4. The Use of Electrostatic Lens Systems for Suppressing Divergence in High Energy Beams

In this section the effect of a succession of electrostatic lenses with cylindrical symmetry will be investigated. It is found that the beam will diverge to some extent except for certain special cases. The velocity of the particles will be assumed large enough so that space charge may be neglected. The focusing effect of a succession of two-dimensional lenses has been treated by Rose[4] who also took into account the effect of a time variation of the potential difference across the electrodes. In the following analysis of electric lenses with cylindrical symmetry no time variation of the fields will be considered.

The differential equation of the path of a positive ion through the nth lens for $(dr/dz)^2\ll 1$ is

$$2(U_n-V)^{\frac{1}{2}}\frac{d}{dz}\left[(U_n-V)^{\frac{1}{2}}\frac{dr}{dz}\right]=-\frac{\partial V}{\partial r}, \quad (24)$$

where V is the potential at the point r, z, such that $V(r,0)=0$ and U_n is the voltage the ion has fallen through by the time it has reached the median plane $z=0$ as illustrated in Fig. 8. In the following calculation only those ion paths will be considered for which the potential at any point in the lens may be represented by $V(r,z)=V(0,z)-(d^2V/dz^2)(r^2/4)$. When this expression is used Eq. (24) becomes

$$\frac{d^2r}{dz^2}-\frac{dV/dz}{2(U_n-V)}\cdot\frac{dr}{dz}-\frac{1}{4(U_n-V)}\cdot\frac{d^2V}{dz^2}r=0. \quad (25)$$

It may be readily be shown[5] that

$$r=(U_n-V)^{-\frac{1}{4}}\psi, \quad (26)$$

where ψ satisfies the differential equation

$$\frac{d^2\psi}{dz^2}+\frac{3}{16}\left\{\frac{dV/dz}{U_n-V}\right\}^2\psi=0. \quad (27)$$

Since this discussion pertains to particles having a high energy, powers of V_0/U_n higher than the first will be neglected where $2V_0$ is the potential difference across the lens. In this approximation Eq. (27) reduces to $d^2\psi/dz^2=0$ so that

$$r=(A+Bz)\{U_n-V(r,z)\}^{-\frac{1}{4}} \quad (28)$$

and

$$\frac{dr}{dz}=B\{U_n-V(r,z)\}^{-\frac{1}{4}}+\tfrac{1}{4}(A+Bz)\{U_n-V(r,z)\}^{-5/4}\frac{dV}{dz}. \quad (29)$$

This shows that the path of the particle sufficiently far from the median plane to either side is a straight line as shown in Fig. 8 because V

[4] M. E. Rose, Phys. Rev. **53**, 392 (1938).

[5] E.g., see E. T. Whittaker and G. N. Watson, *Modern Analysis* (Cambridge University Press, 1920), p. 194.

becomes constant and $dV/dz=0$ here. If these straight portions of the path are continued to the median plane their points of intersection with this plane will be a distance Δr_n apart. The slopes of the straight line portion of the paths to the left and right of $z=0$ will be designated as $\alpha_{n-\frac{1}{2}}$ and $\alpha_{n+\frac{1}{2}}$, respectively, and the difference in slope will be $\Delta\alpha_n=\alpha_{n+\frac{1}{2}}-\alpha_{n-\frac{1}{2}}$. The effect of any one lens will be determined by the values of Δr_n and $\Delta\alpha_n$. These quantities may now be calculated from Eq. (28). For large negative values of z, $V(r,z)=V_0$ and for large positive z $V(r,z)=-V_0$. The constants A and B in Eq. (28) may be determined by noting that $r=r_n$ for $z=0$ and $dr/dz\}_{z=-\infty}=\alpha_{n-\frac{1}{2}}$ and $dr/dz\}_{z=+\infty}=\alpha_{n+\frac{1}{2}}$ and have the values

$$A=U_n^{\frac{1}{2}}r_n, \tag{30}$$

$$B=\alpha_{n-\frac{1}{2}}\{U_n-V_0\}^{+\frac{1}{2}}=\alpha_{n+\frac{1}{2}}\{U_n+V_0\}^{+\frac{1}{2}}. \tag{31}$$

Consequently the paths of the particle on the right and left of the median plane are

$$r_R=\left(1-\frac{V(r,z)}{U_n}\right)^{-\frac{1}{2}}r_n+\left[\frac{1-V(r,z)/U_n}{1+V_0/U_n}\right]^{-\frac{1}{2}}\alpha_{n+\frac{1}{2}}z,$$

$$r_L=\left(1-\frac{V(r,z)}{U_n}\right)^{-\frac{1}{2}}r_n+\left[\frac{1-V/U_n}{1-V_0/U_n}\right]\alpha_{n-\frac{1}{2}}z.$$

The value of Δr_n, computed from these expressions as mentioned above, is

$$\Delta r_n=\left(1+\frac{V_0}{U_n}\right)^{-\frac{1}{2}}r_n-\left(1-\frac{V_0}{U_n}\right)^{-\frac{1}{2}}r_n$$

$$\leqq-\frac{1}{2}\frac{V_0}{U_n}r_n. \tag{32}$$

It is easily found that

$$\Delta\alpha=\left.\frac{dr}{dz}\right\}_{z=\infty}-\left.\frac{dr}{dz}\right\}_{z=-\infty}$$

$$=\left[\left\{\frac{1+V_0/U_n}{1-V_0/U_n}\right\}^{-\frac{1}{2}}-1\right]\alpha_{n-\frac{1}{2}}\leqq-\frac{1}{2}\frac{V_0}{U_n}\alpha_{n-\frac{1}{2}}. \tag{33}$$

The change in r_n per lens depends on the slope of the particles' path and distance l_n between the $(n-1)$st and nth lens and the displacement Δr_n. Thus we may write

$$dr_n/dn=\alpha_{n-\frac{1}{2}}l_n+\Delta r_n.$$

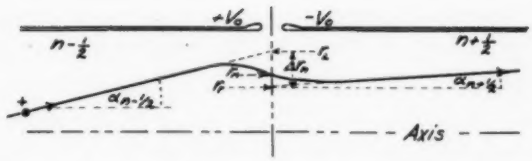

FIG. 8. The effect of a cylindrical electric lens on the path of a charged particle near the axis.

By differentiating this equation and eliminating $\alpha_{n-\frac{1}{2}}$ one obtains the differential equation for the particles' path through a succession of lenses namely

$$\frac{d^2r_n}{dn^2}=\left\{\frac{dr}{dn}-\Delta r_n\right\}\frac{1}{l_n}\frac{dl_n}{dn}+\frac{d}{dn}\Delta r_n+l_n\Delta\alpha. \tag{34}$$

When it is assumed that the particle receives the same increase in energy at each lens, $U_n=2V_0n$ and this together with expressions (32), (33) and (34) gives

$$\frac{d^2r_n}{dn^2}-\left(\frac{1}{l_n}\frac{dl_n}{dn}-\frac{1}{2n}\right)\frac{dr_n}{dn}-\frac{1}{4nl_n}\frac{dl_n}{dn}r_n=0, \tag{35}$$

where terms of the order $1/n^2$ have been neglected. For generality, let the lenses be spaced according to the law

$$l_n=l_0n^m, \tag{36}$$

in which case the solution of Eq. (35) neglecting terms in $1/n^2$ and higher is

$$r_n=An^{(2m+1)/2}+B. \tag{37}$$

This result is interesting in that when the law of spacing of the lenses is such that $m>-\frac{1}{2}$, the ion beam will always diverge but when $m<-\frac{1}{2}$ the beam will converge. In the case of a linear resonance accelerator[6] the lengths are given by

$$l_n=l_0n^{\frac{1}{2}},$$

so that here the beam diverges according to the law

$$V_n=An+B.$$

Another lens of interest may be handled in much the same manner, namely, the lens obtained by placing a plane grid over the face of the high velocity electrode of the previously considered cylindrical lens. In this case the

[6] P. L. Hartman and Lloyd P. Smith, Rev. Sci. Inst. **10**, 223 (1939).

potential of the grid at $z=0$ and at greater values of z is assumed to be zero, and at values of large negative z is assumed to be $2V_0$. Instead, however, of taking $(dr/dz)_{z=\infty}=\alpha_{n+1}$ to evaluate constants, it is necessary to take $(dV/dz)_{z=0}=\alpha_{n+1}$ and evaluate constants with this and the previous boundary conditions, the reason being that the derivatives of the potential are discontinuous at this point. Carrying through the same procedure used previously in evaluating the lens effects one finds the same Δr_n:

$$\Delta r_n \leqq -V_0 r_n/2U_n. \tag{38}$$

For $\Delta\alpha$ one obtains the somewhat different result

$$\Delta\alpha \leqq -\frac{V_0}{2U_n}\alpha_{n-1}+\frac{r_n}{4U_n}\left(\frac{dV}{dz}\right)_{z=0}. \tag{39}$$

Here $(dV/dz)_{z=0}$ is interpreted as being the limit of the electric field as z approaches zero from the negative side. Since $(dV/dz)_{z=0}$ is negative, this term gives the lens stronger focusing action than the ordinary cylindrical lens.

For a succession of such lenses such as previously considered for the symmetrical cylindrical lens one obtains the differential equation for r_n

$$\frac{d^2r_n}{dn^2}-\left(\frac{1}{l_n}\frac{dl_n}{dn}-\frac{1}{2n}\right)\frac{dr_n}{dn} -\left\{\frac{1}{4nl_n}\frac{dl_n}{dn}+\frac{l_n}{8nV_0}\left(\frac{dV}{dz}\right)_{z=0}\right\}r_n=0. \tag{40}$$

Again taking $l_n=l_0n^m$ one finds the equation to have the solution

$$r_n=Sn^{+(2m-1)/4}$$

where

$$\frac{d^2S}{dn^2}-\frac{l_0n^{m-1}}{8V_0}\left(\frac{dV}{dz}\right)_{z=0}S=0.$$

Solving this by the W.K.B. method and substituting above gives for a succession of lenses of this type

$$r_n=n^{m/4}\left[-\frac{l_0}{8V_0}\left(\frac{dV}{dz}\right)_{z=0}\right]^{-\frac{1}{4}} \times\exp\left[\pm i\left\{-\frac{l_0}{8V_0}\left(\frac{dV}{dz}\right)_{z=0}\right\}^{\frac{1}{2}}\frac{2n^{m+1/2}}{m+1}\right]. \tag{41}$$

It is seen that this is an oscillating function the amplitude and wave-length increasing or decreasing depending on m. When $m<0$ the solution converges and for $m>0$ the solution diverges, the results being markedly different in this respect from the ordinary cylindrical lens. For the linear resonance accelerator referred to above, where $m=\frac{1}{2}$ one has

$$r_n=n^{1/8}\left[-\frac{l_0}{8V_0}\left(\frac{dv}{dz}\right)_{z=0}\right]^{-\frac{1}{4}} \times\exp\left[\pm i\left\{-\frac{l_0}{8V_0}\left(\frac{dV}{dz}\right)_{z=0}\right\}^{\frac{1}{2}}\frac{4}{3}n^{3/4}\right].$$

The beam diverges very much less in this case than for the symmetrical cylindrical lens discussed above.

Instead of merely taking l_n to be some particular function of n one could also take U_n to be some other function of n than $2nV_0$ and determine requirements for a focused beam.

All the results here obtained are independent of the e/m value of the accelerated particle.

5. Experimental Attempts at Low Velocity Focusing

In connection with the confining of low energy ion beams of considerable intensity, it may be of interest to consider some experiments made in this connection in work on an acceleration device of the linear resonance type. In the particular device it was desired to pass the beam of ions from the source through a delivery tube about 2.5 centimeters in diameter to the accelerator, a distance of about 30 centimeters. The source was a low voltage type[7] and it was desirable to refrain from the use of high voltages to confine the ion beam. But with low voltages of a couple of kilovolts or less, a beam of only about a microampere was obtainable at the accelerator when perhaps a milliampere or so was delivered by the source.

The first attempt at improvement consisted of mounting inside, and coaxial with the delivery tube, a helical grid about 2 centimeters in diameter and biased negatively with respect to the delivery tube around it. It was thought that

[7] G. W. Scott, Phys. Rev. **56**, 954 (1939).

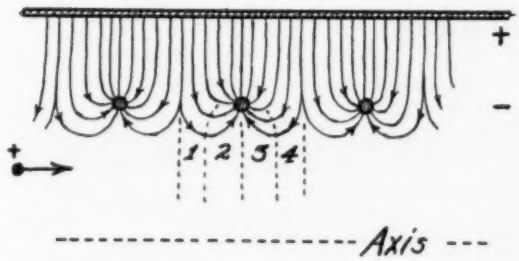

FIG. 9. The electric field in a cylindrical grid type of focusing device.

there might be sufficient field penetration from the outside cylinder to keep the beam confined within the grid. As shown in the sketch of Fig. 9 the grid wires do act as lenses with non-image-forming properties. In region 1 of each wire in the grid there is convergent action and in region 2 divergent action acting for a shorter period of time due to the particle's higher velocity. Again, region 3 is diverging but also acting for a shorter time than the convergent action of region 4 due to the particle's slower velocity in region 4. One cannot say easily what the net lens action will be, due to the stronger field in near the grid wire than away from it. At any rate not much improvement over the ordinary tube was noted.

A second attempt was made with another non-image-forming device. A 5-mil tungsten wire was stretched along the axis of the tube and biased negatively with respect to the tube itself, giving rise to a purely radial field driving particles toward the axis. With about 700 volts potential difference between the wire and the tube, a beam of about 50 microamperes of 2000 volt hydrogen ions was obtained at the accelerator end. With the wire heated to copious electron emission temperature a current of the same order of magnitude was obtained with no radial field other than that due to the voltage drop in the wire itself, which was less than 50 volts. The greater part of the focusing here was due primarily to some ion space charge neutralization.

A third improvement was made with the use of cylindrical lenses. It is, of course, well known that a cylindrical lens produces convergence whether or not it accelerates or decelerates the particles passing through it. With this in mind, a series of about twenty cylindrical lenses were mounted within the delivery tube, which alternately accelerated and decelerated the particles giving rise to a considerable net radial deflection. With about 300 volts between successive cylinders, a current of about 150 microamperes was obtained at the acceleration end of the delivery tube.

The most satisfactory arrangement so far was had by surrounding the delivery tube with a solenoid producing a magnetic field of a couple hundred gauss. Electrons were fired into the delivery tube from the accelerator end and ions in at the other end. The electrons produce a "potential trough" through which the ions may pass. If both beams of particles have the same energy, for space charge neutralization the currents must be in the ratio of the square roots of their masses. This arrangement has allowed currents as high as 1.5 milliamperes of ions to be discharged into the accelerator system. There is sometimes considerable ion production in the tube itself, as may be evidenced by the fact that it performs quite well when only electrons are fired in at both ends.

Work is under way at the present time toward the maintenance of a beam by increasing the potential along the axis as the $\frac{4}{3}$ power of the distance as indicated by Eq. (21), for balancing out the space charge radial field.

Letter to the Editor

The Mechanism of Static Friction

Amontons' law of friction,[1] which places tangential frictional force directly proportional to load, has long been an accepted relationship, but there has been much difference of opinion concerning its theoretical explanation. Coulomb[2] proposed that the force of friction is due to the opposition which the normal load produces when interlocking asperities of opposing solid surfaces must be lifted over each other. As a second possible mechanism he suggested that opposition to slip might be caused by the interaction of the force fields of opposing solid surfaces. However, he rejected this latter possibility for cases where Amontons' law held.

During the past three years an extensive investigation of friction and related phenomena has been carried on under the joint cooperation of the Cincinnati Milling Machine Company and the University of Cincinnati. It is the purpose of the present publication to show, on the basis of the results of this investigation, that interaction of surface force fields is as much a part of the mechanism of static friction as is interlocking of surface irregularities.

First, to harmonize the two views, let us consider contact between two *ideally smooth* solids of different curvature. There can be no interlocking of irregularities here. However, let it be assumed that the surface fields do interact at the area of actual contact, A, and thus a finite tangential force, F, will be required to initiate relative sliding. Then as a consequence, F must be proportional to A, or $F=SA$, S thus being the force per unit area necessary to cause slip or shear of the contact area. It follows, then, that if the frictional force, F, is to be also proportional to normal force, N, i.e., if Amontons' law is to hold, A must be proportional to N, or $N=HA$. Thus H, the compressive force per unit area of actual contact, is a constant of the material, and so independent of load. That this last conclusion is generally true has been mentioned by Tomlinson (as having been observed by Stott)[3] and has been more fully confirmed by Bowden and Tabor.[4] It is readily observed on a macroscopic scale in ordinary engineering hardness testing (although the constancy of H is there somewhat obscured by the phenomenon of work hardening). Hence H is what is generally known as the mean pressure hardness of the softer of two contacting solids. Now, by definition, $\mu=F/N$. From the above, therefore, $\mu_A=SA/HA=S/H$, where μ_A is the coefficient of *static* friction for cases where no interlocking of asperities takes place.

Let us now consider contact similar to the above between a pair of *rough* flat surfaces for which the value of S *is zero*. It is apparent that the angle of repose for these ideal solids will be approximately equal to the average angle, θ, which the planes of slip (in this case the tiny surface "hillsides") make with the general plane of the surfaces. Thus the coefficient of friction, μ_B, will be equal to tan θ. Bikerman and Rideal[5] have recently suggested this same conclusion, but have assumed that this term alone is the source of *all* friction.

In the foregoing we have shown, then, that when $\theta=0$, $\mu=\mu_A=S/H$, and when $S=0$, $\mu=\mu_B=\tan\theta$. It follows therefore that, in general, $\mu=\mu_A+\mu_B=S/H+\tan\theta$, which we now propose as the general equation of static friction.

That any interlocking of surface irregularities must have some effect on static friction is self evident, but the existence of the term S/H in this expression for μ demands thorough verification. This has been furnished in the course of the previously mentioned investigation of friction. Coefficients of static friction were determined for metal surfaces dry turned in a lathe and quickly transferred to a vacuum chamber. Strict precautions were taken to prevent contamination of the freshly exposed metal. The surfaces were therefore clean except for a certain amount of adsorbed gas, and were probably quite fully work-hardened by the machining process. Details of the experimental work and apparatus will be given in a more complete discussion to be published later.

The results of the investigation are in agreement with the theory outlined above. They may be summarized as follows:

(1) The coefficient of friction was independent of load (except for very minute loads) thus verifying Amontons' law for the case of these clean surfaces, and for the range of loads used in obtaining the succeeding facts.

(2) For like-metal pairs, the points of contact were severely torn and scored after a single slip, indicating actual shearing of the metal itself, and thus a very high value for S.

(3) Carefully polished like-metal pairs were prepared by a dry rouge technique which left the surfaces sufficiently clean to be freely wet by water. These gave virtually the same coefficients of friction as the rough machined surfaces, even for the very first slip on an unscratched finish. This indicates that the effect of surface roughness is ordinarily negligible when the metal itself shears, (i.e., the planes of shear are practically parallel to the surface).

(4) For like-metal pairs, values of μ were independent of temperature and approximately equal to one for metals of cubic crystal structure tested below their annealing range. When the metals were heated above their annealing temperature, however, the coefficient of friction increased to much higher values, and this increase was maintained after cooling and even after an exposure to air equivalent to that experienced by a newly prepared specimen.

Quantitative confirmation of the correctness of the term S/H will be published later.

M. E. Merchant

Research Department,
Cincinnati Milling Machine Company,
Cincinnati, Ohio,
January 18, 1940.

[1] Amontons, Mem. Acad. Roy. Sci. 206 (1699); 96 (1704).
[2] Coulomb, Mem. Acad, Roy. Sci. 161 (1785).
[3] G. A. Tomlinson, Phil. Mag. **7**, 905 (1929), see p. 920.
[4] F. P. Bowden and D. Tabor, Proc. Roy. Soc. **A169**, 391 (1939).
[5] J. J. Bikerman and E. K. Rideal, Phil. Mag. **27**, 687 (1939).

Wratten Light Filters

for Photography, Photomicrography, Spectroscopy, Photometry, and Astronomy

WRATTEN LIGHT FILTERS are universally used in widely separated fields of scientific research.

The Wratten list includes filters for use with all types of color-sensitive films and plates. Over one hundred different filters are available.

Complete spectrophotometric data are given in the Eastman publication, *Wratten Light Filters;* price, 50 cents. A price list of filters will be furnished free on request.

EASTMAN KODAK COMPANY

Research Laboratories **ROCHESTER, N. Y.**

GEIGER-MUELLER TUBES with a WIDE PLATEAU

by Professor Francis R. Shonka, De Paul University, Chicago

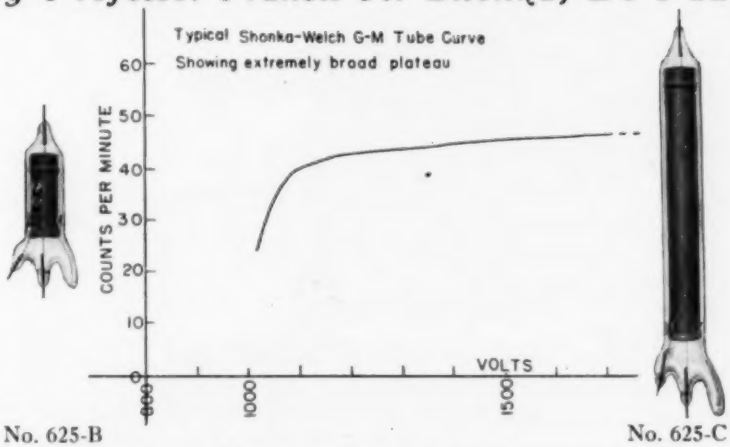

No. 625-B No. 625-C

Special sizes available on order

SPECIAL FEATURES:

Extremely Wide Plateau.

Eliminates the need for highly stabilized voltage supply.

High Efficiency and Stability.

Offered in two stock sizes:

No. 625B—short tube, 60 mm long.....each, $25.00

No. 625C—long tube, 180 mm long.....each, $30.00

For full information, write

W. M. Welch Scientific Company

Established 1880

1515 Sedgwick Street Chicago, Illinois, U.S.A.

WELCH

Catalog lists over 10,000 items for Science Laboratories

Associates of the Institute

FOR the most part, the expenses incurred in carrying out the work of the American Institute of Physics are defrayed by its Founder Societies. The institute exists to do the work which these Societies have assigned to it—work toward objectives which they have in common. These Societies are being materially aided by a significant added contribution from the dues of the Associates of the Institute. The Associates are a group of forward looking companies and laboratories who believe it is valuable to them and to America to maintain a vigorous advance of physical science. In aiding the Institute they are helping physicists to secure for themselves and their science the necessary opportunities and facilities for effective service to industry and to society in general.

The Associates of the Institute are

Agfa Ansco Corporation
Allegheny Steel Company
Aluminum Company of America
American Telephone and Telegraph Company
Bausch & Lomb Optical Company
Bell Telephone Laboratories
Crane Company
Dow Chemical Company
E. I. du Pont de Nemours & Company
Eastman Kodak Company
General Electric Company
General Motors Corporation
Gulf Research & Development Company
Libbey-Owens-Ford Glass Company
Loomis Laboratory
Massachusetts Institute of Technology, Department of Physics
Massachusetts Institute of Technology, Division of Industrial Cooperation
Radio Corporation of America
Research Corporation
Shell Development Company
Sperry Gyroscope Company, Inc.
Westinghouse Electric & Manufacturing Company

The American Institute of Physics cordially invites other interested corporations to become its Associates and will welcome their inquiries addressed to the Director.

American Institute of Physics
175 Fifth Avenue, New York, N. Y.

MATTER, MOTION AND ELECTRICITY

A Modern Approach to General Physics

By H. D. Smyth, Princeton University, and C. W. Ufford, Allegheny College

647 pages, 6 x 9. $3.75

IN this outstanding new book, intended primarily for students with a background of high school physics, the authors review fundamental principles and definitions, while presenting a fresh approach that avoids a repetition of the conventional beginners' course. Modern physics is introduced earlier than usual. A feature of the book is the wealth of illustrative examples and stimulating problems.

"This book seems to be the first attempt in many years at a searching reorganization of the materials of physics suitable for a general introductory course of college level, and it is one of the first to present a consistent and clean cut organization of the subject in keeping with the now well established and commonly accepted modern concepts regarding matter and energy."

—Professor J. C. Hubbard, Johns Hopkins University

Send for a copy on approval

McGRAW-HILL BOOK COMPANY, INC.

330 West 42nd Street **New York, N. Y.**

RAMAN SPECTROGRAPH

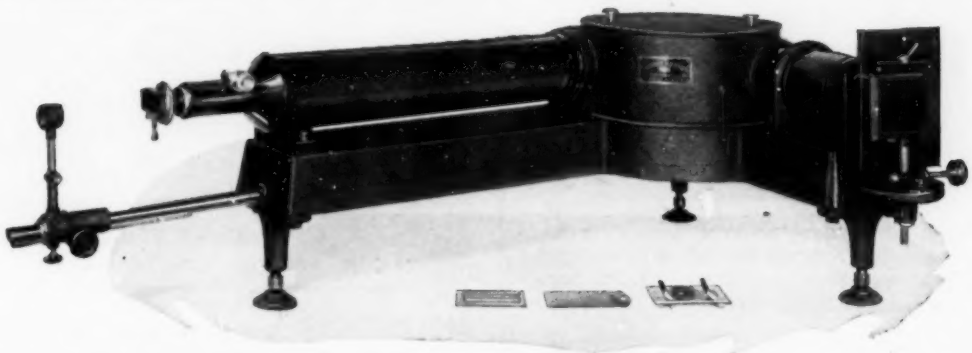

Excellent resolution and permanence of adjustment characterize the GAERTNER Raman Spectrograph. Supplied with either 12″ focus F/3.5 or 20″ focus, F/6.3 camera.

Write for catalogue L2.

THE GAERTNER SCIENTIFIC CORPORATION

1212 WRIGHTWOOD AVE. **CHICAGO, U.S.A.**

FIRST SURFACE MIRRORS

by High Vacuum Deposition

EVAPCO first surface are excellent for projection mirrors and other uses that require an opaque mirror of high reflectivity that does not tarnish or give double image.

DUOLUX semi-transparent for one exposure three color cameras, range finders, or wherever an accurate beam-splitter is needed. Made to order for all practical transmission —reflection ratios.

EVAPORATED METAL FILMS CORP.

ITHACA, N. Y.

The RCA SIGNALYST *is here!*

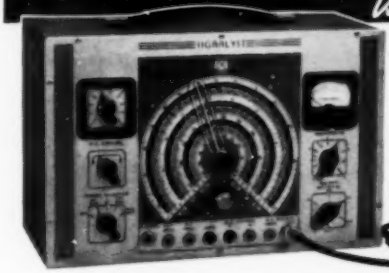

The New Signal Generator
Range 120 KC to 120 MC
In Fundamentals

New service instrument is important companion to the Rider Chanalyst and Rider VoltOhmyst

Dollar for dollar, feature for feature, the new RCA SIGNALYST... is the best buy in Signal Generators. Its amazing range is greater than any test oscillator... Its accuracy and stability are excellent... Stray signal leakage is kept at a minimum... AC operated with regulated power supply! It is an instrument that will find many applications in the laboratory in radio and television work. $107.50 Net

Over 335 million RCA radio tubes have been purchased by radio users. In tubes, as in parts and test equipment, it pays to go RCA All the Way

RCA Test Equipment

RCA Manufacturing Co., Inc., Camden, N. J.
A Service of Radio Corporation of America

TYPE B POTENTIOMETER

A high-grade, general-purpose laboratory potentiometer with 3 ranges: 1.6, .16 and .016 volts. Extremely accurate and convenient. Used in leading standardizing laboratories.

Described in Bulletin No. 270 which also lists Rubicon portable potentiometers.

Other products: standards of resistance, inductance and capacitance, Wheatstone and Kelvin bridges, resistance boxes, galvanometers, electrometers, permeameters, colorimeters.

RUBICON COMPANY

29 North 6th Street Philadelphia, Penna.

STABILIZED A-C VOLTAGE

INPUT 95-130 volts
Instantaneous action
A magnetic unit

OUTPUT
115 volts ±½%
Stabilizes at any load within rating

No moving parts. Nothing to wear out.

RAYTHEON Voltage Stabiliser

APPLICATIONS Broadly it insures stable operation of all precision apparatus obtaining its power from an A.C. source, for example:—

- Insures constant brilliancy from all types of lamps.
- Improves the operation of X-ray equipment.
- Stabilizes all electronic apparatus.

Write for Bulletin 48-71JP.

RAYTHEON MFG. CO. WALTHAM, MASS.

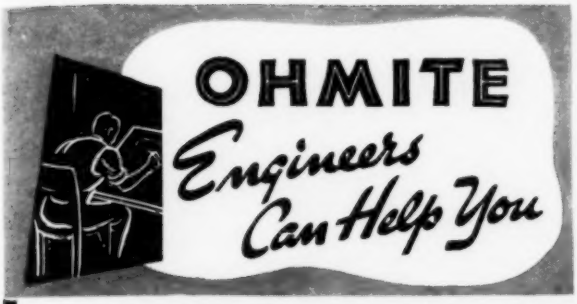

OHMITE
Engineers Can Help You

Send Us Your "Specs" to get the *Right Rheostat*

Don't worry about that Rheostat problem! Ohmite Engineers, with their wide specialized experience, can help you solve it quickly, dependably, economically! Send in your "Specs"—often the right Rheostat can be found in the wide range of Ohmite stock types and sizes. Or, Rheostats can be made-to-order promptly to meet your exact requirements.

OHMITE MFG. CO.
4888 Flournoy St., Chicago

Write for Catalog 17

***Be Right with* OHMITE**
RHEOSTATS · RESISTORS · TAP SWITCHES

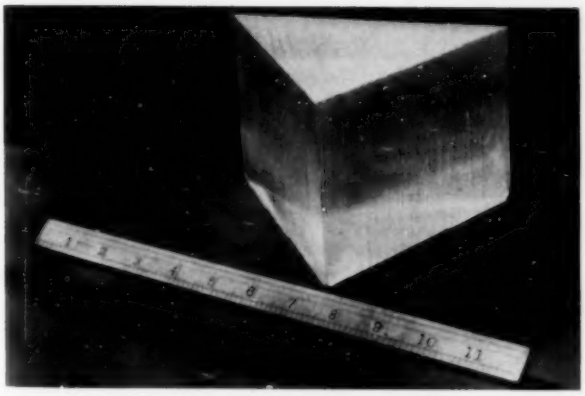

An eight pound rock salt prism blank cut from a twenty-five pound single crystal

SYNTHETIC CRYSTAL OPTICS

For infrared and ultraviolet spectroscopy and for polarizing optics. . . . Single crystals of Lithium Fluoride, Sodium Chloride, Sodium Nitrate, and Potassium Bromide. . . . Write for information.

THE HARSHAW CHEMICAL CO.
SPECIAL PRODUCTS DIVISION CLEVELAND, OHIO

EPPLEY
THERMOPILES
for
RADIANT ENERGY
MEASUREMENTS

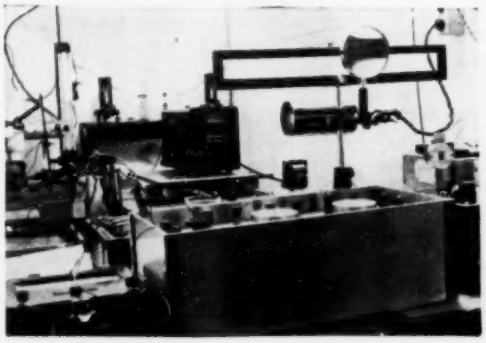

A view of some of the apparatus used for calibrating thermopiles at the Eppley Laboratory, Inc.

Adequate manufacturing, testing and calibrating equipment in the hands of our skilled and experienced technicians insures satisfaction to the users of Eppley Thermopiles.

We are prepared to furnish thermopiles of either bismuth-silver or copper-constantan, mounted in vacuum or air type cases. We also furnish thermopiles and mountings especially designed to meet individual needs. A card will bring you our Bulletin R–3 which contains illustrations, sample curves, complete descriptive matter, prices, references, etc., with regard to Eppley Thermopiles.

EPLAB

THE EPPLEY LABORATORY, INC.
SCIENTIFIC INSTRUMENTS
NEWPORT, R.I.
U. S. A.

JAGABI

"Lubri-tact"

RHEOSTATS

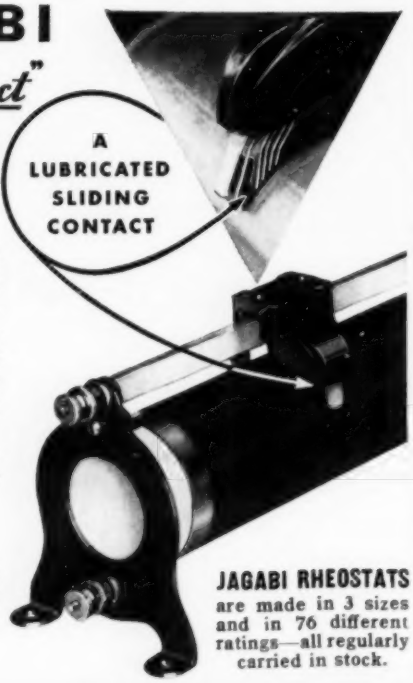

have a graphited carbon lubricator associated with the contact brushes. Eliminates scratching and abrasion—gives smoother operation and a better contact. Makes Jagabi Rheostats *better* rheostats.

Write for Bulletin 1620-R which lists new lower prices.

JAGABI RHEOSTATS are made in 3 sizes and in 76 different ratings—all regularly carried in stock.

JAMES G. BIDDLE CO.
1211-13 ARCH STREET *Electrical and Scientific Instruments* PHILADELPHIA, PA.

Eyes for the Future look through

POLAROID*

Light Controls

Already in use in variable windows, anti-glare day glasses and desk lamps, Polaroid developments foreshadow 3-dimensional color movies, glareless auto headlights, many other important new devices. Instruction in light polarization has logically become a part of every science course, elementary or advanced.

For school and college science departments, Polaroid filters come in economical, convenient form, with kits for performing many dramatic experiments.

Polaroid Kit No. 324, $10.

Polaroid Kit No. 324, $25.

Write Division 4 for free handbook and survey of applications.

POLAROID CORPORATION
720 Main Street, Cambridge, Mass.

*T. M. REG. U. S. PAT. OFF.

INDEX TO ADVERTISERS

Name	*Page*
BAUSCH & LOMB OPTICAL CO. ..... Makers of Microscopes, Microtomes, Colorimeters, Refractometers, Spectrometers, Balopticons, Photomicrographic and Microprojection Apparatus and related instruments. Also makers of Orthogon Eyeglass Lenses for Better Vision.	ii
JAMES G. BIDDLE COMPANY ..... "Jagabi" Rheostats; Adam Hilger and Kipp & Zonen Optical Instruments; "Pointolite" Lamps; Electrical Testing and Speed-measuring Instruments.	viii
CENTRAL SCIENTIFIC COMPANY .....Cover 4 Manufacturers of Cenco Physical Apparatus and Instruments to meet all requirements of University, College and High School Physics Laboratories. Specializing in high vacuum pumps and development of instruments and apparatus for various sciences.	
EASTMAN KODAK COMPANY ..... Purified Organic Chemicals for research purposes; Plates for Photography, Photomicrography, Spectroscopy, Photometry, Astronomy; Wratten Light Filters; Cameras and Films.	iii
THE EPPLEY LABORATORY, INC. ..... Standard Cells, thermopiles, pyrheliometers and temperature bridges.	vii
EVAPORATED METAL FILMS CORPORATION ..... First surface and semi-transparent mirrors by high vacuum deposition.	vi
GAERTNER SCIENTIFIC CORPORATION ..... Spectroscopes, Spectrometers, Spectrographs, Spectrophotometers, Heliostats, Measuring Microscopes, Comparators, Cathetometers, Reading Telescopes, Interferometers, Chronographs, Dividing Machines, etc.	v
GENERAL RADIO COMPANY .....Cover 3 Manufacturers of electronic measuring instruments; vacuum-tube voltmeters, amplifiers and oscillators; wave analyzers, noise meters and analyzers, stroboscopes; laboratory standards of capacitance, inductance and frequency; impedance bridges, decade resistors and condensers; air condensers and variable inductors; rheostats, Variacs, transformers; other laboratory accessories.	
HARSHAW CHEMICAL COMPANY ..... Optical Lithium Fluoride grown in single crystal to predetermined size. Industrial Chemicals.	vii
LEEDS & NORTHRUP COMPANY ..... Manufacturers of Galvanometers, Resistors, Bridges, Condensers, Inductances, Potentiometers, Testing Sets; Temperature Measuring, Recording and Controlling Apparatus; Instruments for Measuring and Controlling Conductivity of Electrolytes and Hydrogen Ion Concentrations.	i
MCGRAW-HILL BOOK COMPANY, INC.	v
OHMITE MANUFACTURING COMPANY ..... Manufacturers of close control rheostats, fixed and adjustable power resistors, precision and non-inductive resistors, attenuators, tapswitches and R.F. chokes.	vii
POLAROID CORPORATION ..... Polaroid experimental kit for demonstration. Polarized light. Handbook. Sheet Polaroid.	viii
RAYTHEON MFG. COMPANY ..... Voltage stabilizers and regulators. Electrical measurement and control instruments.	vi
RCA MANUFACTURING COMPANY, INC. ..... RCA Oscillators and Oscillographs, RCA Test Equipment, RCA Ultra-Sensitive DC Meter.	vi
RUBICON COMPANY ..... Galvanometers, electrometers, potentiometers, Wheatstone and Kelvin bridges, resistance boxes, hydrogen ion and conductivity apparatus.	vi
W. M. WELCH SCIENTIFIC COMPANY ..... Scientific instruments—laboratory apparatus. Catalog lists 10,000 items.	iii

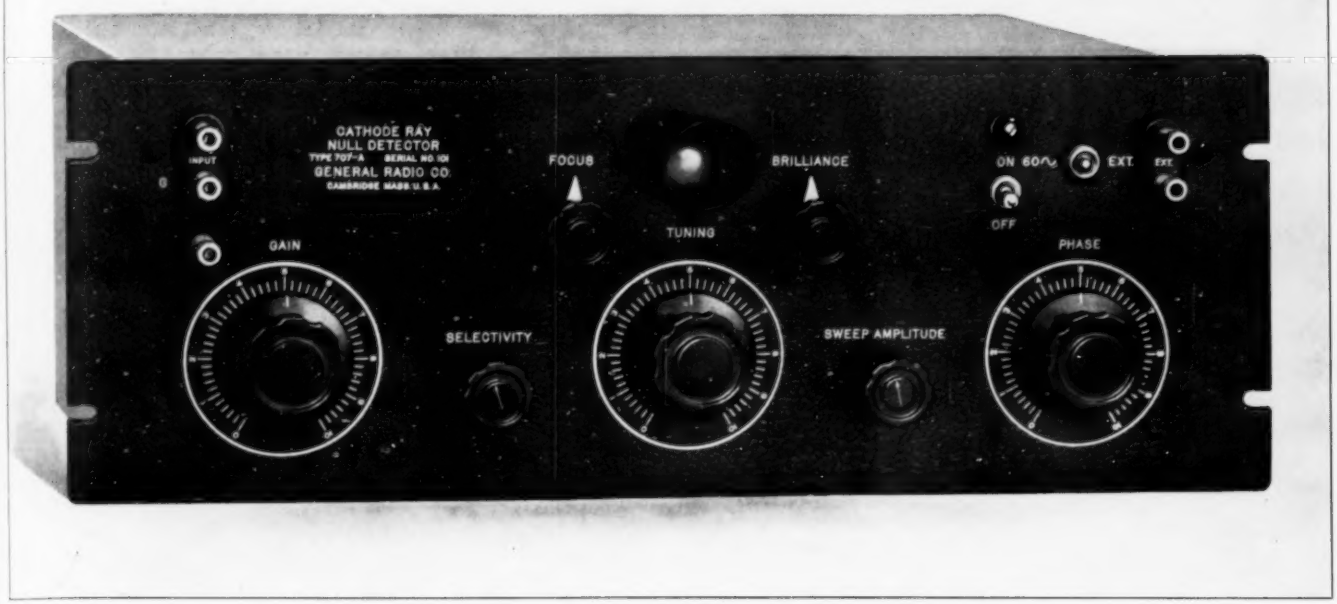

IMPROVED NULL DETECTOR

for a-c Impedance Bridges

SENSITIVE • RUGGED • CONVENIENT TO OPERATE

THE G-R TYPE 707-A NULL DETECTOR uses a one-inch cathode-ray tube in a new non-inductive degenerative amplifier circuit, with tuning and phasing networks and sweep and sensitivity controls. This new detector offers many advantages which include:

- Operation in noisy locations
- Not affected by strong fields
- May be used at all frequencies up to 20 kilocycles
- Separately indicates balance of the resistive and the reactive components
- Makes possible precise balancing of either component with only moderately close balance of the other
- Precise measurement of the steady component can be made while the other varies erratically
- Shows immediately any drift of either or both components
- Provides positive indication of the direction of off-balance for either component as selected
- Can be calibrated to show the degree of unbalance
- Can be used at all times at maximum sensitivity, even with the bridge far off balance
- Supplies instantaneous response
- Will withstand any overload caused by marked off-balance, and is instantaneous in recovery

The input impedance of the null detector is 1 megohm. Its sensitivity is 100 μv at 60 cycles and 200 to 300 μv at 1000 cycles. Its selectivity is 40 db against the second harmonic. Plug-in units tune the amplifier to any operating frequency desired between 20 and 2,000 cycles, with a continuous tuning range of $\pm 5\%$ for each unit.

TYPE 707-A CATHODE-RAY NULL INDICATOR $195.00

WRITE FOR BULLETIN 554 FOR COMPLETE INFORMATION

GENERAL RADIO COMPANY

Cambridge, Massachusetts

Branches in New York and Los Angeles

For Demonstrations of the

PIEZO-ELECTRIC EFFECT

81330

81335

80796

ROCHELLE SALT CRYSTAL

A nearly flawless half crystal, of approximately 350 grams weight and measuring 10 by 8 cm, in which the piezo-electric effect is very large and reversible. By cementing tinfoil coatings on opposite faces, alternating emf can be applied to cause it to vibrate. With the output of a radio receiver, audible sounds are emitted.

81330 **Piezo-Electric Crystal** ..... Each $10.00

PIEZO-ELECTRIC DEMONSTRATION

Shows production of an electric charge by mechanical distortion of a Rochelle salt crystal and the converse effect. When crystal is tapped, the neon bulb flashes. A shock is received when terminals are touched with moistened fingers. When neon bulb is replaced by a connection to the output of a radio receiver and a paper cone attached to the upper end of the crystal mounting, audible sounds are produced.

81335 **Piezo-Electric Demonstration Apparatus** ..... Each $16.50

PIEZO-ELECTRIC TELEPHONE RECEIVER

A commercial application of the piezo-electric effect which is excellent for laboratory work with alternating currents. Can be used for long periods without fatigue and loss of sensitivity of the ear. Especially suited for balancing A.C. bridges. It is non-magnetic, has high impedance, high current sensitivity, draws negligible current, and vibrates with great amplitude in response to applied potentials. Provided with head band and standard 5-foot telephone cord with pin tips.

80796 **Piezo-Electric Telephone Receiver** ..... Each $3.50

CENTRAL SCIENTIFIC COMPANY

SCIENTIFIC INSTRUMENTS & LABORATORY APPARATUS

CHICAGO
1700 Irving Park Blvd.,
Lakeview Station

TRADE MARK CENCO REG. U.S. PAT. OFF.

BOSTON
79 Amherst St.,
Cambridge A Station

LANCASTER PRESS, INC., LANCASTER, PA.